Development of anode materials for rechargeable batteries

A thesis
submitted in partial fulfilment of the requirements
for the degree of

Doctor of Philosophy

by

Neha Sharma

Indian Institute of Science Education and Research (IISER)-Pune

2019

Dedicated to

My late grandfather

Mr. Jaswant Krishan Rampal

(without you it would not have been possible)

भारतीय विज्ञान शिक्षा एवं अनुसंधान संस्थान, पुणे
INDIAN INSTITUTE OF SCIENCE EDUCATION AND RESEARCH (IISER) PUNE
(An Autonomous Institution of Ministry of Human Resource Development, Govt. of India)
Dr. Homi Bhabha Road, Pune – 411008.

DECLARATION

I declare that this written submission represents my ideas in my own words and wherever other's ideas have been included; I have adequately cited and referenced the original sources. I also declare that I have adhered to all the principles of academic honesty and integrity and have not misrepresented or fabricated or falsified any idea / data / fact / source in my submission. I understand that violation of the above will cause for disciplinary action by the Institute and can also evoke penal action from the sources which have thus not been properly cited or from whom proper permission has not been taken when needed.

Ms. Neha Sharma
(ID: 20143297)

Date: 18th January 2019

Dr. Musthafa Muhammed
Assistant Professor
Department of Department,
IISER Pune

CERTIFICATE

Certified that the work incorporated in the thesis entitled "**Development of anode materials for rechargeable batteries**" submitted by **Ms. Neha** was carried out by the candidate, under my supervision. The work presented here or any part of it has not been included in any other thesis submitted previously for the award of any degree or diploma from any other university or institution. For the completion of thesis, few results are taken from collaborators after their permissions and are clearly mentioned in the thesis.

Date: 18th January 2019

Dr. Musthafa Muhammed
(Research Supervisor)

Dr. Satishchandra Ogale

Professor Emeritus

Department of Physics,

IISER Pune

CERTIFICATE

Certified that the work incorporated in the thesis entitled "**Development of anode materials for rechargeable batteries**" submitted by **Ms. Neha** was carried out by the candidate, under my supervision. The work presented here or any part of it has not been included in any other thesis submitted previously for the award of any degree or diploma from any other university or institution. For the completion of thesis, few results are taken from collaborators after their permissions and are clearly mentioned in the thesis.

Date: 18th January 2019

Prof. Satishchandra Ogale

(Research Co-Supervisor)

x

Acknowledgement

As I approach the completion of my PhD program, I would express my gratitude and thanks to all the people who helped me directly and indirectly to complete this arduous yet enjoyable journey and making things easy and pleasant for me.

At the outset, I would take the opportunity to thank my supervisors Dr. Musthafa Muhammed and Prof. Satishchandra Ogale for giving me the opportunity to work with them. Their precious guidance and support throughout my working tenure has enabled me to finish my PhD in the given time frame and whatever I have learnt during this course of time is because of them. They have not only helped me with professional advice and supervision, but on personal fronts as well by taking care of me and thinking about my health and career all the time.

I would particularly mention Prof. Ogale here being concerned about me and instructing my fellow students to take care of me in my bad health and motivating me all the time. His positive approach and evergreen enthusiasm for research is indeed a motivation for all the people working around him. His attitude of giving priority to the work of students and being always there to help them is undeniably awesome.

I would like to extend my gratitude to the former director of IISER Pune, Prof. K. N. Ganesh, for allowing me to make my choice of guide after a substantial period of my PhD duration. Along with him Dr. V. G. Anand, former dean doctoral studies, had also been very supportive during that whole process. I truly applaud their initiative and efforts in helping a student.

I thank IISER Pune for giving me opportunity to work in a top notch institute such as IISER Pune itself, for the research funding and the fellowship. I thank the current director of IISER Pune Prof. Jayant Udgaonkar for providing us all with all the first rate research facilities, healthy research environment and a charming campus. I thank the Department of Chemistry and the Department Chair for all the resources they have given us to conduct our research and not letting the work stop under any conditions.

I thank my RAC members Dr. R. Vaidhyanathan and Prof. Sreekumar Kurungot for their useful suggestions during the RAC meetings that helped me in improving my work. I also wish to thank IISER Pune faculties for all the help and support at various situations and my course work mentors for their good teachings. I have spent a good

Synopsis

This thesis is on the investigation of electrode materials for alkali ion batteries such as Li and Na ion batteries. Although the battery is composed of various inherent components such as cathode, anode, electrolyte and separator, the anode has been given the primary attention in the present work. It is well known that the battery performance metrics is certainly effected by the type of anode material chosen and their behavior determines the stability and life of the battery. There are wide range of anode materials and they typically play a crucial role in determining the overall battery energy density and power density. Along these lines, according to the literature and the ongoing research in the field, certain problems were designed and the background and motivation for the same is discussed in the beginning of every chapter.

Chapter 1. Introduction: In this chapter, the importance of energy storage is reviewed and emphasized based on the energy demand and consumption statistics. The types of energy resources and their advantages and disadvantages are also screened. The sector wise energy utilization reveals that currently the non-renewable energy resources are being relied upon to fulfill the energy requirements of modern society. These resources not only pose a threat of being depleted over the course of time but also are very harmful for the environment. The renewable energy resources are clean and harmless without any emissions but they have been scarcely utilized. The reason for this is their intermittence due to characteristic weather fluctuations and difficulty in harnessing them as per our demand. This generates immense interest in energy storage and energy conversion devices. Batteries and supercapacitors are primary energy storage devices used for a wide range of applications spanning grid scale to small gadgets. Battery history starts from the Baghdad battery which was invented around 250 B.C. Since then batteries underwent many changes and developments and there were many prototypes like Daniel cell, Voltaic pile, Lead acid battery, Zinc-Carbon cell, Na-S battery etc. It should be noted that each of them was designed as an improvement over the previous model. Present day batteries are Li ion batteries which finds major applications in almost all electronic gadgets. The other chemistries such as Na ion, Mg ion, air batteries and redox flow batteries are active as well but not to the expected scale. The batteries still have to take over the fossil fuels and present battery chemistries have not achieved the optimization stage yet for completely replacing fossil fuels. The development and use of rechargeable batteries have led to the price increment in the basic materials

consumed by battery industry. There are many considerations in the battery design like the choice of cheap and safe materials which are at the same time eco-friendly. The energy density and power density of the batteries still fall short for many applications and they are yet to beat gasoline in this regard. This chapter paves the motivation of the work in related field.

Chapter 2. Alkali ion batteries: This chapter briefly explains the working of the Li ion batteries and discusses the battery components and their types with respect to their storage mechanism. The cathodes for Li ion battery are layered compounds with Li. They mainly consist of a 3d transition element responsible for the redox reaction and Li uptake. The other type of cathodes known are polyanionic compounds. The famous cathode for Li ion battery is $LiCoO_2$ (LCO) proposed by Goodenough in 1980s. To increase the energy density of Li ion batteries other cathode materials have been discovered other than LCO. But the transition elements present in the structure substitute Li sometimes and cause instability in the structure. Apart from this they tend to dissolve in electrolytes hence have poor cycling capability. The polyanionic compounds are considered to be a better choice than layered compounds. The anodes are of three types depending upon their charge storage mechanism. The intercalation type anodes do not react with the Li ion chemically thus the ion gets intercalated between the layers or gets adsorbed onto the material. The intercalation materials are safe to use and very robust in their performance. Graphite is the best example of intercalation anodes. But these materials have limited specific capacities and thus low energy densities. The alloying type anodes like Sn, Sb, Si etc. can alloy with Li ion taking more than one ion. This makes them good materials to achieve high energy densities. But as they take 3-4 Li ions, volume expansion in the materials and rapid capacity decay are serious challenges. Several strategies like downsizing the particles and making composite with carbon are adapted for improving their performance. The third type of anode materials is conversion and they undergo displacement reaction and take high number of Li ions like alloying materials. They also suffer from issues like alloying materials and hence have not been commercialized. The electrolytes used in batteries are of different types- carbonates based, ether based and ionic liquids. The electrolytes are chosen in such a manner that they have sufficient viscosity and high ion mobility. Some electrolyte systems are specific for specific anodes and cathodes. The separators used in batteries are of two types the Whatmann and polypropylene where

polypropylene is considered to be thermally stable than Whatmann. The high cost and limited reserves of Li makes Na as an alternative but Na ion batteries have not yet been able to replace Li ion batteries. This is because of their bigger ionic size causing structural distortion in cathodes and anodes. The fast diffusion kinetics of Na ion imparts the device high rate capability as compared to Li ion batteries but the difficulties in their implementation are still a hindrance. The batteries also suffer from aging, self-discharge and leakage which degrade their performance. The battery performance is analyzed based on few factors namely the energy density, power density, C-rate performance, cycling stability etc.

Chapter 3. Nanotubular hard carbon derived from renewable natural seed gel as high performance sodium-ion battery anode: Na ion batteries have been the focus to replace Li ion batteries in future and hence there is constant endeavor to improve the current energy density of Na ion battery. In anodes, Graphite which is a very suitable material for Li ion batteries is not at all compatible with Na ion batteries because of the bigger ionic size of Na. The interlayer spacing of graphite is not appropriate for Na ion giving rise to the use of other carbon based materials like hard carbon with enhanced d-spacing. Many bio wastes like banana peels, coconut shells, pomelo peels, and walnut shells have been used as the hard carbon source. Other than bio wastes, naturally occurring compounds such as glucose, grass, algae, phytic acid have been also used to obtain hard carbon. In this chapter, a Basil seed derived natural gel is employed as a source of hard carbon called as natural gel derived hard carbon (NGHC). The basil seeds are soaked in D.I. water and their mucilage is extracted and freeze dried. The simple high temperature pyrolysis yields a hard carbon which is characterized using PXRD, RAMAN, XPS and BET analysis. The NGHC exists in nanotubular form as seen in SEM and TEM.

The electrochemical behavior of NGHC is analyzed by impedance spectroscopy and cyclic voltammetry followed by the charge discharge measurements. The NGHC shows a reversible specific capacity of 195 mAh g^{-1} at a current density of 100 mA g^{-1} with high cyclic stability up to 300 cycles. The comparison with commercial hard carbon also states that the NGHC is better in terms of specific capacity and rate performance.

Chapter 4. Carbon caged Si nanoparticles with high capacity and cycling stability for Li-ion battery anode: Si is an alloying anode and has a theoretical specific capacity

of 4200 mAh g^{-1} as it can take 4.4 Li ions during alloying. As a result of this, the final alloy is much bigger in volume than pure Si. This makes the structure to expand which is termed as volume expansion. To counteract this issue, people have tried making nano size Si in different morphologies so that the overall size of the Li$_x$Si alloy remains smaller than that of a micro sized Si. Another approach to tackle this is making core shell structure where the shell acts as buffer for volume expansion as well as composite with volume expansion accommodation material such as carbonaceous compounds. In this work, we adopted a strategy to encapsulate Si nanoparticles in a carbon cage. The carbon source was the natural gel from basil seed. The target of this approach was to uniformly embed Si NPs in carbon nanostructure. The seeds were soaked in Si NPs dispersed aqueous solution and during swelling they absorbed the Si NPs uniformly. The Si NPs loaded gel was freeze dried and then pyrolyzed in Ar at 1000 °C to obtain carbon caged Si NPs. The Si NPs containing gel derived carbon (Si-GDC) consists of the Si as well as carbon features reflected in PXRD and RAMAN. The impedance also reveals the reduced interfacial resistance because of carbon present in the composite and the CV also exhibits the Si alloying and carbon intercalation peaks. The Si-GDC has good rate performance giving 700 mAh g^{-1} at 2 A g^{-1} and high stability of 250 cycles at 1 A g^{-1} with final specific capacity of 1460 mAh g^{-1}.

Chapter 5. A hard carbon and Li$_4$Ti$_5$O$_{12}$ based physically mixed anode for superior Li-battery performance with significantly reduced Li content: A case of synergistic materials cooperation: Li$_4$Ti$_5$O$_{12}$ (LTO) is a very promising anode material for Li ion battery and it has a good rate performance due to the small diffusion channels for Li ion and is widely used anode at commercial level. The low specific capacity and poor electronic conductivity are major drawbacks of LTO which need to be addressed to enhance its performance. The carbons have specific capacities higher than LTO and are highly conducting. The extremely low intercalation potentials and low current density for the ion adsorption make them viable for metal plating and reduce their overall power density. This chapter presents the idea of combining these two to resolve their shortcomings and improve their performance. A simple physical mixture of LTO and hard carbon in two ratios 50-50 and 20-80 is tested as anode for Li ion battery. At low current density, the specific capacities reach near that of hard carbon. The rate performance proves that the mixtures perform better than hard carbon as carbon nanopores need very low currents for ion adsorption. The long term cycling

stability at 6 A g^{-1} up to 3000 cycles is a strong evidence for this synergistic phenomenon and even the 20 wt % LTO containing anode performs similar to LTO with little change in the specific capacity at high current density. The SEM images of all anodes taken at different cycling stages show that the SEI layer is robust in case of mixed anodes due to the synergistic effect.

The full cells of all the anodes with LiCoO$_2$ cathode reflect the anode dominance in charge discharge behavior. The LCO//LTO full cell has low operating window of 2.5 V whereas the LCO//HC and LCO//mixed anodes can be charged up to 3.5 V. The specific energy densities and cycling performance of full cells with mixed anodes are seen to be much better than the full cells with pristine anodes.

Chapter 6. Single phase Cu$_3$SnS$_4$ nanoparticles as high capacity Li-ion battery anode: In this chapter, conversion type Cu$_3$SnS$_4$ is demonstrated for Li ion battery application. Few materials allow conversion followed by alloying process for the charge storage. One of the elements in such compounds undergo displacement reaction and forms a matrix which does not contribute to the capacity. The other element alloys with Li and gets dispersed in the matrix of previous element. Binary and ternary sulfides like SnS$_2$, transition metal chalcogenides like MoS$_2$ are such examples. The sulfides have electrolyte dissolution problem and in every cycle, the poly sulfides irreversibly get trapped in electrolyte which causes low coulombic efficiency and capacity fading. The poly sulfides pass through the separator and travel to the other side leading to shuttle effect in batteries. In this study, a ternary metal sulfide Cu$_3$SnS$_4$ (CTS) is selected for the Li ion battery anode. The high Cu: Sn ratio enables the Cu^0 to act as matrix for Sn volume expansion and minimize the sulphur dissolution. The CTS nanoparticles show 1082 mAh g^{-1} at 0.2 A g^{-1}. It is highly stable up to 950 cycles with specific capacity of 890 mAh g^{-1} at 0.5 A g^{-1}. The comparison with similar materials shows that the CTS NPs stand out among those in terms of stability and capacity.

Appendix. A flexible Li ion battery for drug delivery application: In this work, a metal organic framework (MOF) is used as an anode for Li ion battery. The MOFs have unique structural properties and their pore size and flexibility can be tuned by varying the linkers. They are porous materials and can thus be used as intercalation anodes. In this study, a Fe metal containing MOF shows a very high specific capacity and cycling stability up to 1100 cycles. The full cell shows an energy density of 360 Wh/kg and a

robust stability up to 1000 cycles without any capacity decay. The flexible battery was made by using free standing electrodes made by using carbon nanotubes (CNTs) and polydimethylsiloxane (PDMS). The flexible battery could power a transdermal skin patch to generate enough heat required for the drug delivery which is evident from IR imaging.

Summary and outlook: Here, the new methodologies and their significance in the field is explained. The relevance of the results obtained is establish describing their importance. In the future direction, the improvement in full cell performance and enhancement in capacity is proposed by the use of different cathode. The conversion based cathode FeF3 with any other cathode as composite is proposed for its capacity fading issue during lithiation. Finally, metal batteries are put as a possible systems with much higher energy density and power density and the use of aerogels as the conducting free standing host matrix for Li metal is suggested.

Contents

Chapter 1

Introduction

Abstract

The significant dependence of the modern society on energy for a variety of daily needs brings the context to the issue of smart and careful use of the energy resources provided to us by nature. The non-renewable resources are depleting rapidly due the developmental needs of the ever growing population around the world and this has already caused severe adverse effects on the environment and health. If this is not checked on an urgent priority basis the society awaits a disastrous and uncertain future. The renewable resources on the other hand are fragmentary, temperamental and in many cases dilutely dispersed. Thus harvesting them efficiently when they are in their full strength and storing the harvested energy for subsequent use as needed is the only smart and viable option. There are a number of ways to harvest and storage energy from such sources, however in this work we focus on electrical energy storage which is the most important frontier because the modern society is essentially electrically driven. Amongst such storage devices the electrochemical and electrical energy storage systems are perhaps the most popular due to their applicability for diverse application sectors including mobile systems. The main electrochemical energy storage devices include batteries and supercapacitors, and their variants. Batteries render high energy density and good power density, and their development has been taking place over several decades with modifications in each component to improve their performance and make them safer to use. The modern day batteries are majorly alkali ion batteries although other chemistries also being intensely explored. These issues and challenges are reviewed in this chapter to set the stage for the work reported in this thesis.

1.1 Present scenario of energy consumption

Energy drives the engines of growth, development and progress of modern civilization. Sun is the primary source of energy providing light and heat via its broadband spectral radiation. Energy is used in various forms for various processes and converted from one form to another continuously in nature. In modern life we are heavily dependent on energy to meet our daily requirements.[1] We need energy to run our household jobs, for transportation and also in production or industrial work. Figure 1 shows various forms of energy being utilized in several areas including residential and commercial needs.

1.1.1   Energy Consumption statistics

The energy consumption statistics are given in Figure 2 in various sectors of society. It is evident from the histograms that most of the energy is consumed in transportation and it is generated form oil resources. Industrial areas rely on oil majorly but have their energy generated from coal and natural gas as well in substantial amount.
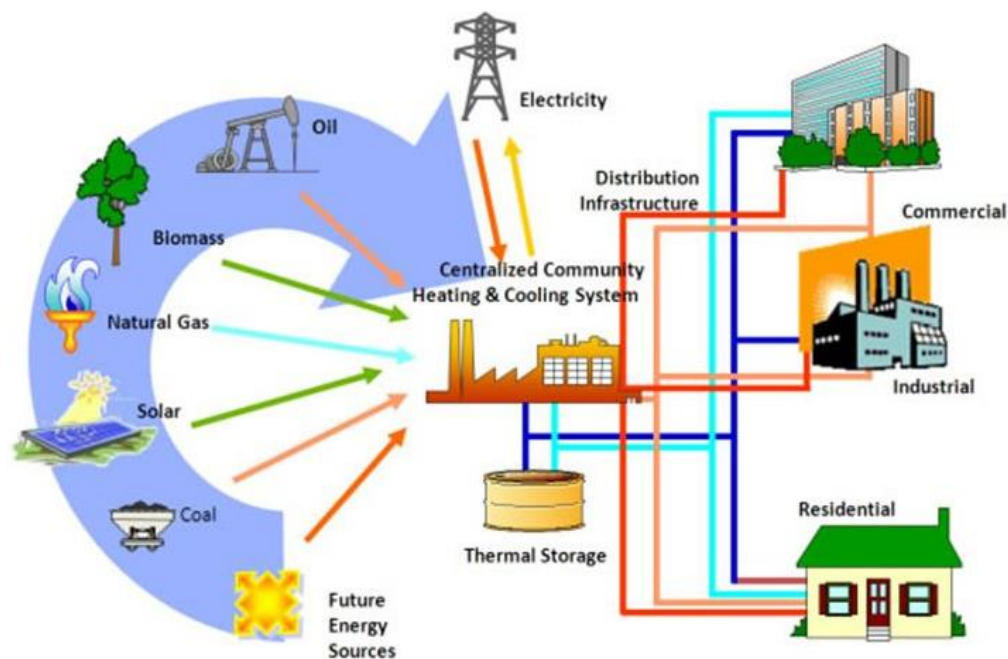
Figure 1. Daily life usage requirements of energy. (http://www.fvbenergy.com/wp-content/uploads/2012/12/renewable-energy-chart.jpg).

Total Energy Consumption by Fuel

Renewable Energy 7%
Nuclear/Electric Power 8%
Oil 39%
Coal 22%
Natural Gas 23%

Sector Energy Consumption by Fuel Type

Transportation: 96% | 2% | 2%
Industrial: 46% | 37% | 8% | 9%
Residential and Commercial: 75% | 19% | 5% | 1%
Electric Power: 52% | 21% | 17% | 9% | 2%

Oil | Natural Gas | Coal | Renewable Energy | Nuclear/Electrical Power

Source: Updated AEO 2009 Tables A1, A2 and A17

Figure 2. Energy consumption percentage by sector. https://www.ecofys.com/en /publication/deep-renovation-of-buildings.

The nation wise energy consumption per person seen from Figure 3 is pretty non-uniform with the developed countries consuming most of the resources. The developing countries have moderate consumption whereas the under developed countries have very less share of resources to consume and their utilization per capita is very low. However, given the large population of the developing and underdeveloped world, the total actual energy requirement is extremely high.
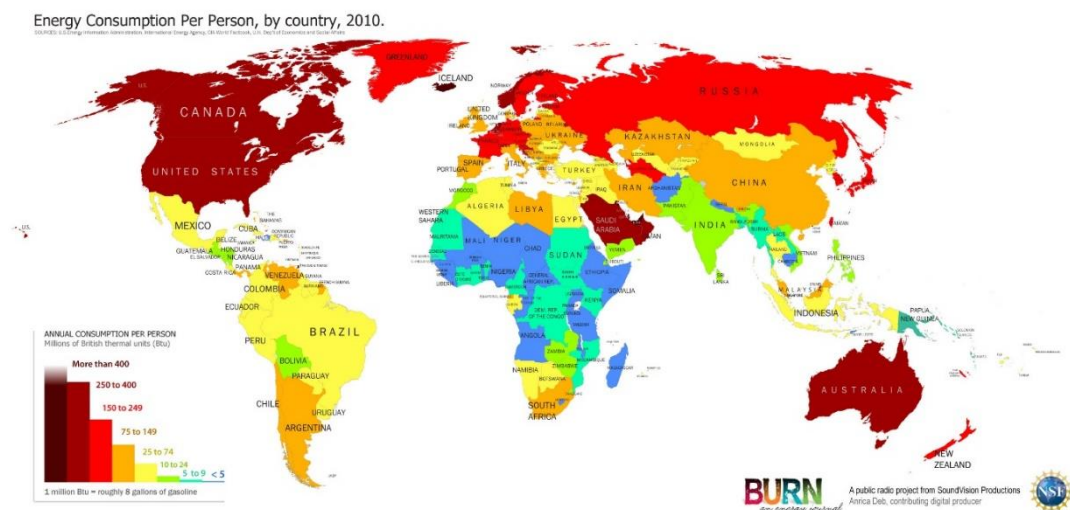
Figure 3. Energy consumption per person by country. http:// burnanenergyjournal.com /how-much-energy-are-we-using/.

1.2 Energy Resources

The available sources of energy (Figures 4, 5) can be broadly classified in to two categories. 1) Renewable Energy and 2) Non-renewable Energy. Renewable Energy is the energy from renewable resources which are naturally available and are abundant.[2] Non-renewable energy resources are those which are present in limited amount and are viable to extinction, if exploited excessively.
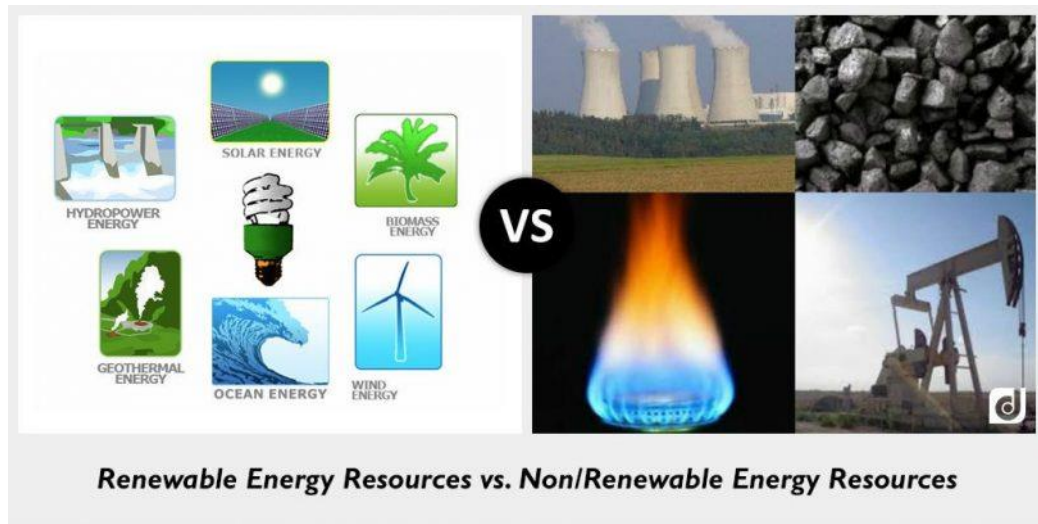
Figure 4. Types of energy resources. https://www.picemaps.com/images-of-non-renewable-resources/.
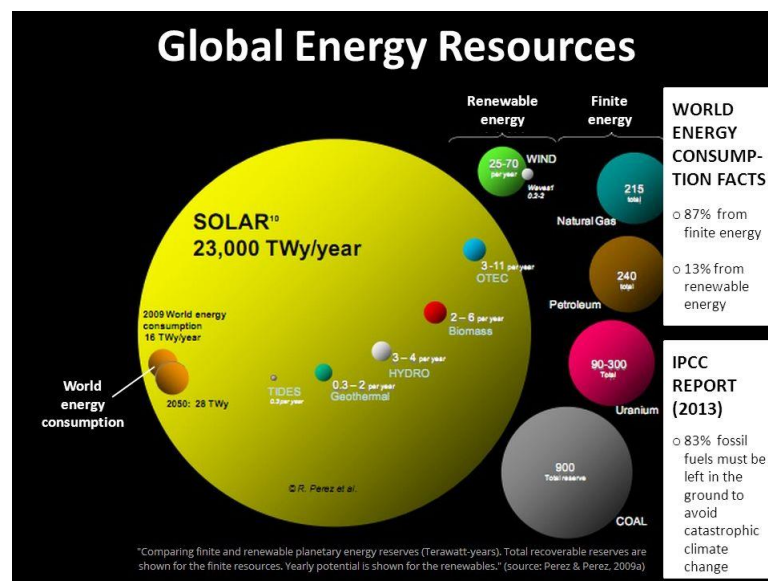
Figure 5. Various energy resources. https://www.southmountain.com/blog/2017/07/local-sustainable-economies and-way/.

1.2.1 Non-renewable energy resources

Fossil fuels such as coal, petroleum and natural gas are some examples that come under the category of non-renewable resources. Due to intense heat and pressure the organic matter buried in earth's crust got converted into fossil fuels.[3] The fossil fuels are limited as it takes millions of years for the decomposition and conversion process. It is believed that they were formed during carboniferous period around 350 million years ago. It is obvious to say that the non-renewable resources are not abundant like renewable ones and should not be inconsiderately used.

1.2.1.1 Harmful Effects by over consumption of Fossil Fuels

As mentioned in the above section, non-renewable resources are present in limited amount in earth's crust and hence need to be used judiciously. The present energy requirements are mainly tied to the non-renewable resources and we need to be very careful in their utilization. The current usage of fossil fuels to meet the energy demands is indeed at alarmingly high rates and poses a threat about their exhaustion in coming decades.[4] The over usage is not the only concern when it comes to the status of non-renewable resources of energy in present world. The effects caused by their burning are equally menacing. The burning of fossil fuels produces carbon dioxide which leads to the greenhouse effect. Along with carbon dioxide, sulphur oxides are also released.[5] The global climate change is one of the adverse effect of greenhouse effect which in turn is responsible for the habitat change of many species. Several species have gone extinct as they could not adapt to the change in the environmental conditions.

Figure 6. Adverse effects of over usage of non-renewable energy resources. https://www.lifeextension.com/Magazine/2017/6/Consequences-Of-Air-Pollution.

Several others are in danger of extinction and have been declared as endangered species. The food chain is also disturbed as many important components of food chain are missing. Earth which is till now (excluding the attempts of finding life existence possibilities on mars) considered as the only planet where the conditions for the existence of life are appropriate than no other planet in the solar system, is now facing the serious issues of environmental pollution, climate change and extinction of living beings.[6]

1.2.2 Renewable energy resources

The renewable energy resources like solar energy, wind energy, tidal wave energy, geothermal energy and several others are plentiful for earth and are never going to get exhausted. They are harmless when used and have no emissions. The renewable energy resources which are scrutinized as alternatives to non-renewable energy resources and also regarded as solution to the problems caused by the employment of fossil fuel are however not sufficient to meet the ever increasing energy demands because of current limitations of harvesting and storing them.[7]

Figure 7. Harvesting of renewable energy resources. (http://www.sustainableei.com/ naturalresources.php).

1.3 Need for energy storage

The increase in population and rapid industrialization steered the destruction of harmony between nature and mankind. The energy dependence of mankind in the modern world has gone to a far extent and as it is fulfilled mostly by the non-renewable resources of energy, their depletion would be highly unfavorable for sustainability.[8] Restoring sustainable development is the need of the hour. The sustainable development means fulfilling our energy requirements using the natural resources without harming the ecosystem. The non-uniformity in their distribution worldwide is itself a hindrance in their implication to replace their counterparts. For instance, solar energy cannot be utilized as an energy resource in the regions where sunlight is present only for limited period of the year or with low insolation. Similar issues are there in the utilization of other renewable energy resources like wind energy, tidal energy, geothermal energy etc., as their sources show characteristic fluctuations. This scenario calls for energy conservation and energy storage. The attention towards these two have particularly grown from past few decades since the issues caused by fossil fuels are alarming and need to be addressed immediately. Alternatives have been searched for and their wise utilization has been emphasized. The concept of clean and green energy has been introduced where emission free and environmental friendly methods are used for energy conversion and storage.

1.4 Energy storage systems

Being aware of the energy resources present for our use, now we look to the various energy storage technologies which would facilitate the energy usage at any given time frame and at any place irrespective of the availability statistics of any particular energy resource. An energy storage system or device is the one which stores energy and releases it in a desired form when required. The various energy storage forms could be mechanical storage which further can be hydroelectricity, pumped storage, flywheel energy storage, gravitational potential energy, thermal storage. The thermal energy storage systems capture heat and cold and are based on the physical characteristics of the materials such as latent heat. The phase change materials and the thermochemical energy storage are included in this class. Then there exists the chemical storage which is basically a hydrogen storage like in a fuel cell.
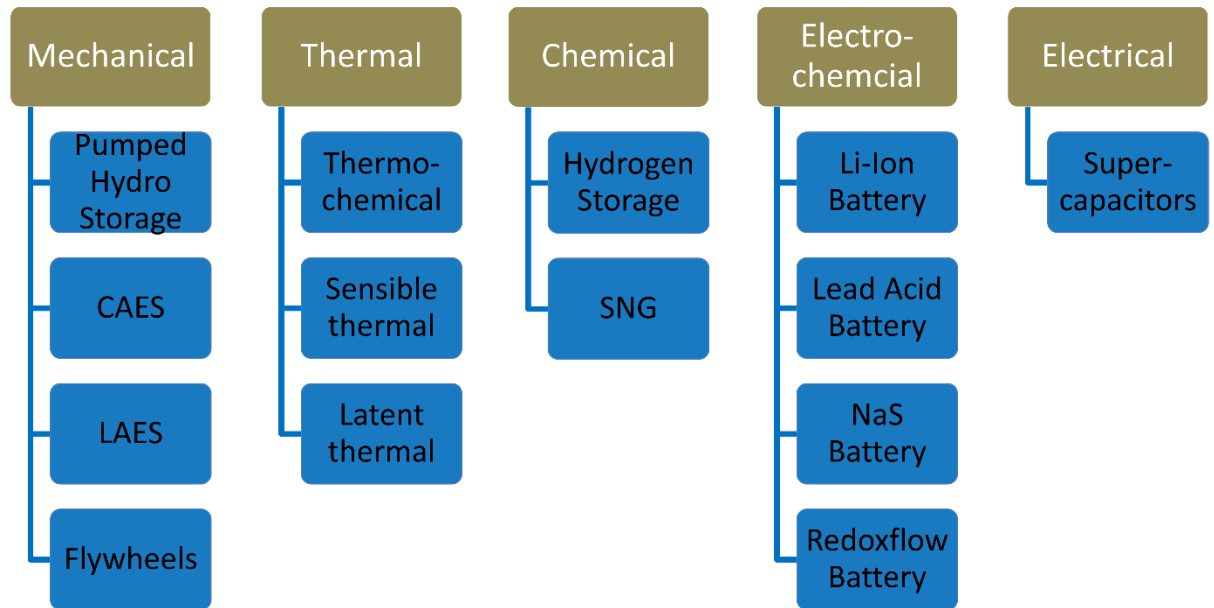
Figure 8. Classification of energy storage technologies.

The electrical energy storage devices are categorized as capacitors that store electrical energy electrostatically and superconducting magnets in which a direct flow of current induces magnetic field in a superconducting coil.[9] The electrochemical energy storage devices include the chemical energy stored in the device and include batteries of all types.

Out of all the above mentioned energy storage technologies, electrochemical and chemical energy storage are definitely of great significance based on the energy usage sectors. As seen from Figure 2, most of the energy is required for transportation and residential applications. For these applications, one needs a convenient, portable and easy handling energy storage system. The electrical and electrochemical energy storage systems satisfy these norms and hence are utterly important to be flourished.

1.5 Electrochemical energy storage devices

In this work, the electrochemical energy storage devices are the primary focus and hence will be described more elaborately. The primary components of an electrochemical energy storage device are:

Cathode: The positive electrode which undergoes reduction during the discharge process.

Anode: The negative electrode which undergoes oxidation during the discharge reaction.

Separator: A material that prevents cathode and anode to be in direct contact with each other hence preventing the short circuiting of the half cells.

Electrolyte: A medium which facilitates ion flow from one direction to another. Based on the type of device it can be aqueous, alkaline or organic.

The major electrochemical energy storage and conversion devices are capacitors, supercapacitors, batteries and fuel cells.

1.5.1 Capacitors: The conventional capacitors compose of two conducting plates separated by a dielectric medium. This is called as the parallel plate configuration of capacitors. The capacitance C is calculated by the following equation:

$$C = \varepsilon \frac{A}{d}$$

The A is the area of the plates and d is the distance between them. ε is the permittivity of the dielectric. The unit of the capacitance is Farad (F) and the typical capacitors for general applications have the capacitance in the range of picofarad (pF) to millifarads (mF). The capacitor stores the potential energy between the plates in terms of electric energy. The process is non-Faradaic in nature. The capacitors have very high power density but very low energy density.

1.5.2 Supercapacitors: A supercapacitor differs from a capacitor in terms of the amount of energy it can store. Supercapacitors are known as ultracapacitors since they have high energy density and capacity as compared to conventional capacitors.[10][11] A supercapacitor employs porous carbon material as electrodes and stores charge electrostatically. The supercapacitors have high power density as the charge storage/release happens at very high rates. The supercapacitors are employed in the applications where instant power is required. They are further classified into two types depending upon the charge storage process, 1) Electrochemical Double Layer Capacitors (EDLCs) and 2) Pseudocapacitors.

1.5.2.1 Electrochemical Double Layer Capacitors (EDLCs): The EDLCs store charge in the electric double layer created at the electrode/electrolyte interface hence the name EDLC.[12]
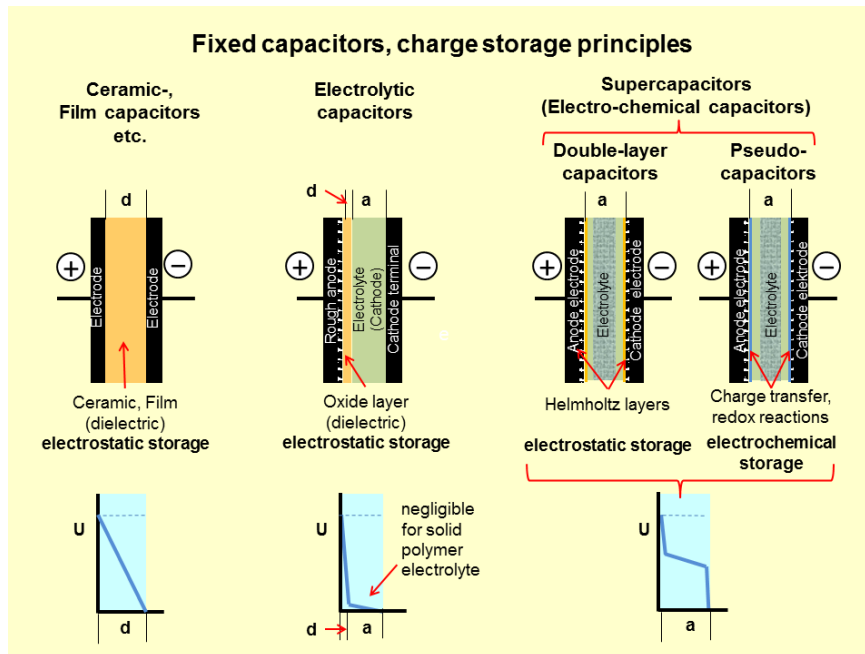
Figure 9. A schematic representation of supercapacitor (Source – Wikipedia).

These are highly stable and robust as no chemical reaction is involved in charge storage.[13]The working principle is demonstrated in Figure 10 (a).[14] The energy storage in the electrical double layer capacitor (EDLC) takes place by the charge separation at the interface between the electrolyte and electrode. The electrolyte is usually aqueous solution of salts like H_2SO_4 or KOH. The charging and discharging processes in the EDLC ideally involve no electron transfer across the electrical double layer at the electrode/electrolyte interface. Thus they are non-Faradaic in nature. EDLCs have remarkably long cycle life because of electrostatic charge storage and absence of chemical reaction.

1.5.2.2 Pseudocapacitors: The pseudocapacitors are similar to EDLC except that they involve redox process along with double layer for the charge storage.[15] Sometimes intercalation also takes place in pseudocapacitors.[16][17] In pseudocapacitors, surface confined redox reactions (Faradaic reactions) occur in the material. The electron transfer in a pseudo-capacitive material brings a net charge into the material. This is neutralized through the intercalation of ions of the opposite charge from the electrolyte

into the electrode. This is the reason why they are compared to batteries. However, the difficulties for ion transport and substantial solid phase changes in pseudocapacitors makes them inferior to the EDLCs in terms of power density.
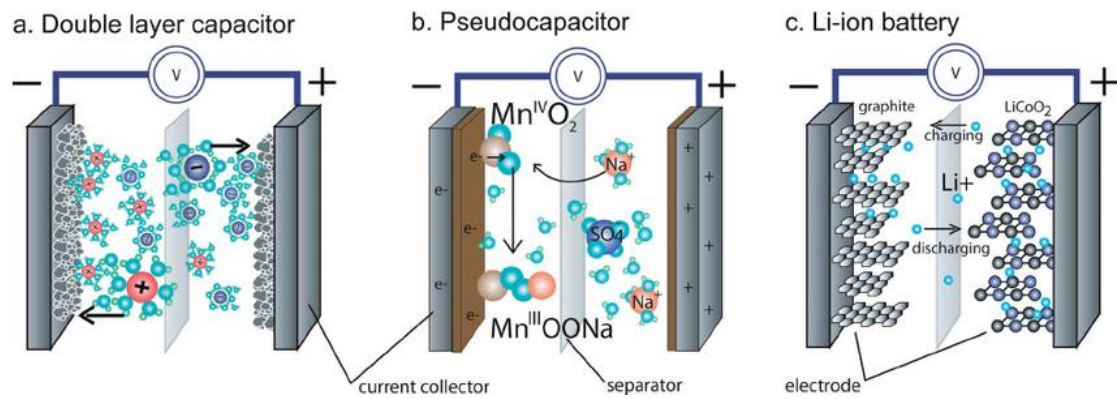
Figure 10. Working principle of (a) EDLC; (b) pseudocapacitors and (c) battery. Copyright Royal Society of Chemistry. Reproduced with the permission of Ref [14].

1.5.3 Batteries

A battery is essentially a device that stores chemical energy which gets converted into electrical energy during the discharge process.[18] The major components of a battery are illustrated in Figure 10 (c). Unlike the supercapacitors, batteries are totally Faradaic devices. The charge storage takes place by means of oxidation and reduction process in the whole of the electrodes. It implies that batteries constitute of bulk storage in spite of surface storage. The batteries have a specific electrochemical potential at which the Faradaic reaction occurs by the transfer of electrons. The batteries charging discharging time is usually much longer than EDLCs and pseudocapacitors as evident from Figure 8. The EDLCs exhibit the capacitive behavior corresponding to the adsorption of ions on the surface of the electrode and the time scales are in seconds. Pseudocapacitors undergo Faradaic reaction along with intercalation which is reflected in their charge discharge nature. Batteries have their charging discharging time scales ranging from minutes to hours. The batteries have high energy density and a well-defined potential window which can be tuned based on the chosen electrolyte. The power density of the batteries can be enhanced by using the high rate capability materials. Batteries have wide range of operating potential as well. The aqueous electrolytes based batteries operate up to 1.23 V as beyond this the water splitting is thermodynamically feasible. By employing non-aqueous batteries, the potential window can be raised up to 4 V.
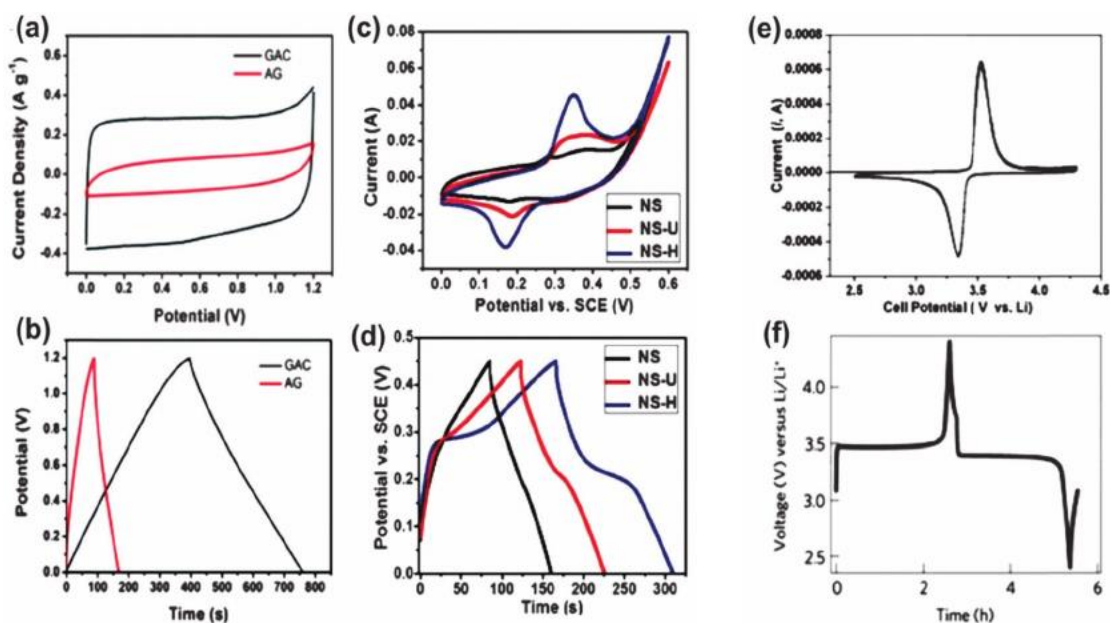
Figure 11. Charge discharge characteristics of (a), (b) EDLCs; (c), (d) psueodocapacitors and (e), (f) battery. Copyright Royal Society of Chemistry. Reproduced with the permission of Ref [17].

1.5.4 Fuel Cells: A fuel cell differs from a battery since it requires continuous source of fuel and oxygen or any oxidizing agent for its operation whereas a battery use already stored chemical energy. The fuel cell converts chemical energy of a fuel into electrical energy with the production of water and heat.[19][20] The functioning of a fuel cell is demonstrated in Figure 12. When hydrogen ions move from anode to cathode and combine with oxygen at cathode, electric current is generated by the electrons flowing in the outer circuit with the evolution of water at the cathode side.[21] There are several types of fuel cells namely Proton Exchange Membrane Fuel Cells (PEMFCs), Phosphoric Acid Fuel Cells (PAFCs), Solid Acid Fuel Cells (SAFCs), Alkaline Fuel Cells (AFCs), Solid Oxide Fuel Cells (SOFCs) and Molten Carbonate Fuel Cells (MOFCs).[22] Although the fuel cells offer a clean and emission free output, they can be used only at the bulk scale like grid scale power generation. The aforementioned electrochemical energy storage devices are employed for various purposes. The applications vary from stationary storage to appliances or small gadgets.
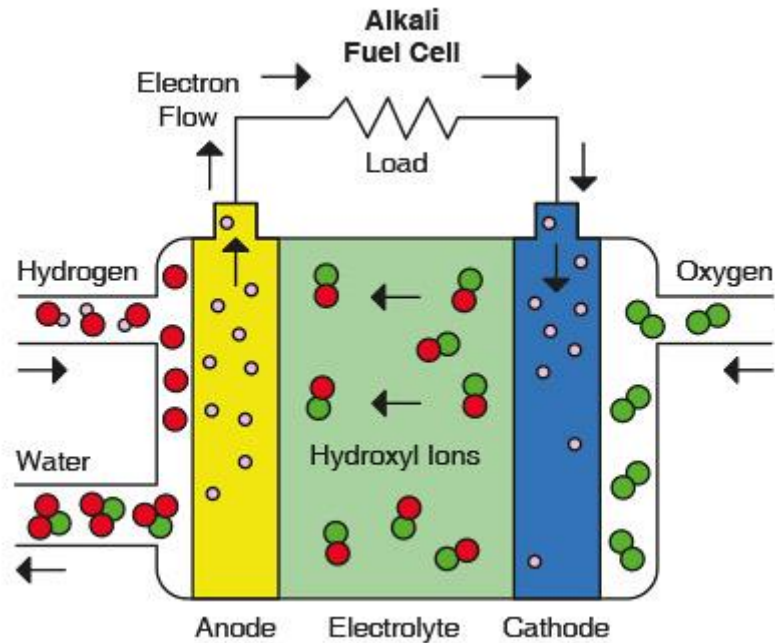
Figure 12. Alkali fuel cell prototype. https://www.researchgate.net/publication/ 290770006_Fuel_Cells_Their_Applications.

1.5.5 Comparison of different devices:

The supercapacitors have high power density and are used for applications where large amount of energy in a short time interval. Batteries and Fuel Cells are devices of high energy density and can be used in applications demanding continuous supply of electrical energy. These devices are used in combinations as well to deliver power and energy simultaneously. The performance of these devices is evaluated in terms of the power density and energy density they are able to provide. The same can be analyzed from the Ragone plot given in Figure 13.[23] It shows the power vs. energy densities of various clean energy storage devices. The capacitors possess very high power density but low energy density. The fuel cells have high energy density but low power density. The supercapacitors and batteries are moderate in their performance. Batteries particularly are of interest as they have high energy density with reasonably good cycle life. They have the potential of tenability in terms of energy density and power density. They span a large area of applications from big to small scale. These are used in mobile applications, various gadgets as well as in grid storage. Battery development is going on from a long historical duration undergoing several changes in their chemistry, design and materials.
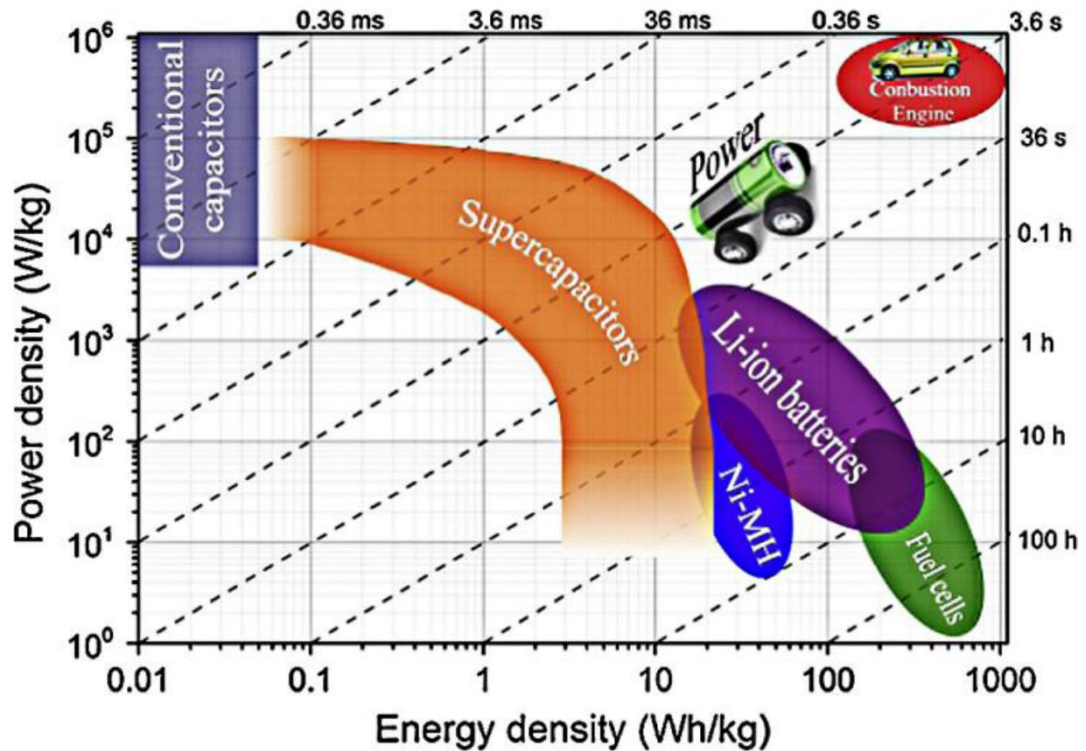
Figure 13. Ragone plot for various energy storage and conversion devices Reproduced with the permission of Ref [23].

Although the basic components of batteries remain the same but to improve the performance and enhance the parameters crucial for certain usage, many chemistries have been tried. Once a certain type of chemistry was developed, its loop holes or the difficulties in its practical usage were eradicated by proposing changes in existing materials or design. Based on all that we have many types of batteries being invented. Some of them are still in use and few of them were discarded if they were not good enough in their operation or pose a difficulty in handling. In the next section, the types of batteries and related mechanisms have been discussed.

1.6 Types of Batteries

Batteries are classified broadly on the basis of their function and life cycle. The two categories into which batteries are divided majorly are 1) primary batteries and 2) secondary batteries.

Primary Batteries: These batteries have a fixed life span and can't be recharged once their cycle life is finished. They stop functioning once the chemicals are used up and the components need to be replaced for further generation of electricity.

Secondary Batteries: Also popularly called as rechargeable batteries now, these batteries have a longer life span and can be recharged over multiple cycles. The chemical processes taking place in such batteries are reversible.

1.7 Evolution of Batteries

Today's long lasting batteries used in gadgets and grid storage are the outcome of the years of evolution in battery technology starting from galvanic cells to Li air batteries. The battery history reveals how the batteries were designed initially from very common ingredients and many of the earlier battery materials were toxic. The shortcomings were improved over the years to produce recyclable and safer batteries. The evolution of batteries is briefly described below:

1.7.1 Baghdad Battery: Most historians believe the first battery invented to be from Alessandro Volta in late 18th century but some archaeological facts prove the existence of batteries from 250 B.C. The 1938, Wilhelm Konig, a German Archaeologist discovered an earthenware jars of 5 inch in Khujut Rabu near Baghdad, hence the name Baghdad Battery.[24]
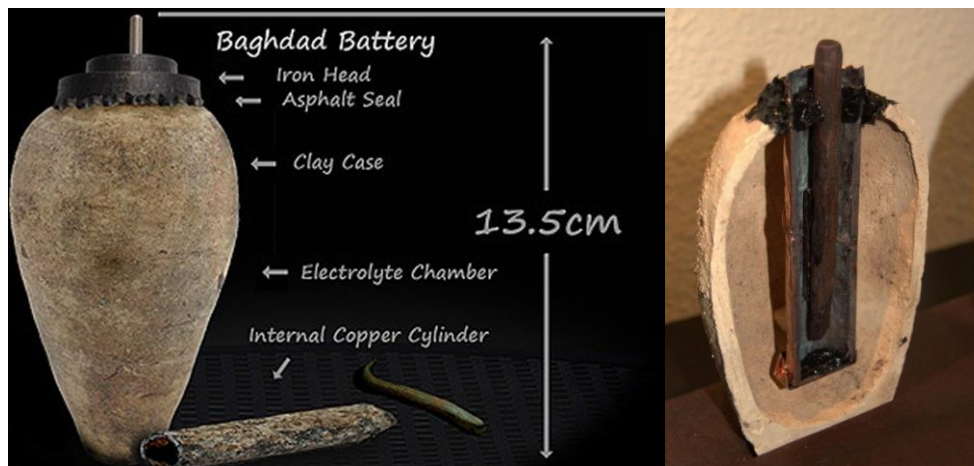
Figure 14. Baghdad battery. (https://factsofworld4u.blogspot.com/2015/10/baghdad-battery-first-battery-ever-built.html).

The jar consisted of a copper cylinder sealed with asphalt encasing an iron rod which was suspended from an asphalt stopper at the top of the copper cylinder. The iron rod was corroded showing evidence of presence of some acidic medium inside the

assembly. He theorized that these jars were the galvanic cells and could have been used for electroplating of gold on ornaments.

1.7.2 Voltaic Pile: In 1749, Benjamin Franklin during his experiments with electricity called a set of linked capacitors as battery.[25] These were interconnected metal coated glass panels which were charged by a static generator and discharged by making contact with the electrode. These led basis of the piling of cells to be later called as battery. However, Alessandro Volta, an Italian physicist invented the first true battery in 1799 using Copper (Cu) and Zinc (Zn) discs separated by a brine solution soaked paper. These discs were piled onto each other to give continuous electricity where a set of Cu and Zn disc generated 0.76 Volts (V).[26] The stacking of discs could provide higher voltages. Nonetheless, there were some flaws in this system including the corrosion of discs, hydrogen bubbles plate formation on copper, separator crushing due to heavy weight etc.
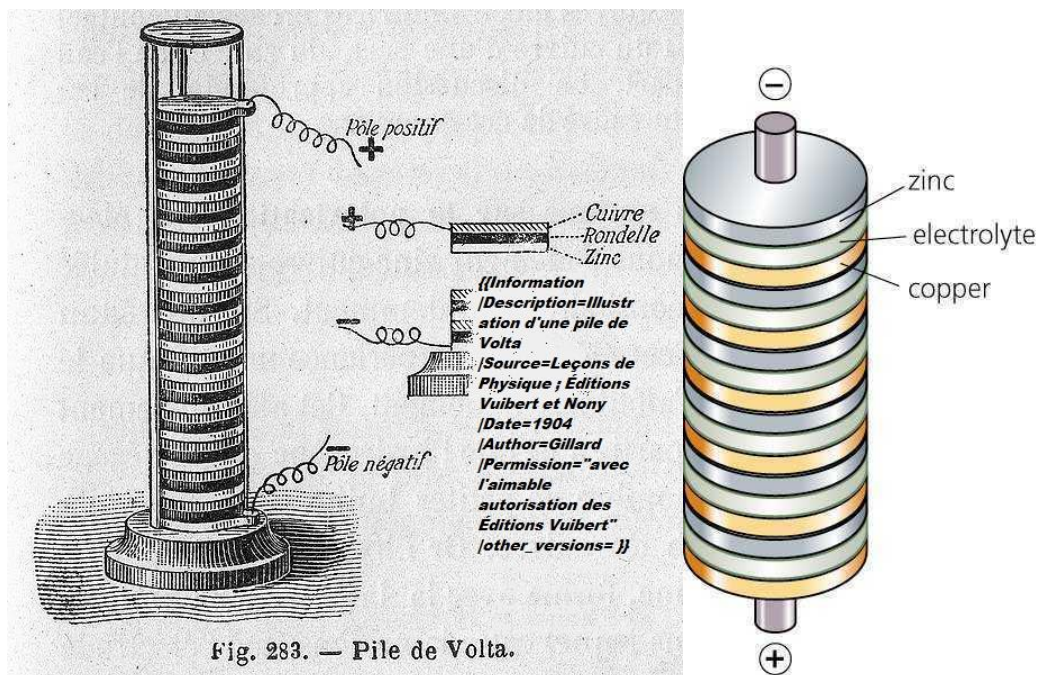
Figure 15. A Voltaic Pile. (http://www.yourdictionary.com/voltaic-pile).

1.7.3 Daniel Cell: Daniel Cell was invented by English chemist John F. Daniel in 1836. He proposed the solution to the hydrogen bubble problem of Voltaic Pile by introducing second electrolyte.[27] The Daniel cell consisted of two glass beakers one containing copper plate dipped in the copper sulfate solution and other containing zinc plate in a

zinc sulfate solution. The two beakers were connected by a porous plug.[28] The positive terminal was connected to the copper plate and the negative terminal to the zinc plate. The two terminals are connected by a salt bridge making the ions to move from one electrode to other and keeping the solutions electrically neutral.[29] There were several other batteries designed including Bird's Cell which used plaster of Paris to isolate two electrolytes and allow diffusion of ions from one solution to another. Porous pot cell was another improvement over the Bird's Cell design where a porous earthenware containing zinc electrode and zinc sulfate solution was immersed into the copper can containing copper sulfate. Gravity cell used one glassware and exploited the density of the copper. The copper cathode used to be placed at the bottom immersed in copper sulfate solution and the zinc anode used to be suspended. The zinc sulfate used to form a top layer on the copper sulfate due to the high density of copper and the polarity of the cell. This way the internal resistance of the cell was minimized.
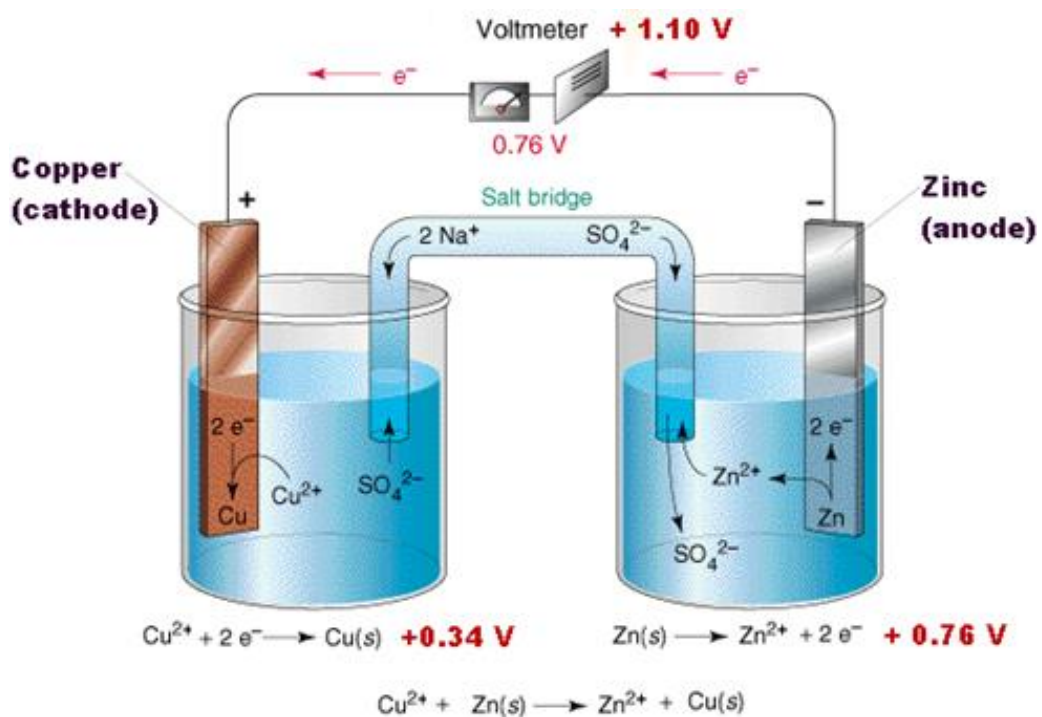
Figure 16. A Daniel Cell. (https://onllogy.blogspot.com/2015/01/electrochemical-cell-and-its-types.html).

1.7.4 Lead Acid Battery: Gaston Planté, a French physician invented the first rechargeable or secondary battery in 1859 called as Lead Acid battery.[30][31] The battery consisted of lead plates as anodes immersed in sulphuric acid and the cathode

used was lead oxide giving lead sulfate as the discharge product.[32] By applying reverse current the process could be reversible and thus the battery could be recharged.[33][34] This battery is used for stationary applications where weight is not a concern. The improvisations were made over the years but the basic principle remains the same.
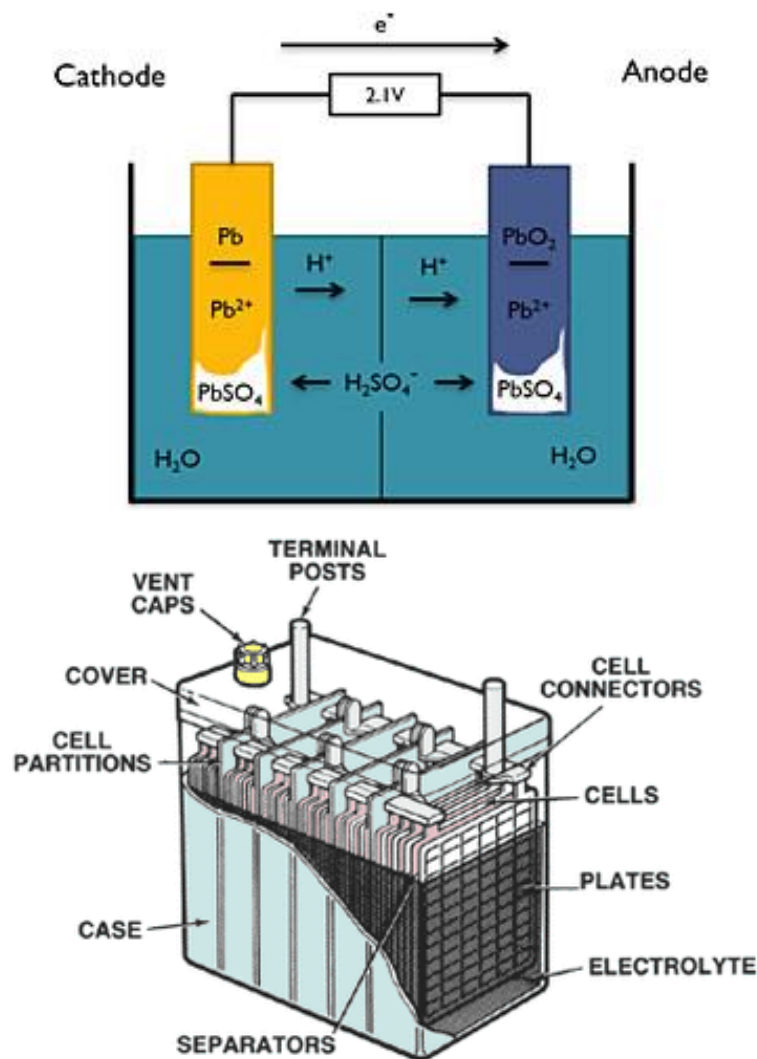
Figure 17. A Lead Acid battery working principle and its construction. Copyright John Wiley and Sons. Reproduced with the permission of Ref [31]. https://www. infinitumstore.com/articles/ archives/01-2008.

1.7.5 Leclanché Cell: The carbon coated manganese dioxide cathode and zinc anode dipped in ammonium chloride solution for use as a battery was invented by Georges

Leclanché in 1866.[35] This battery provided output of 1.6 V.[36][37] This cell was famous for its applications in signaling and telegraphy.
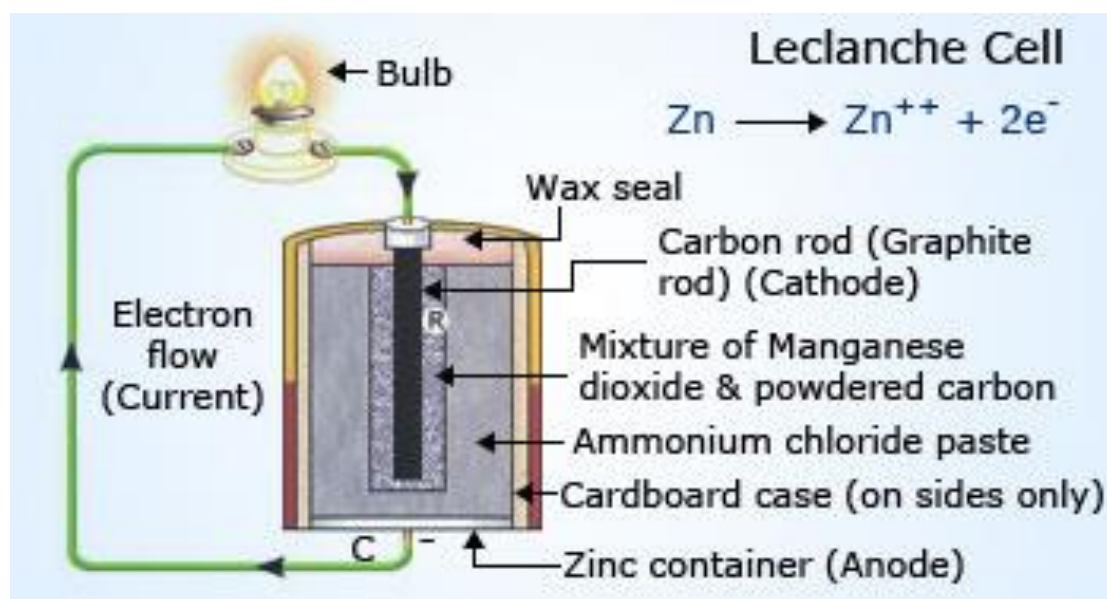
Figure 18. A Leclanché Cell. (By courtesy of Encyclopaedia Britannica, Inc., copyright 2005 (Leclanché cell); used with permission.).

1.7.6 Zinc-carbon Cell: With the various modifications in the cell designs and choice of electrode materials, there were concerns with the portability and practical use of batteries. Scientist tried to make the batteries convenient for use by immobilizing the electrolyte.[38] In this regard, the first dry cell proposed was Zinc-carbon cell by Carl Gassner in 1886.[39] The cell composed of ammonium chloride and zinc chloride mixed with plaster of Paris to make a paste. The manganese dioxide cathode with carbon mixed in it was dip coated with the electrolyte and then wrapped by a zinc anode shell.[40] This design was compact and more rigid with no spillage issues and handling problems. The Zinc-carbon cell generated potential of 1.5 V and required no maintenance. This battery was handy and used in common applications and was key factor in development of flashlight.
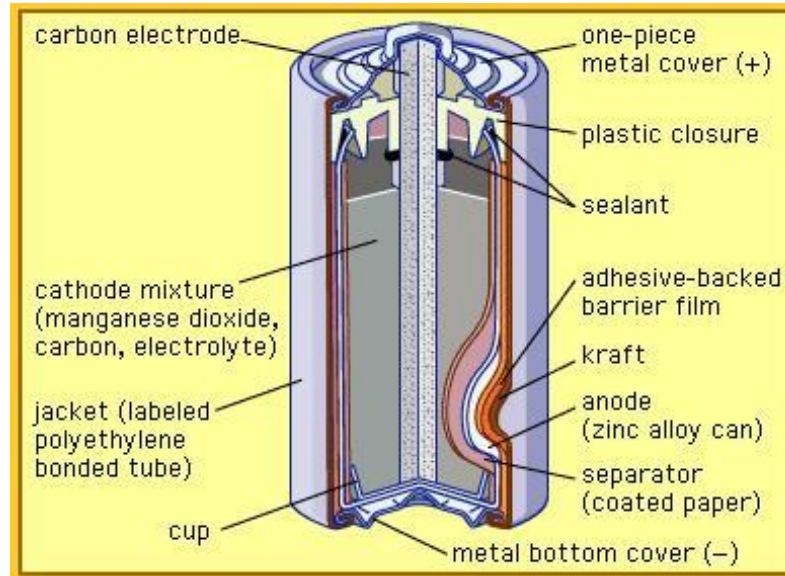
Figure 19. A Zinc-carbon cell. (By courtesy of Encyclopaedia Britannica, Inc., copyright 2005 (zinc-carbon cell); used with permission.).

1.7.7 Nickel-Cadmium (Ni-Cd) Battery: As an improvement over lead acid battery, Ni-Cd battery came into existence by Waldemer Jungner's invention in 1899.[41][42] This battery used potassium hydroxide electrolyte and thus was the first alkaline battery. This battery was capable of providing more energy density than lead acid battery but the shortcoming was its high cost.[43]
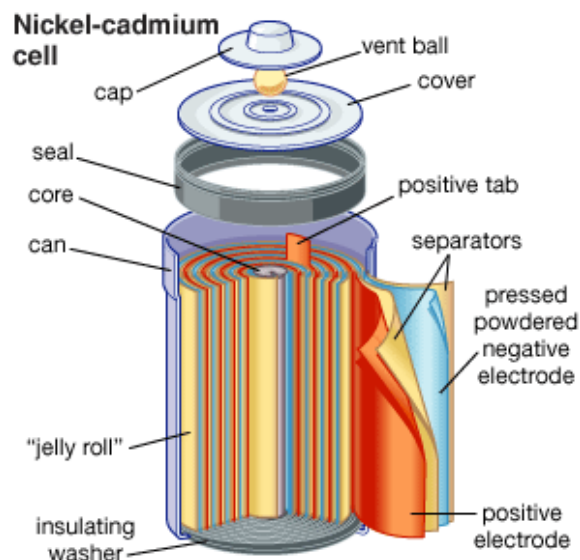
Figure 20. A Ni-Cd battery components. (By courtesy of Encyclopaedia Britannica, Inc., copyright 2007 (nickel-cadmium cell); used with permission.).

1.7.7 Ni-metal hydride Battery: Ni-metal hydride battery called as Ni-MH is analogous to Ni-Cd battery except the anode part.[44] The positive electrode is nickel hydroxide and the anode is usually an intermetallic compound of the nature AB5 or AB2 for example LaNi$_5$ or TiNi$_2$, a hydrogen absorbing alloy.[45][46] These were commercially made available in 1989 as a variation of Ni-hydrogen battery developed in 1970's. Ni-MH batteries use alkaline electrolyte and are long lasting and non-toxic as compared to Ni-Cd batteries. The output voltage of the battery is 1.4-1.6 V and is safer and maintenance free.
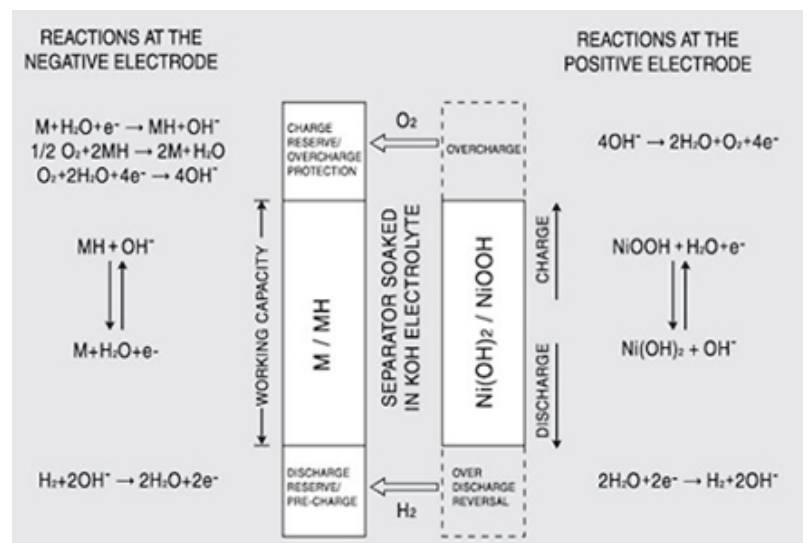
Figure 21. Components and reaction mechanism of a Ni-metal hydride battery. (http://www.gbattery.com/english/technical/nimh).

1.7.8 Na-Sulphur Battery: Kummer and Weber discovered a 2D fast Na+ ion transport in β-Al$_2$O$_3$ in 1967. This led to the solid electrolyte based batteries. Following this discovery at Ford Motors Co., a Na/ β-Al$_2$O$_3$ /Sulphur system was proposed and this is very efficient in stationary storage systems.[47][48] In this battery Na is in molten state and thus the battery is molten salt battery. The operating temperatures for Na-S battery are 300-350 °C.[49] The battery has low self-discharge as the electrolyte selectively conducts Na ions but does not conduct electrons giving long shelf life and cycle life to battery.[50] This battery is economical as it is constructed from cheap materials and thus best suited for stationary and large scale applications.
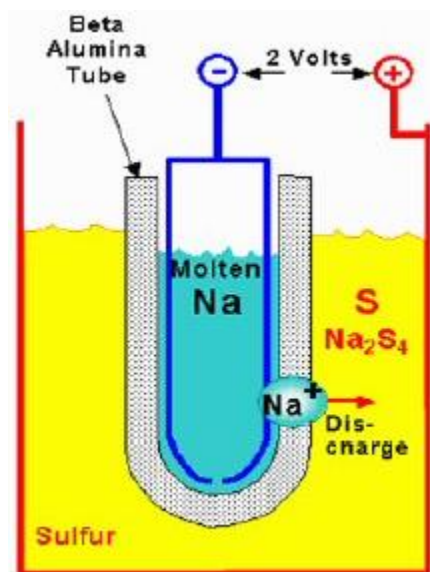
Figure 22. Na-S battery schematic Copyright Elsevier. Reproduced with the permission of Ref [48].

1.8 Present battery Chemistries (Post 1960's)

1.8.1 Lithium (Li) ion Batteries: The Li ion battery era started in 1980 with the contribution of American scientist John B. Goodenough when he proposed a Li containing oxide $LiCoO_2$ (LCO) as a cathode material. Same year, Rachid Yazami from Morocco discovered graphite anode with solid electrolyte.[51] The first Li ion battery prototype was built by Japan in 1985 and the Li ion battery commercialization was done by Sony in 1991. Li ion batteries have electromotive force up to 3.6 V and are now commercially used for large scale as well as small scale applications. Li polymer batteries were also developed using a polymer or gel based electrolyte to mitigate the issues associated with the use of liquid electrolytes which are generally carbonates based and are flammable, posing a threat to the safety of the device.

1.8.2 Other Types of Batteries: Since the non-aqueous rechargeable batteries are into the business, many other battery chemistries are into research. To increase the energy and power density of the current Li ion battery technology, other technologies such as Li-Sulphur, Li-air batteries, Li metal batteries, $Li-CO_2$ batteries, Zn-air batteries, Redox-flow batteries are being the topic of research and development.[52] These batteries are at the early stage of development and it will take some time for them to come at par with Li ion battery systems.[53][54]

As the Li reserves are known to be reserved in the earth's crust, alternatives are being hunted. Among them, Sodium (Na) ion batteries have already gained the attention and are commercial.[55][56] Along with these, Magnesium (Mg), Potassium (K) and Calcium (Ca) ion batteries are also being explored.[57][58][59] Nonetheless, being heavier than Li, Na and other ion batteries would never be closer to Li ion batteries in terms of energy and power density. Nevertheless, in large scale applications where weight is not a concern, Na ion batteries have already flourished as a possible replacement to Li ion batteries.[60]
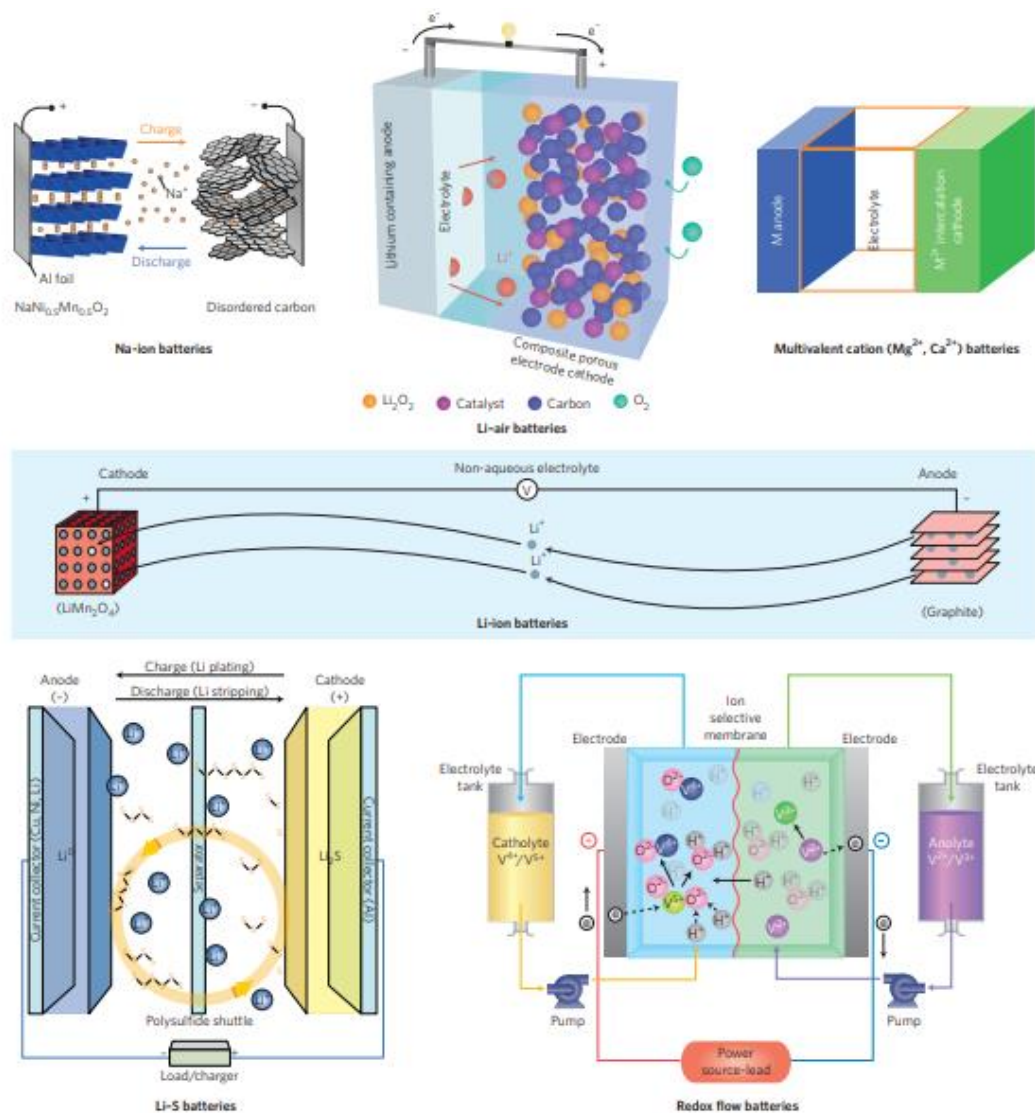
Figure 23. Different types of batteries. Copyright Springer Nature. Reproduced with the permission of Ref [58].

1.9 Battery Challenges

As we see the Li ion batteries are having the potential to meet the energy demands of the modern society and serve all the needs. These batteries have already been the active part of our household appliances and we are dependent on them for our daily needs. However, we have not yet made our society completely independent of fossil fuels. A major role in fulfilling modern era's energy requirements is still being played by the non-renewable energy resources. The reason to this state is the key challenges which Li ion battery system has not been able to meet till date. The issues faced by Li ion and related battery systems are listed below which are a major factor and hindrance in their complete evolution.[61]

1.9.1 Increase in Energy Density: The major challenge for the Li ion and related battery chemistries is to compete with the already existing battery types in the market and gasoline in terms of performance and price. For instance, Li ion batteries are able to provide energy density of 250 Wh/Kg which is 10-15 folds lesser than gasoline (3000 Wh/L) and is cheaper as well. The same is true if it is compared to the Lead acid battery technology.[62][63] Lead acid battery spans total 60% of automobile applications and Li ion batteries are no closer to this scenario. To increase the energy density and raise the performance of current systems, new cathode materials have to be engineered which possess very high redox potentials or have capability to take more than one ions reversibly to increase the specific capacity.[64][65]
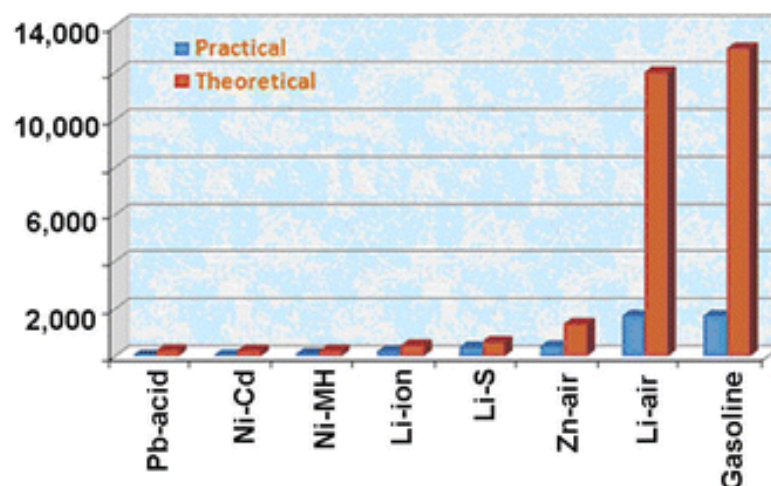
Figure 24. Bar graph representation of practical and theoretical energy density of various batteries. Copyright Elsevier. Reproduced with the permission of Ref [62].
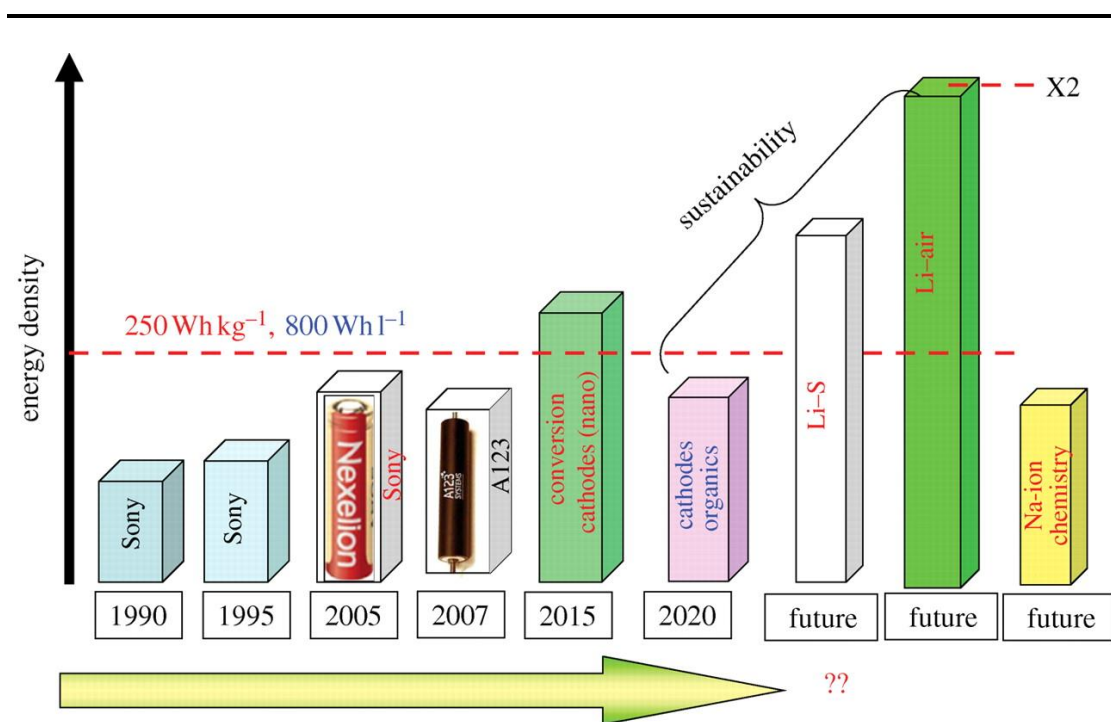
Figure 25. Energy density evaluation of various battery chemistries. Copyright Royal Society of Chemistry. Reproduced with the permission of Ref [66].

1.9.2 Safety: No doubt Li ion batteries enjoy commercial success due to their demand in portable electronics and to some extent electric vehicles (EVs) but they come with the risk of safety. The materials used to bring cost down to compete with existing technology compromise with the safety.[66] For instance, the additives used to modify the electrode electrolyte interface to for stability or capacity enhancement would not be safe if used beyond certain temperatures and certain chemical environments. Sometimes less reducing materials which form thin solid electrolyte interface (SEI) layer such as $Li_4Ti_5O_{12}$ are used with highly oxidizing positive electrode like $LiCoO_2$ (LCO). This reduces the safety value of the device. Use of solid electrolytes including polymer and inorganic electrolytes seems to be a solution to attain safety as well as performance in terms of high energy density but unfortunately till date researchers have not been able to provide a material which is cost effective and performs equally well as the liquid counterparts. Figure 26 is a representation of the same argument. It shows how all parameters responsible for battery performance are inter connected to each other.[67] While designing the material, one has to be very careful about the operating voltage as well as the compatibility of the electrolyte. The optimized combination of both only can lead to a prolonged and good battery performance.
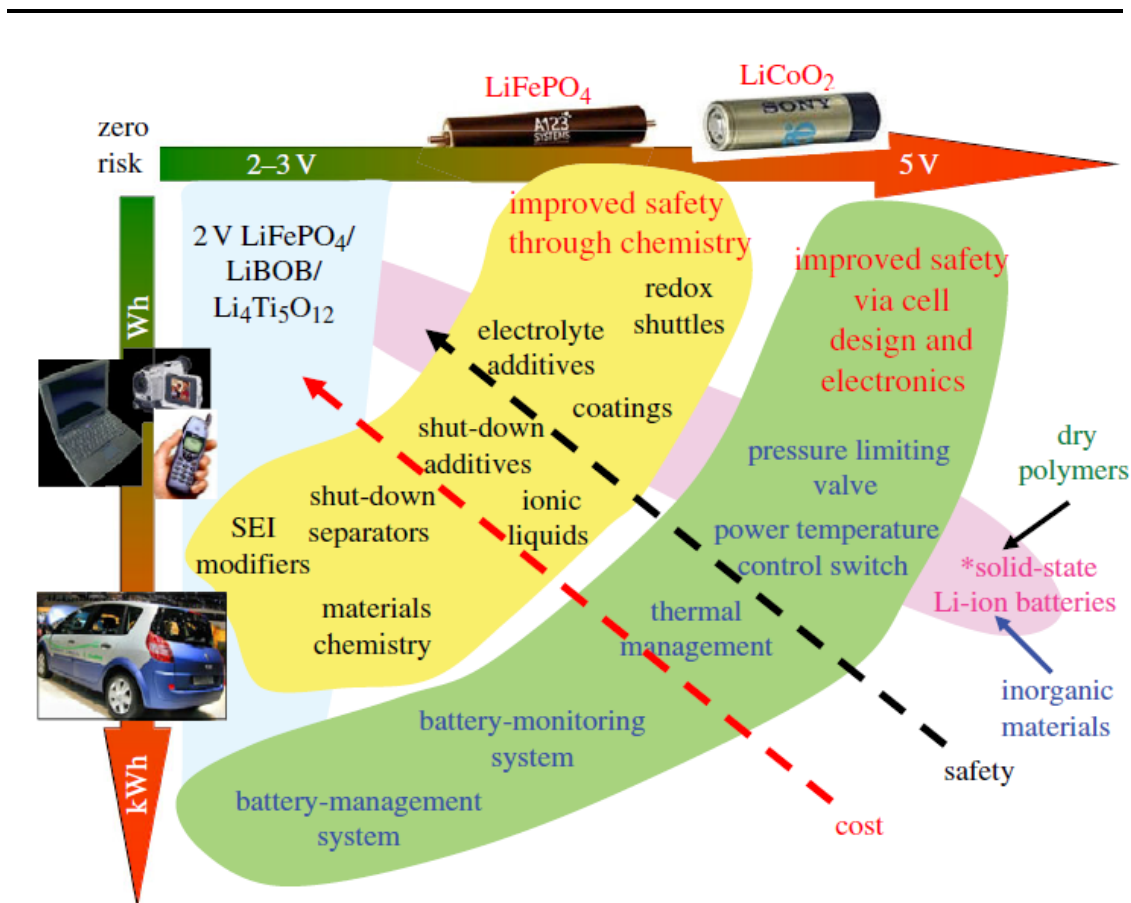
Figure 26. Safety aspects of Li ion battery. Copyright Royal Society of Chemistry. Reproduced with the permission of Ref [66].

To increase the power density or energy density of the device and to bring down the cost, the quality component should not be compromised at all to ensure safer devices.

1.9.3 Cost: One should always be aware of the fact that cost and safety go hand-in-hand. If one compromises with the cost, then safety will be at risk. We need to adopt for materials which are cost effective and their production should not shake the battery industry processes.[68] Figure 27 depicts the comparison of Li and Na metal reserves in earth's crust. The statistics shown here are on the basis of elemental composition of brine found in Chile, where the Li reserves are found to be concentrated. As we have limited Li reserves and most of them are concentrated in brines found in Chile, the cost of Li has touched high values than ever. The battery industry is estimated to consume 46% of the total Li extracted.[69] This is not only limited to the Li consumption, it has to do with the other elements used in battery as well.

a Demand for lithium and cobalt for the battery industry, 2016–2050

Present Ni/Co-rich cathode mixtures

Fictive Ni/Co-poor cathode mixtures

b Lithium and cobalt production and reserves

- Large batteries
- Small batteries

- Total amount produced, 2016–2050
- Total amount produced, 2016–2050 with 2% annual growth
- Reserves

c Battery industry's present share of the demand for lithium and cobalt

Lithium
46%   54%

Cobalt
50%   50%

- Batteries
- Other industries

Figure 27. Demand and supply mismatch risk of Li and Co. Copyright Springer Nature. Reproduced with the permission of Ref [69].

More common to talk about are Co and Ni which are also less abundant but are epicenter of battery chemistry as the positive electrodes used in Li ion battery are Co and Ni based. This can be very well understood from Figure 28. Thus, the new cathodes designed should have high power and energy densities which in turn should be cost effective and safe.

1.9.4 Clean and Green Li ion batteries: Even though the Li ion battery chemistry is considered as green, the electrode production and the battery recycling add to the energy consumption and does not satisfy the green chemistry criteria.

a Elemental composition of brine from the Salar de Atacama, Chile

9.10 wt% Na
2.36 wt% K
0.97 wt% Mg
0.16 wt% B
0.04 wt% Li
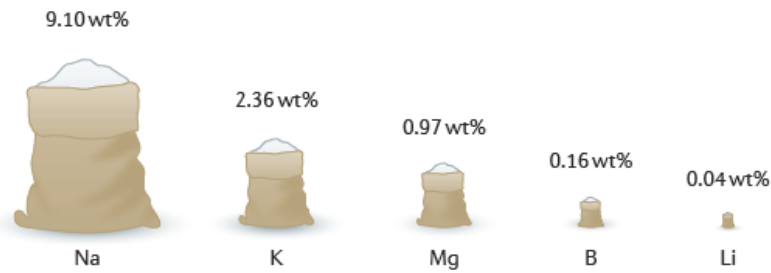
b Production of metallic elements from mining

Primary production:
18.5 kt Co
2.2 Mt Ni
9.8 Mt Mn
17.6 Mt Cu
57.6 Mt Al
1,992 Mt Fe

Co-production:
970 kt Cu (5%)
61.5 kt Co (50%)
43 kt Co (35%)
<300 kt Mn (<3%)
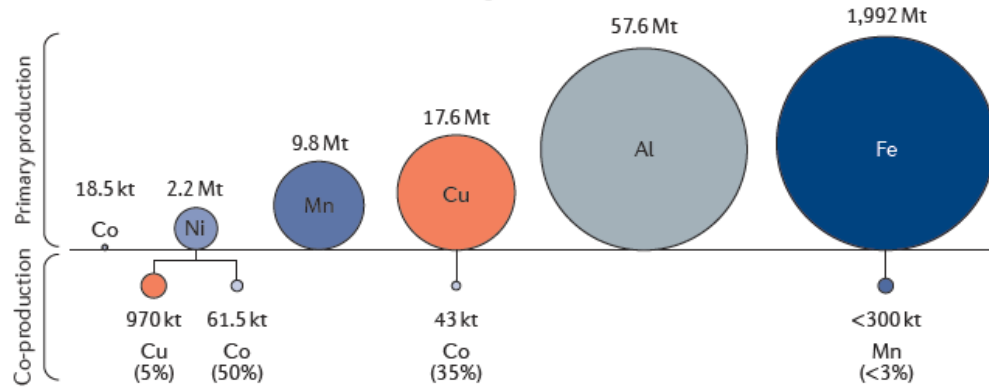
Figure 28. Statistics reflecting elemental abundance for battery industry. Copyright Springer Nature. Reproduced with the permission of Ref [69].

The steps involved cause CO_2 emissions and thus cannot be accepted without worrying about the harm caused. The synthesis process are not environmentally benign and sometimes costly as well.[70] To achieve sustainable and green batteries, these issues need to be pondered over deeply. The efforts should be devoted towards the greener synthesis procedures and also in better recycling techniques.[71][72]

1.10 Aim and scope of the thesis: This thesis primarily focuses on the design and testing of new anode materials and architectures for the Li and Na ion batteries in the light of the stringent requirements to be fulfilled by an anode material. It deals with the synthesis, characterization and application of various materials as anodes in the Li and Na ion batteries. The materials designed are based on the type of the mechanism they adapt to function as an anode and the problems faced by the similar compounds already reported in the literature. In the working chapters to follow, certain issues have been explained and the material design and synthesis to overcome those issues and achieve better performance are explained.

Chapter 2 explains the trends in the state of the art alkali ion batteries specifically Li ion batteries. The components of Li ion batteries and the materials used are explained in detail. The charge storage mechanisms in different materials is also presented and briefly discussed. An elaborate discussion on Li and Na ion batteries is provided thereafter. Finally, the battery related technical terms and battery issues which cause degradation in battery performance are reviewed.

Chapter 3 explains the importance of hard carbon as an intercalation anode in Na ion batteries. In this chapter, the cheap and abundant water-swelling basil seeds are used to obtain hard carbon by controlled pyrolysis and the battery performance realized by using such material is provided and analyzed.

Chapter 4 presents work on an interesting materials design via the incorporation of Si NPs in the basil seed gel for uniform distribution of Si NPs into the carbon sheets during the synthesis and its evaluation as Li-ion battery anode material. The obtained Si-carbon composite shows very high specific capacity and stability with minimized volume expansion.

Chapter 5 is on the combination of two intercalation type materials namely $Li_4Ti_5O_{12}$ and hard carbon. The work provides an insight into the synergy between these two materials combined together to enhance the overall performance and to overcome their respective shortcomings. The mixed anodes are shown to perform far better than the individual materials in half cell as well as full cell configurations.

Chapter 6 deals with the last category of charge storage materials which are conversion cum alloying compounds. A ternary metal sulfide is chosen to tackle the electrolyte dissolution problem very pronounced in sulfide based batteries. The Cu_3SnS_4 NPs show an excellent performance as a Li ion battery anode. The results and possible mechanisms are provided at length in the corresponding chapters.

Appendix proposes the use of a Fe based metal organic framework (MOF) as anode in a full cell flexible device to heat the transdermal patch for drug delivery application.

References

[1]   A.E. Akinlo, Energy consumption and economic growth: Evidence from 11 Sub-Sahara African countries, Energy Econ. 30 (2008) 2391–2400. doi:10.1016/j.eneco.2008.01.008.

[2]   R. Perez, M. Perez, A Fundamental Look At Supply Side Energy Reserves For The Planet, Int. Energy Agency SHC Program. Sol. Updat. 62 (2015) 4–6. doi:http://dx.doi.org/10.1016/j.enconman.2015.02.007.

[3]   C.T. Tugcu, I. Ozturk, A. Aslan, Renewable and non-renewable energy consumption and economic growth relationship revisited: Evidence from G7 countries, Energy Econ. 34 (2012) 1942–1950. doi:10.1016/j.eneco.2012.08.021.

[4]   A.K. Tiwari, Comparative performance of renewable and nonrenewable energy source on economic growth and CO2 emissions of europe and eurasian countries: A PVAR approach, Econ. Bull. 31 (2011) 2356–2372.

[5]   R. Latawiec, P. Woyciechowski, J.K. Kowalski, Sustainable Concrete Performance—CO2-Emission, Environ. . 5 (2018). doi:10.3390/environments5020027.

[6]   N. Apergis, J.E. Payne, Energy consumption and economic growth in Central America: Evidence from a panel cointegration and error correction model, Energy Econ. 31 (2009) 211–216. doi:10.1016/j.eneco.2008.09.002.

[7]   K. Ellegård, J. Palm, Visualizing energy consumption activities as a tool for making everyday life more sustainable, Appl. Energy. 88 (2011) 1920–1926. doi:https://doi.org/10.1016/j.apenergy.2010.11.019.

[8]   B.R. Keeble, The Brundtland report: 'Our common future,' Med. War. 4 (1988) 17–25. doi:10.1080/07488008808408783.

[9]   Chapter_1_Modified, (n.d.).

[10]   L. Guan, L. Yu, G.Z. Chen, Capacitive and non-capacitive faradaic charge storage, Electrochim. Acta. 206 (2016) 464–478. doi:10.1016/j.electacta.2016.01.213.

[11]   J. Huang, B.G. Sumpter, V. Meunier, A universal model for nanoporous carbon supercapacitors applicable to diverse pore regimes, carbon materials, and electrolytes,

Chem. - A Eur. J. 14 (2008) 6614–6626. doi:10.1002/chem.200800639.

[12]   E. Frackowiak, K. Fic, M. Meller, G. Lota, Electrochemistry serving people and nature: High-energy ecocapacitors based on redox-active electrolytes, ChemSusChem. 5 (2012) 1181–1185. doi:10.1002/cssc.201200227.

[13]   B. Akinwolemiwa, C. Peng, G.Z. Chen, Redox Electrolytes in Supercapacitors, J. Electrochem. Soc. 162 (2015) A5054–A5059. doi:10.1149/2.0111505jes.

[14]   K. Jost, G. Dion, Y. Gogotsi, Textile energy storage in perspective, J. Mater. Chem. A. 2 (2014) 10776–10787. doi:10.1039/c4ta00203b.

[15]   S.W. Zhang, G.Z. Chen, Manganese oxide based materials for supercapacitors, Energy Mater. 3 (2008) 186–200. doi:10.1179/174892409X427940.

[16]   L. Su, L. Gong, H. Lü, Q. Xü, Enhanced low-temperature capacitance of MnO2nanorods in a redox-active electrolyte, J. Power Sources. 248 (2014) 212–217. doi:10.1016/j.jpowsour.2013.09.047.

[17]   D. Dubal, O. Ayyad, V. Ruiz, P. Gómez-Romero, ChemInform Abstract: Hybrid Energy Storage: The Merging of Battery and Supercapacitor Chemistries, 2015. doi:10.1039/c4cs00266k.

[18]   D.P. Dubal, O. Ayyad, V. Ruiz, P. Gómez-Romero, Hybrid energy storage: The merging of battery and supercapacitor chemistries, Chem. Soc. Rev. 44 (2015) 1777–1790. doi:10.1039/c4cs00266k.

[19]   E. Perry Murray, T. Tsai, S.A. Barnett, A direct-methane fuel cell with a ceria-based anode, Nature. 400 (1999) 649–651. doi:10.1038/23220.

[20]   K. Kordesch, J.C.T. Oliveira, T.U. Graz, F U T U R E a P P L I C a T I O N S , With Special C O N S I D E R a T I O N of T H E, 13 (1988) 411–427.

[21]   S. Park, J.M. Vohs, R.J. Gorte, Direct oxidation of hydrocarbons in a solid-oxide fuel cell, Nature. 404 (2000) 265–267. doi:10.1038/35005040.

[22]   J. Suntivich, H.A. Gasteiger, N. Yabuuchi, H. Nakanishi, J.B. Goodenough, Y. Shao-Horn, Design principles for oxygen-reduction activity on perovskite oxide catalysts for fuel cells and metal-air batteries, Nat. Chem. 3 (2011) 546–550.

doi:10.1038/nchem.1069.

[23] C. Wang, E. Zhou, W. He, X. Deng, J. Huang, M. Ding, X. Wei, X. Liu, X. Xu, NiCo2O4-Based Supercapacitor Nanomaterials, Nanomater. . 7 (2017). doi:10.3390/nano7020041.

[24] L. Flank, The Baghdad Battery: An Update, (2015). http://conhecimentohoje.com.br/Recentes921_Anexo_01.pdf.

[25] P. Scharlin, R. Battino, The Voltaic pile: A stimulating general chemistry experiment, J. Chem. Educ. 68 (1991) 665. doi:10.1021/ed068p665.

[26] W.Y. Ng, Conversion of potentials in voltammetry and potentiometry, J. Chem. Educ. 65 (1988) 727. doi:10.1021/ed065p727.2.

[27] P. Salles, R. Gauche, P. Virmond, A qualitative model of Daniell cell for chemical education, Intell. Tutoring Syst. (2004) 870–872.

[28] A. Boulabiar, K. Bouraoui, M. Chastrette, M. Abderrabba, A Historical Analysis of the Daniell Cell and Electrochemistry.pdf, J. Chem. Educ. 81 (2004) 3–6.

[29] F. Rogers, P.A. Huddle, M.D. White, Using a Teaching Model to Correct Known Misconceptions in Electrochemistry, J. Chem. Educ. 77 (2000) 104. doi:10.1021/ed077p104.

[30] A.N. Ogude, J.D. Bradley, Ionic Conduction and Electrical Neutrality in Operating Electrochemical Cells: Pre-College and College Student Interpretations, J. Chem. Educ. 71 (1994) 29. doi:10.1021/ed071p29.

[31] B. Dawoud, E. Amer, D. Gross, Experimental investigation of an adsorptive thermal energy storage, Int. J. Energy Res. 31 (2007) 135–147. doi:10.1002/er.

[32] K.R. Bullock, Lead/acid batteries, J. Power Sources. 51 (1994) 1–17. doi:10.1016/0378-7753(94)01952-5.

[33] R.S. Treptow, The Lead-Acid Battery: Its Voltage in Theory and in Practice, J. Chem. Educ. 79 (2002) 334. doi:10.1021/ed079p334.

[34] P. Ruetschi, Reveiw on the Lead-Acid Battery Science and Technology, J. Power

Sources. 2 (1977) 3–24. doi:10.1016/0378-7753(77)85003-9.

[35] Z. Rogulski, A. Czerwin, Cathode modification in the Leclanche, J. Solid State Electrochem. 7 (2003) 118–121. doi:10.1007/s10008-002-0322-3.

[36] A. Kozawa, Primary Batteries—Leclanché Systems BT - Comprehensive Treatise of Electrochemistry: Volume 3: Electrochemical Energy Conversion and Storage, in: J.O. Bockris, B.E. Conway, E. Yeager, R.E. White (Eds.), Springer US, Boston, MA, 1981: pp. 207–218. doi:10.1007/978-1-4615-6687-8_5.

[37] T.H.E. Effect, O.F. Applying, C.E.M.F. To, L. Cell, The effect of applying a counter e.m.f. to a leclanche cell.', (1938) 587–602.

[38] K. Kordesch, Alkaline manganese dioxide zinc batteries, Batteries. 1 (1974) 241–384.

[39] K. V. Kordesch, C. Fabjan, J. Daniel-Ivad, J. Oliveira, Rechargeable zinc-carbon hybrid cells, J. Power Sources. 65 (1997) 77–80. doi:10.1016/S0378-7753(97)02470-1.

[40] M.H. Khan, A.S.W. Kurny, Characterization of Spent Household Zinc-Carbon Dry Cell Batteries in the Process of Recovery of Value Metals, 11 (2012) 641–651.

[41] A. Green, Characteristics of the nickel-cadmium battery for energy storage, Power Eng. J. 13 (1999) 117–121. doi:10.1049/pe:19990303.

[42] Ref 40.Pdf, (n.d.).

[43] F. Putois, Market for nickel-cadmium batteries, J. Power Sources. 57 (1995) 67–70. doi:10.1016/0378-7753(95)02243-0.

[44] K.-H. Young, Research in Nickel/Metal Hydride Batteries 2017, Batteries. 4 (2018) 9. doi:10.3390/batteries4010009.

[45] A. Ni, N. Cd, M.A. Zelinsky, J.M. Koch, K. Young, Performance Comparison of Rechargeable Batteries for Stationary Applications (Ni/MH vs. Ni–Cd and VRLA), Batteries. 4 (2017) 1. doi:10.3390/batteries4010001.

[46] J. Koch, K.-H. Young, J. Nei, C. Hu, B. Reichman, Performance Comparison between AB5 and Superlattice Metal Hydride Alloys in Sealed Cells, Batteries. 3 (2017) 35.

doi:10.3390/batteries3040035.

[47]   S. Wei, S. Xu, A. Agrawral, S. Choudhury, Y. Lu, Z. Tu, L. Ma, L.A. Archer, A
        stable room-temperature sodium-sulfur battery, Nat. Commun. 7 (2016) 1–10.
        doi:10.1038/ncomms11722.

[48]   H. Chen, T.N. Cong, W. Yang, C. Tan, Y. Li, Y. Ding, Progress in electrical energy
        storage system: A critical review, Prog. Nat. Sci. 19 (2009) 291–312.
        doi:10.1016/j.pnsc.2008.07.014.

[49]   E. Rudnik, Thermal Properties of, J. Therm. Anal. Calorim. 88 (2007) 495–498.
        doi:10.1081/E-ENN.

[50]   H. Näfe, Thermodynamic Stability and Electronic Conductivity of Na-beta-Alumina,
        J. Electrochem. Soc. 143 (1996). doi:10.1149/1.1836563.

[51]   C. Pillot, The Rechargeable Battery Market and Main Trends 2015-2025, Adv.
        Automot. Batter. Conf. (2016).

[52]   N.B. Aetukuri, B.D. McCloskey, J.M. Garciá, L.E. Krupp, V. Viswanathan, A.C.
        Luntz, Solvating additives drive solution-mediated electrochemistry and enhance
        toroid growth in non-aqueous Li-O2batteries, Nat. Chem. 7 (2015) 50–56.
        doi:10.1038/nchem.2132.

[53]   D. Larcher, J.M. Tarascon, Towards greener and more sustainable batteries for
        electrical energy storage, Nat. Chem. 7 (2015) 19–29. doi:10.1038/nchem.2085.

[54]   X. Sun, P. Bonnick, V. Duffort, M. Liu, Z. Rong, K.A. Persson, G. Ceder, L.F. Nazar,
        A high capacity thiospinel cathode for Mg batteries, Energy Environ. Sci. 9 (2016)
        2273–2277. doi:10.1039/c6ee00724d.

[55]   N. Yabuuchi, K. Kubota, M. Dahbi, S. Komaba, Research development on sodium-
        ion batteries, Chem. Rev. 114 (2014) 11636–11682. doi:10.1021/cr500192f.

[56]   M.R. Palacín, Recent advances in rechargeable battery materials: A chemist's
        perspective, Chem. Soc. Rev. 38 (2009) 2565–2575. doi:10.1039/b820555h.

[57]   J. Muldoon, C.B. Bucur, T. Gregory, Quest for nonaqueous multivalent secondary
        batteries: Magnesium and beyond, Chem. Rev. 114 (2014) 11683–11720.

doi:10.1021/cr500049y.

[58] C.P. Grey, J.M. Tarascon, Sustainability and in situ monitoring in battery development, Nat. Mater. 16 (2016) 45–56. doi:10.1038/nmat4777.

[59] A. Ponrouch, C. Frontera, F. Bardé, M.R. Palacín, Towards a calcium-based rechargeable battery, Nat. Mater. 15 (2016) 169–172. doi:10.1038/nmat4462.

[60] S. Yagi, T. Ichitsubo, Y. Shirai, S. Yanai, T. Doi, K. Murase, E. Matsubara, A concept of dual-salt polyvalent-metal storage battery, J. Mater. Chem. A. 2 (2014) 1144–1149. doi:10.1039/c3ta13668j.

[61] P. Poizot, F. Dolhem, Clean energy new deal for a sustainable world: from non-CO2 generating energy sources to greener electrochemical storage devices, Energy Environ. Sci. 4 (2011) 2003. doi:10.1039/c0ee00731e.

[62] J. Wang, Y. Li, X. Sun, Challenges and opportunities of nanostructured materials for aprotic rechargeable lithium-air batteries, Nano Energy. 2 (2013) 443–467. doi:10.1016/j.nanoen.2012.11.014.

[63] X.G. Zhang, Fibrous zinc anodes for high power batteries, J. Power Sources. 163 (2006) 591–597. doi:10.1016/j.jpowsour.2006.09.034.

[64] Q. Pang, D. Kundu, M. Cuisinier, L.F. Nazar, Surface-enhanced redox chemistry of polysulphides on a metallic and polar host for lithium-sulphur batteries, Nat. Commun. 5 (2014) 1–8. doi:10.1038/ncomms5759.

[65] E. Deiss, F. Holzer, O. Haas, Modeling of an electrically rechargeable alkaline Zn-air battery, Electrochim. Acta. 47 (2002) 3995–4010. doi:10.1016/S0013-4686(02)00316-X.

[66] J.M. Tarascon, Key challenges in future Li-battery research, Philos. Trans. R. Soc. A Math. Phys. Eng. Sci. 368 (2010) 3227–3241. doi:10.1098/rsta.2010.0112.

[67] H. Chen, M. Armand, G. Demailly, F. Dolhem, P. Poizot, J.M. Tarascon, From biomass to a renewable LiXC6O6organic electrode for sustainable li-ion batteries, ChemSusChem. 1 (2008) 348–355. doi:10.1002/cssc.200700161.

[68] B. Dunn, H. Kamath, J.M. Tarascon, Electrical energy storage for the grid: A battery

of choices, Science (80-.). 334 (2011) 928–935. doi:10.1126/science.1212741.

[69]   C. Vaalma, D. Buchholz, M. Weil, S. Passerini, A cost and resource analysis of sodium-ion batteries - Supplementary Information, (2018).

[70]   N. Recham, M. Armand, L. Laffont, J.-M. Tarascon, Eco-Efficient Synthesis of LiFePO[sub 4] with Different Morphologies for Li-Ion Batteries, Electrochem. Solid-State Lett. 12 (2009) A39. doi:10.1149/1.3039090.

[71]   D. Ilic, M. Kilb, K. Holl, H.W. Praas, E. Pytlik, Recent progress in rechargeable nickel/metal hydride and lithium-ion miniature rechargeable batteries, J. Power Sources. 80 (1999) 112–115. doi:10.1016/S0378-7753(99)00067-1.

[72]   J.M. Tarascon, N. Recham, M. Armand, J.N. Chotard, P. Barpanda, W. Walker, L. Dupont, Hunting for better Li-based electrode materials via low temperature inorganic synthesis, Chem. Mater. 22 (2010) 724–739. doi:10.1021/cm9030478.

Chapter 2

Alkali ion batteries

Abstract

The battery design begins with the selection of appropriate couple of positive and negative electrodes based on the electrochemical series. The individual components of an alkali ion battery particularly Li ion battery can be chosen from wide range of materials. The cathodes are generally the Li ion containing oxides or polyanionic compounds and have high operating potentials above 3.5 V. The anodes have three different mechanisms intercalation, alloying and conversion; and different materials show a specific character following one or multiple mechanism for charge storage. The electrolytes are also a crucial component of a battery and electrolytes used in alkali ion batteries and are based on carbonates or ether based solvents. The binders as well affect the battery performance and are specific to different electrode materials. The Na ion batteries are a possible alternative to Li ion batteries as Li reserves are very limited and may get depleted if used at a fast pace; but Na batteries have to overcome their size compatibility and structural stability issues. The battery terminology like power density, C-rate, etc. with the aging and internal resistance of battery responsible for battery degradation are described towards the end in this chapter.

2.1 The electrochemical series

This chapter explains the materials aspect of the alkali ion batteries and the factors affecting the battery life and performance. The Li ion and Na ion batteries being the most popular in this category, the various components and the materials used are described in this chapter. Li metal lies at the bottom of the electrochemical series with the lowest reduction potential of -3.045 V. Any element with the reduction potential more positive than Li can be used as an anode w.r.t. Li metal. Same way any two elements A and B having a difference between their reduction potentials can be used as cathode and anode where the element with more negative potential would be anode and the one with more positive would be cathode.

Reaction	Standard electrode potential (E^0) in volts at 25 °C
$F_2(g) + 2e^- \rightleftharpoons 2F^-(aq)$	+2.87
$H_2O_2(aq) + 2H^+(aq) + 2e^- \rightleftharpoons 2H_2O(l)$	+1.77
$Au^+(aq) + e^- \rightleftharpoons Au(s)$	+1.68
$Cl_2(g) + 2e^- \rightleftharpoons 2Cl^-(aq)$	+1.36
$O_2(g) + 4H^+(aq) + 4e^- \rightleftharpoons 2H_2O(l)$	+1.23
$Br_2(l) + 2e^- \rightleftharpoons 2Br^-(aq)$	+1.09
$Ag^+(aq) + e^- \rightleftharpoons Ag(s)$	+0.80
$Fe^{3+}(aq) + e^- \rightleftharpoons Fe^{2+}(aq)$	+0.77
$O_2(g) + 2H^+(aq) + 2e^- \rightleftharpoons H_2O_2(aq)$	+0.68
$I_2(s) + 2e^- \rightleftharpoons 2I^-(aq)$	+0.54
$O_2(g) + 2H_2O(l) + 4e^- \rightleftharpoons 4OH^-(aq)$	+0.40
$Cu^{2+}(aq) + 2e^- \rightleftharpoons Cu(s)$	+0.34
$Sn^{4+}(aq) + 2e^- \rightleftharpoons Sn^{2+}(aq)$	+0.15
$S(s) + 2H^+(aq) + 2e^- \rightleftharpoons H_2S(g)$	+0.14
$2H^+(aq) + 2e^- \rightleftharpoons H_2(g)$	0.00
$Pb^{2+}(aq) + 2e^- \rightleftharpoons Pb(s)$	−0.13
$Sn^{2+}(aq) + 2e^- \rightleftharpoons Sn(s)$	−0.14
$Ni^{2+}(aq) + 2e^- \rightleftharpoons Ni(s)$	−0.23
$Co^{2+}(aq) + 2e^- \rightleftharpoons Co(s)$	−0.28
$Fe^{2+}(aq) + 2e^- \rightleftharpoons Fe(s)$	−0.44
$Zn^{2+}(aq) + 2e^- \rightleftharpoons Zn(s)$	−0.76
$2H_2O(l) + 2e^- \rightleftharpoons H_2(g) + 2OH^-(aq)$	−0.83
$Mn^{2+}(aq) + 2e^- \rightleftharpoons Mn(s)$	−1.03
$Al^{3+}(aq) + 3e^- \rightleftharpoons Al(s)$	−1.67
$Mg^{2+}(aq) + 2e^- \rightleftharpoons Mg(s)$	−2.34
$Na^+(aq) + e^- \rightleftharpoons Na(s)$	−2.71
$Ca^{2+}(aq) + 2e^- \rightleftharpoons Ca(s)$	−2.87
$K^+(aq) + e^- \rightleftharpoons K(s)$	−2.93
$Li^+(aq) + e^- \rightleftharpoons Li(s)$	−3.02

Figure 1. The electrochemical series. Milazzo, Giulio, et al. Tables of Standard Electrode Potentials. Wiley, 1978.

2.2 Cathodes: A cathode is the positive electrode in the battery and usually a 3d transition metal ion containing compound. The cathodes are of different types namely layered, spinel, olivine and tavorite depending on the crystal structure and atom arrangement. The various cathodes used in Li ion battery are:

2.2.1 Transition metal oxides: The layered transition metal oxides have been used as cathodes since $LiCoO_2$ (LCO) was proposed by Goodenough and commercialized by Sony.[1][2] The layered transition metal oxides contain the Li and the transition metal located in octahedral sites and occupying alternate layers forming a hexagonal symmetry. LCO is a very good cathode material with a theoretical capacity of 274 mAh g^{-1}, high stability, low self-discharge rate and high operating voltage of 4.2 V. But with the growing demand of Li ion battery, the Co cost and supply risk have increased and is a major limitation in its utility in Li ion battery systems.[3] Moreover, the thermal instability, rapid capacity fading at high rates are other concerns associated with its usage as a cathode.[4][5]

$LiNiO_2$ (LNO) is another layered compound with similar structure and almost same theoretical specific capacity as LCO. It has an advantage of relatively lower cost of Ni and is a good choice. It has a major drawback of Ni ions substituting Li ions during synthesis and delithiation process and thus blocking Li diffusion pathways. Its thermal instability is rather high than LCO as Ni^{3+} reduces readily as compared to Co^{3+}.
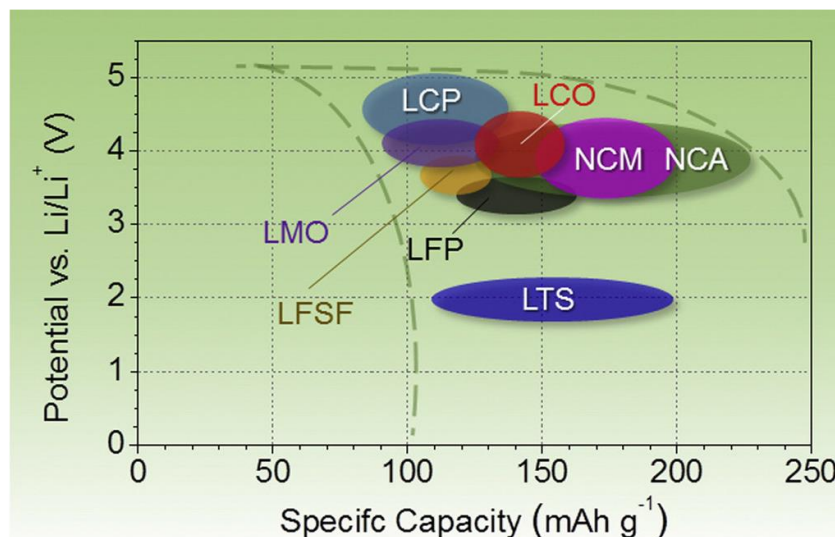

Figure 2. Various cathodes and their operating potentials. Copyright Elsevier. Reproduced with the permission of Ref [6].

The partial substitution of Co by Ni can be a possible remedy for this and doping of Mg and Al were also found to be effective to counteract the thermal instability. $LiNi_{0.8}Co_{0.15}Al_{0.05}O_2$ (NCA) is thus used widely and has high discharge capacity of 200 mAh g^{-1} and longer stability as compared to conventional Co based cathodes.[6] However, the performance fades rapidly at high temperatures due to solid electrolyte interphase and cracks development at grain boundaries. $LiMnO_2$ (LMO) is yet another choice for the cathode material for Li ion battery as Mn is cheaper and less toxic as compared to Co and Ni.[7][8] Unfortunately, LMO has poor cycling performance due to the change in the structure from layered to spinel during Li extraction and Mn dissolution into electrolyte at high voltage causing Mn ions going to the anode and destabilizing the SEI which in turn affects the cycle life of the device.[9][10] Hence the efforts are being continuously towards the development of cheaper and longer stability cathode materials than LCO. Various substitutions like $Li(Ni_{0.5}Mn_{0.5})O_2$ (NMO), $Li(Ni_xCo_yMn_z)O_2$ are being explored.[11][12]

2.2.2 Polyanionic Compounds: A new class of compounds called as polyanions are also popular cathode materials. These are normally large $(XO_4)^{3-}$ where X= (P, S, Si, Mo) containing compounds and the polyanions occupy lattice positions. The special characteristic of the polyanions is that they increase the cathode working potential thus increasing the power density of the material. For instance, $LiFePO_4$ with its olivine structure has good thermal stability and high power capability.[13] The Li and Fe ions are situated in the octahedral sites and P atoms occupy the tetrahedral sites with distorted hexagonal closed packing of oxygen array. Its low working potential and low ionic and electrical conductivity are a major drawback in its performance. Various nanostructures and composites are usually employed to mitigate these problem.

Another olivine class compound known as cathode material is $LiMnPO_4$ along with $LiCoPO_4$. $LiNi_{0.5}Co_{0.5}PO_4$, $LiMn_{0.33}Fe_{0.33}Co_{0.33}PO_4$ have also been also explored but the improvement in specific capacity values and ionic and electrical conductivities should be improved further.[14][15] Among all these, $Li_3V_2(PO_4)_3$ (LVP) has been found to be the good choice. LVP has high operating voltage of 4 V and high specific capacity of 197 mAh g^{-1}. The LVP/C composites perform very well at high C-rates and attain values very close to the theoretical capacity.
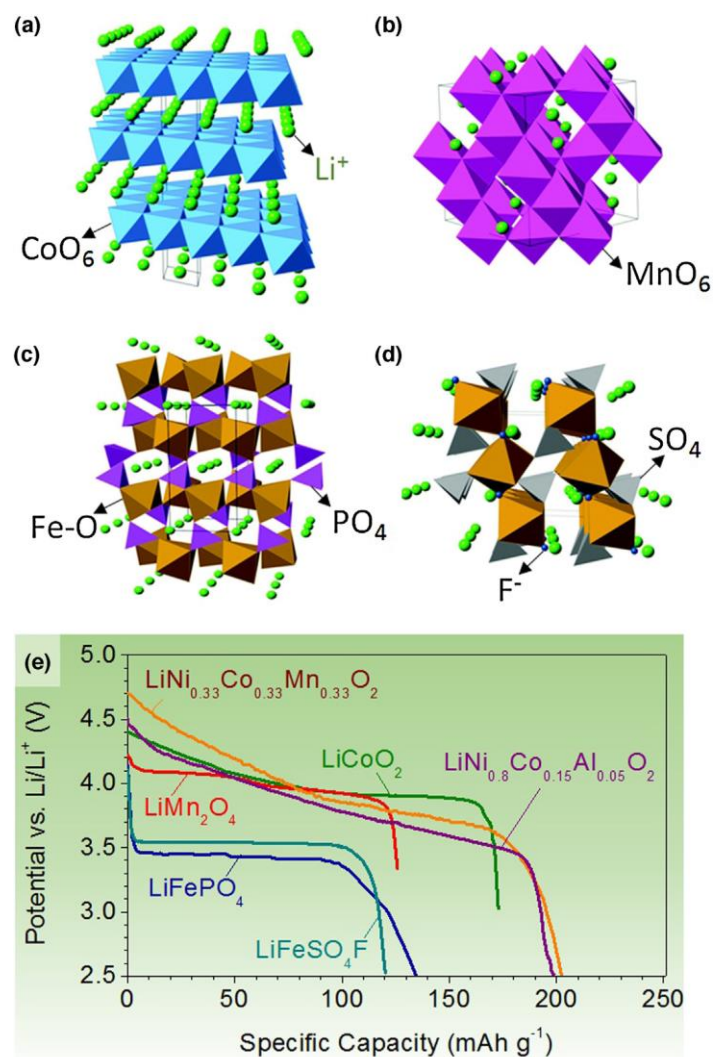
Figure 3. Crystal structures of (a) layered ($LiCoO_2$), (b) spinel ($LiMn_2O_4$), (c) olivine ($LiFePO_4$), and (d) tavorite ($LiFeSO_4F$) and (e) their discharge profiles. Copyright Elsevier. Reproduced with the permission of Ref [6].

2.3 Anodes

Li metal itself has very high specific capacity of 3800 mAh g-1 being the lightest among all alkali metals. Thus, its use as an anode can lead to batteries of very high energy density. But unfortunately, Li metal when used as anode, forms dendrites during high C-rate charging discharging process which can tear the separator and go to cathode sides leading to cell shortening. Apart from that, Li metal is highly unsafe as it can easily catch fire when comes into contact with moisture.

Hence, anodes other than Li metal are required and they are classified into various categories depending upon their Li storage mechanism. The various anode materials are discussed in the coming sections.

2.3.1 Intercalation anodes: These anode materials store Li by means of intercalation via Coulombic and Van der Waals interactions without undergoing and chemical reaction with the metal. Graphite was the first intercalation anode found suitable for Li ion battery. It stores 1 Li per 6 C atoms.[16] The theoretical capacity of graphite is 372 mAh g^{-1} and is highly robust and stable anode material hence a popular choice. The interlayer distance of graphite planes is just appropriate for lithiation and delithiation. The first commercial Li ion battery made use of graphite itself as anode with LCO cathode.[17] However, for certain high energy density applications, graphite might not be suitable and thus other than graphite many carbonaceous materials have also been used as intercalation anodes which can offer higher specific capacities than graphite. These include carbon nanotubes (CNTs), reduced graphene oxide (rGO) and porous carbons.[18][19]

Apart from carbonaceous materials, $Li_4Ti_5O_{12}$ (LTO) is another intercalation anode material which has specific capacity of 175 mAh g^{-1} and operating potential of 1.5 V. LTO has a spinel structure with Li ions occupying the octahedral sites. LTO is a very stable anode and has high rate performance and negligible irreversible capacity loss but suffers from poor ionic and electronic conductivity.[20][21]

2.3.2 Alloying Anodes: The elements Al, Si, Sn, Sb and Ge alloy with Li to give high specific capacities. The alloying takes place at a certain voltage and unlike graphite, the alloying elements can take more than one Li ions leading to specific capacities way higher than conventional graphite anode. As the advanced Li ion batteries need to enhance the energy densities and power densities so they need to opt for high specific capacity compounds. The alloying anodes are good solution for this but they have several issues associated with their use as anode.[22][23] Due to the high Li ion uptake the material undergoes change in its structure and the alloying compounds is much bigger in size than the pristine material, it causes the volume expansion. As a result of the volume expansion, the electrode undergoes cracking and pulverization causing capacity decay.
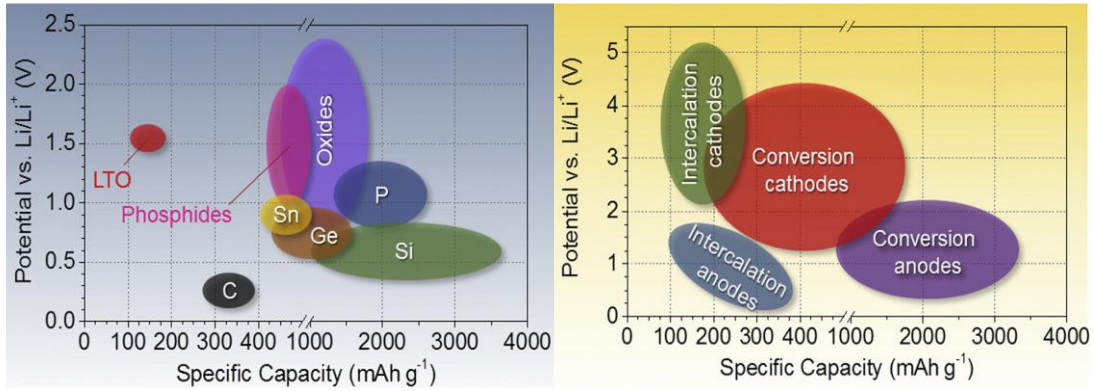
Figure 4. Various anodes and their specific capacities as per their type. Copyright Elsevier. Reproduced with the permission of Ref [6].

The various solutions proposed for this is downsizing the particle size- making the nanostructures or encapsulating the alloying material with the carbon materials such as rGO or CNTs.

2.3.3 Conversion Anodes: Conversion materials undergo displacement reaction during the lithiation process. They are mostly transition row elements coupled with alloying elements.[24][25] The transition metal elements such as Cu changes from ionic state to metallic state and the alloying element takes part in the charging discharging process. The alloy products are embedded in the reduced metal matrix. The example of such compounds are CuSn, SnS_2 etc.[26][27] The reaction mechanism for conversion anodes can be understood from the following equation:

$$M_aX_b + (b.c)A \leftrightarrow a.M + b.A_cX \text{ (A= Li, Na or K)}$$
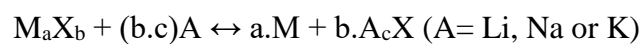
where M is the transition metal which is reduced during conversion reaction and X is non-metal that forms alloy with A. This class of materials has potential of high energy densities but they suffer from the low electronic conductivity and volume expansion. The nanocomposites of these materials are proposed to have better performance.[28][29]

2.4 Electrolytes and additives: A Li salt in a solvent collectively is called as electrolyte and serves the purpose of ion transport medium between the two electrodes. Li ion battery electrolyte normally consists of a Li salt dissolved in a particular concentration in carbonate, ester, ether or ionic liquid solvent.
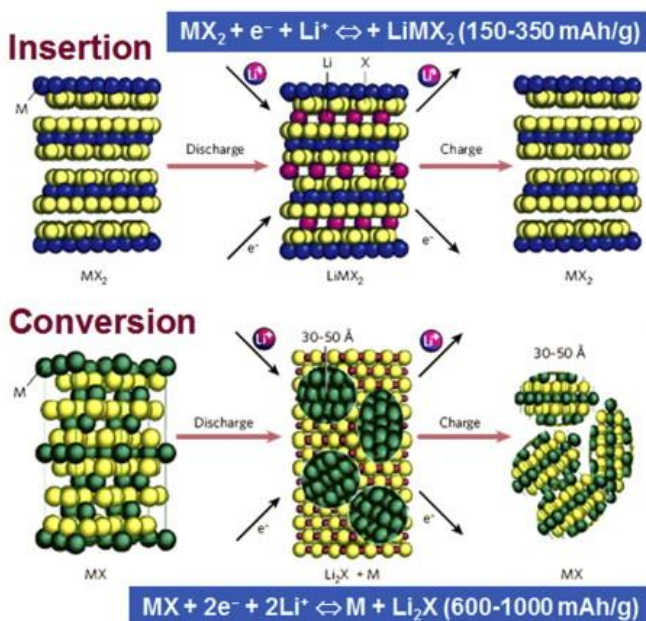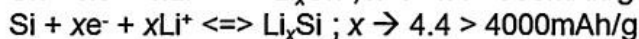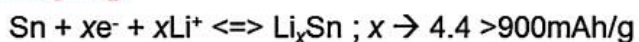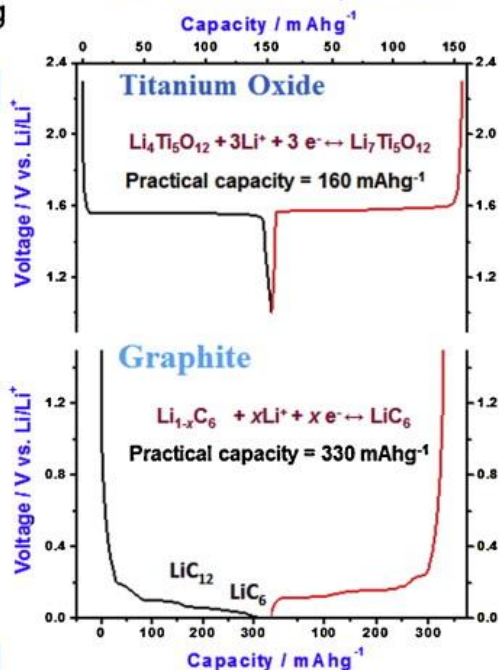
Figure 5. Storage mechanism of intercalation, alloying and conversion anodes. Copyright Elsevier. Reproduced with the permission of Ref [28].

The electrolyte should have the following characteristics: it should be stable over a wide temperature range, it should have a reasonable ionic conductivity, should have large potential window of operation, should have low viscosity and high dissolution for Li salts, should be cheap, environmental friendly and non-toxic.[30] Various Li salts have been used in batteries and $LiPF_6$ being the most common among them. But this salt has HF formation probability which corrodes the Al current collector and therefore is considered unsafe. $LiClO_4$ is used as an alternative as it does not have corrosion issue and has good ionic conductivity but it is explosive and the passivation layer formed is less stable. LiTFSI (Li-bistrifluoromethane sulfonamide) has gained interest lately but has low ionic conductivity and relatively high cost.[31]

Among the solvents, ethylene carbonate (EC) is very common as it has good solubility for the Li salts and high operating voltage > 4.5 V. Apart from this it facilitates the SEI layer formation and is used in combination with other linear carbonates like propylene carbonate (PC), dimethyl carbonate (DMC), diethyl carbonate (DEC).[32][33] This is done to combine low viscosity and high dielectric constant solvents with high viscosity ones.
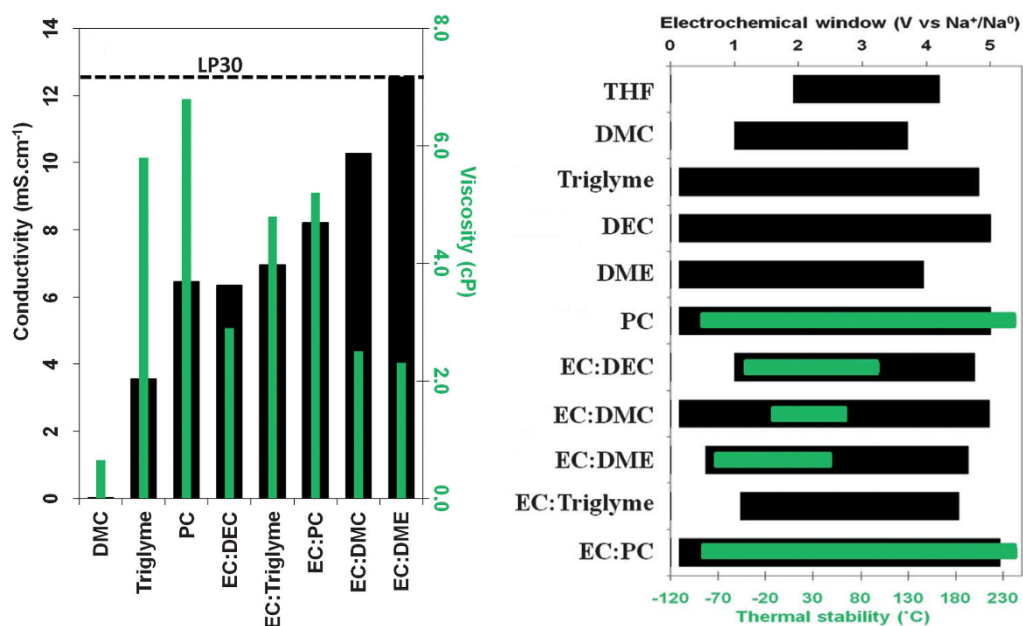
Figure 6. Conductivity and viscosity variation of different electrolyte systems and their thermal stability. Copyright Royal Society of Chemistry. Reproduced with the permission of Ref [30].

Carbonates have flammability issue thus as an alternative, glyme based or ionic liquid electrolytes are also used to enhance thermal stability.[34][35] These electrolytes have low viscosity and are expensive. Some electrolyte systems are designed especially for certain materials to counter the capacity fading or dissolution issue. One such system is ether based dioxolane and dimethyl ether which are used to minimize the sulfide dissolution during cycling.

Additives are also employed to enhance the battery performance. Fluoroethylene carbonate (FEC) and vinylene carbonate (VC) are some examples. FEC increases the LiF content in the SEI layer which contributes towards the stability of SEI and long term cycling stability. Similarly VC is used for providing stability to cathodes.

2.5 Binders: Binders are very crucial for the electrochemical performance of any electrode. Binders are used to make slurry for coating. Commonly used binders are polyvinylidene fluoride (PVDF) which is used for all types of materials including carbonaceous compounds, organic materials etc. Na-carboxymethyl cellulose (Na-

CMC) is used for Si, Sn and Sb etc. Alginate based binders are also used in some cases to improve the stability.[36][37][38]

2.6 Separators: Separators prevent the two electrodes from coming into contact and thus the shortening of the cell. The separator should be a material which is electronically non-conducting but allows the permeation of ions through it. The pore size of the separator should be appropriate for the particular ions. It should not react with the electrolyte and should have high thermal stability.[39] The common separators used in batteries are Whatmann which is a cellulose membrane and is very good conductor of Li as well as Na ions. It is used for a wide range of materials from carbons to composites. Other than Whatmann, polypropylene separators are also used are are called as Celgard. Celgard is of different types- single layer or trilayer and has high thermal stability. Celgard is used for materials with high volume expansion like Si.

2.7 Li vs. Na ion Batteries

Considering the fact that Li reserves are limited in earth's crust and rising cost of Li and Co used in Li ion battery one would immediately accept the urge of seeking alternatives. Na is next to Li in the group and is abundant. This implies that Na can easily replace Li metal in battery but this is not the case in reality. The Li and Na ion chemistries are quite different when it comes to their electrochemical behavior in the device. The key differences are listed below including the advantages and shortcomings of Na over Li metal.

1. First and foremost point is the difference in their atomic size. Thus the structural changes caused by Na during sodiation and desodiation are enhanced as compared to Li. Moreover, because of bigger size, all materials used for Li may not be appropriate for Na. For example in graphite which is the ideal anode for Li ion battery is not suitable for Na ion battery as the interlayer spacing of graphite is not sufficient for Na ion intercalation. Also the bigger size of Na causes adverse structure transformations in the cathodes leading to rapid capacity fading.[40][41][42]

2. Na has low melting point (98 °C) as compared to Li (181 °C) and is chemically more reactive than Li. This makes Na prone for safety issues. In addition, Na is softer than Li and the handling is quite cumbersome. This indirectly suppresses the dendrite formation with the mechanical pressure.[43]
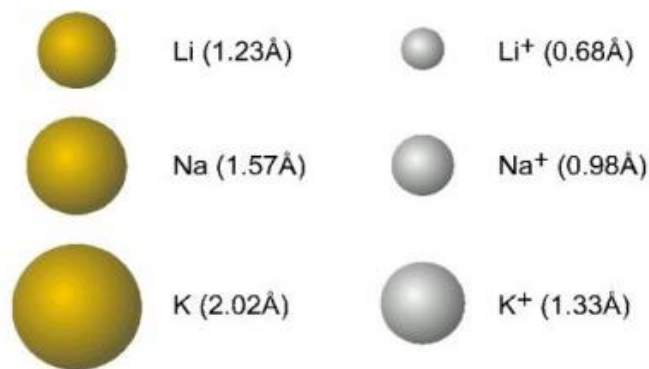
Figure   7.   Atomic   radii   of   alkali   elements   and   ions.
(http://www.mikeblaber.org/oldwine/chm1045/ notes/Bonding/IonSize/Bond03.htm).

3. Na has lower electrochemical potential than Li as seen from the electrochemical series. This leads to the lesser potential difference of the device created when Na is coupled with any material. A Na ion battery would always have low energy and power density as compared to the Li ion battery for a given system of electrodes.[44]

4. Na has higher solvation energies than Li as it is weaker Lewis acid than Li. This is an advantage for Na ion battery as the charge kinetics would not be affected at high rates and the capacity would not degrade if the battery is subjected to high currents which is not the case with Li ion battery as they show poorer rate performance as compared to Na ion battery.[45][46]

5. Na is less reducing than Li. This could be a positive factor for metal batteries. As in Li ion batteries it is found that the solid electrolytes degrade faster in direct contact with metal. This could be less adverse in Na ion based electrolytes.

6. Na ion batteries are cost effective due to the high abundance of Na as compared to Li. The other materials used in Li ion battery can be replaced with cheaper ones in Na ion battery. As an example, Cu is costlier than Al and it is used as current collector in anode side in Li ion battery as Al reacts with Li at potentials lower than 1 V. But in Na ion battery, Al can be used as current collector for both the anode and cathode reducing the manufacturing cost.[47]

In the light of these facts, although there is need to replace Li ion batteries still they continue to be the main players in the market and are used in most of the gadgets. Na ion battery is anticipated to be the future but a lot needs to be established in order to accomplish the desired performance.
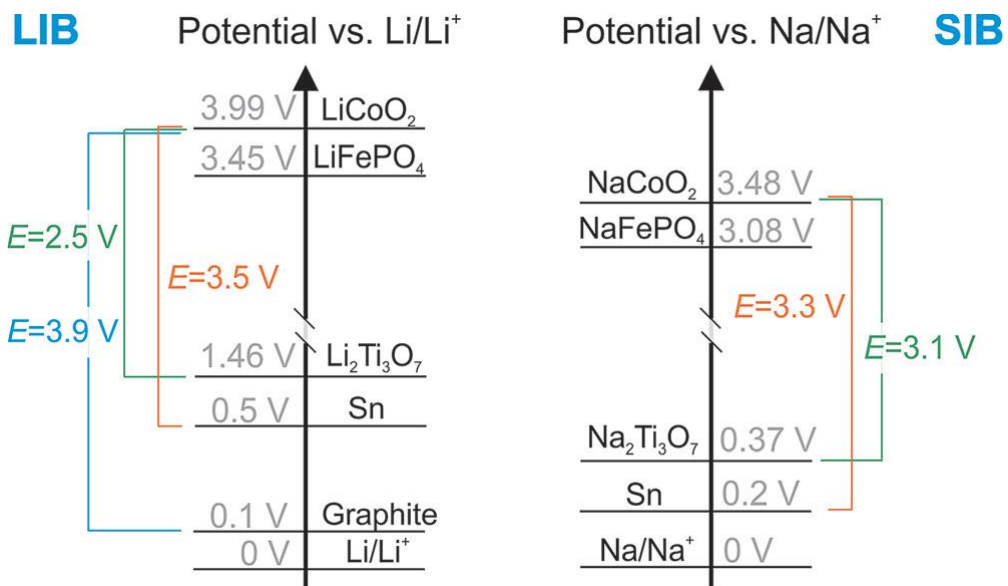
Figure 8. Difference in lithiation and sodiation potentials of same pair of compounds. Copyright John Wiley and Sons. Reproduced with the permission of Ref [44].
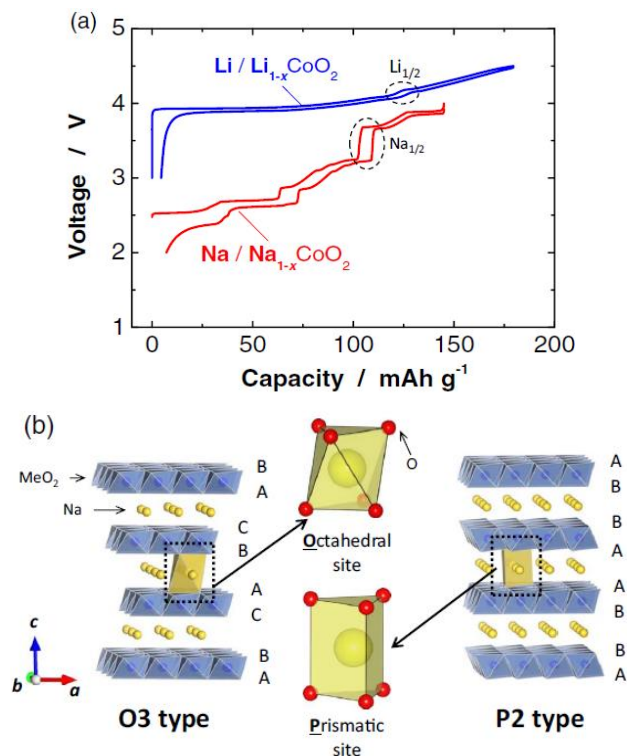
Figure 9. (a) The charge discharge profiles of Li and Na ion battery cathodes. (b) Structural change in layered oxide cathode as a result of bigger size of Na ion. Copyright Electrochemical Society Inc. Reproduced with the permission of Ref [42].

2.8 Terminologies used in battery field

2.8.1 Theoretical capacity: The theoretical capacity of a battery gives the estimation of the specific capacity that can be achieved by the battery. A battery can never exceed its theoretical capacity value. The formula to calculate the theoretical capacity is:

$$C = \frac{n * F}{M.W.* 3.6}$$

where n= no. of Li ions that the material can take

F= Faraday's constant

$= 96500$ C mol^{-1}

M.W. = molecular weight of the compound g mol^{-1}

The units of theoretical capacity are mAh g^{-1}.

2.8.2 Energy density and Power Density: The energy density of a battery is defined as the amount of charge that can be stored in it.[48] The energy density of a battery is calculated as

$$E = QV$$

$$E = (It) * V$$

where E = energy density, Q = charge, I = current, t= time, V = voltage

The units of gravimetric energy density are Wh kg^{-1}.

The power density is defined as the rate at which the battery is capable to store or deliver the charge. The power density formula is given as:

$$P = \frac{E}{t}$$

Accordingly the units are W kg^{-1}.

2.8.3 Solid Electrolyte Interphase (SEI): In the battery, the electrolyte gets reduced on the anode surface and forms a layer which is electronically insulating and ionically conducting. This is called as solid electrolyte interphase (SEI) layer. This process takes

place because of the HOMO and LUMO of cathode and anode and a wide voltage range of electrolyte.[49] For charge transfer to take place, electrolyte molecules reduce on the anode surface giving rise to SEI layer formation. This layer plays a very crucial role in battery performance.
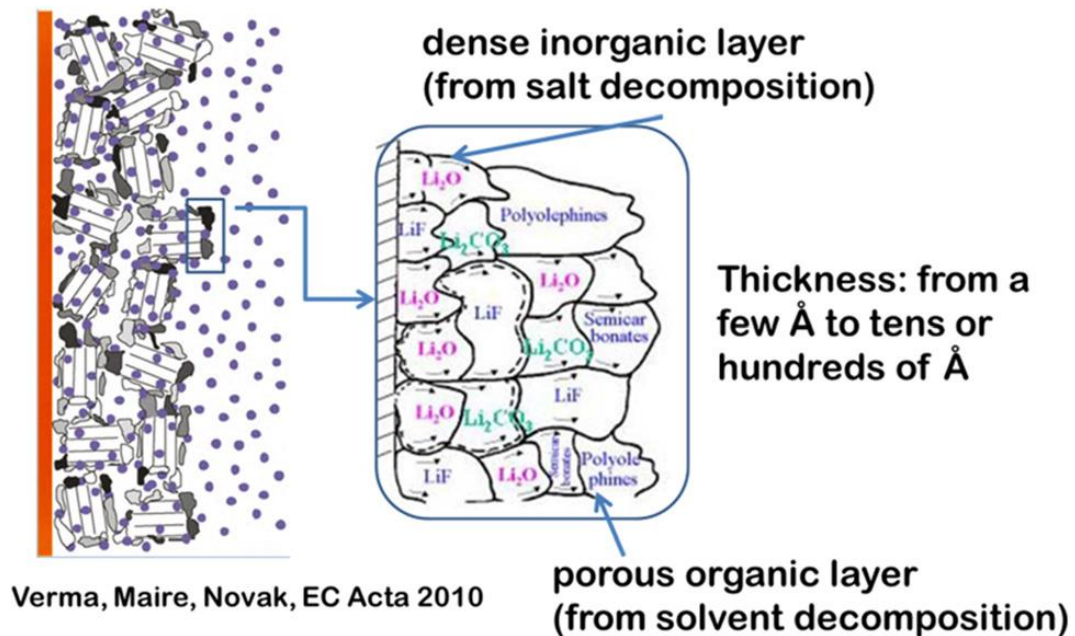
Figure 10. Illustration of SEL layer components. Copyright Elsevier. Reproduced with the permission of Ref [51].

It prevents further reduction of electrolyte on anode surface and provides ion conducting interphase. During SEI formation, significant amount of Li ions is irreversibly consumed leading to the irreversible capacity loss (IRL). The SEI should neither be too thick or too thin. Too thick SEI causes sluggish charge transfer by creating hindrance in permeation of ions. Too thin SEI gets broken during cycling and exposes anode for further electrolyte reduction leading to more Li loss.[50][51]

2.8.4 Impedance: Impedance spectroscopy is a very powerful technique to analyze the battery kinetics. The imaginary vs. real resistance plot also called as Nyquist plot is used for the determination of kinetics of species in a battery.[52] The onset of semi-circle describes the series resistance (R_s) of the system and includes resistance from the circuit, cables, electrodes, contacts etc. It reflects the electrolyte interaction at the anode surface. The double layer capacitance at the electrode/electrolyte interface is represented by C_{dl}. The total resistance of semi-circle is defined as the charge transfer

resistance (R_{CT}) which is the charge or electron transfer resistance of the electrode. The number of semi-circles in the Nyquist plot sometimes can vary from one indicating the presence of charge transfer with a different time constant. The region after the charge transfer resistance is called as Warburg impedance which signifies the diffusion of ions from electrolyte to the electrode also referred to as mass transfer in the electrode.[53]
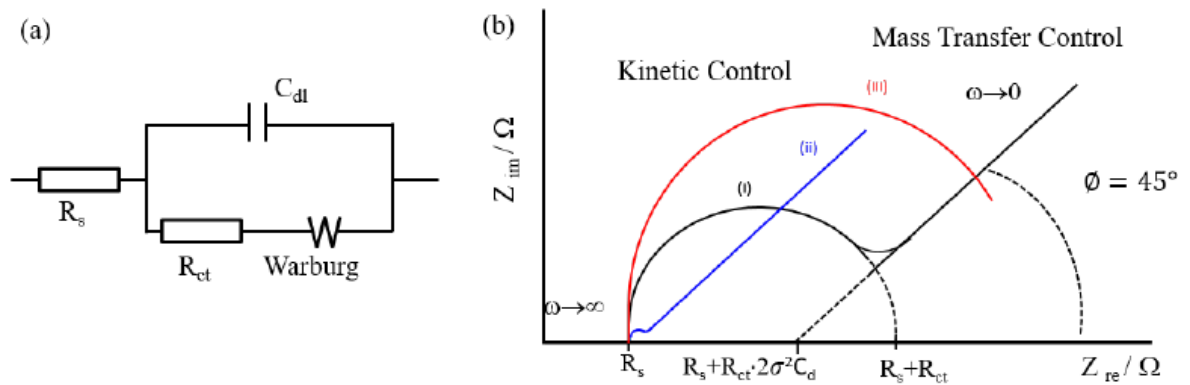
Figure 11. (a) Equivalent circuit and (b) a typical Nyquist plot showing all the components. Reproduced with the permission of Ref [52].

2.8.5 C-Rate: The C-rate is defined as the rate at which the battery will be charged or discharged relative to its maximum capacity that can be achieved. 1C rate would mean the capacity attained during one charge or discharge in 1 hour. The C-rates governs how fast a battery can charge or discharge without losing much of its capacity. Some materials like LTO are unaffected by the rate of charging or discharging as there are shorter Li ion diffusion pathways in the structure which are accessible by the electrolyte even at high C-rate. Carbonaceous materials particular are poorer in rate performance as they need slower rates for the ions to access the nanopores in the material.

2.8.6 Stability: The stability of the battery is crucial factor in determining the longevity of the device. The cycling over several hundreds of cycles without losing the initial capacity would be the ideal situation for any given battery. But realistic battery do degrade with time and with the processes occurring during its function. The battery capacity tends to fade with cycling and the capacity retention is calculated for a given period or number of cycles. The capacity fading could occur due to many reasons such as poor shelf life – if the battery is not used and stored for long time, it might lose its initial performance, side reactions taking place during charging discharging, the

leaching out of material due to dissolvation in electrolyte, electrolyte degradation with time etc.

2.8.7 Coulombic Efficiency: The round trip efficiency determines whether the total number of ions are same in charging and discharging processes. The Coulombic efficiency (C.E.) is given by

$$C.E. = \frac{C\ (Dis)}{C\ (Ch)} * 100\ \%$$

where C (Dis) = Discharge capacity and C (Ch) = Charge capacity

100 % C.E. means that the number of ions travelling towards both the electrodes are same during charging and discharging. If the C.E. is not 100 % that means that the ions are irreversibly lost during discharging process. That might happen if the ions are trapped in nanopores of the material and can't be taken out even if the same potential is applied. Another reason for this is the dissolution of the active material in electrolyte during cycling. In successive cycles the material available is reduced and the C.E. reduces leading to the poor performance. This problem is more prevailing in sulfides.

2.9 Factors affecting battery performance

Every battery would have a life before it stops working. The primary batteries last until the chemicals inside are completely exhausted or no longer in their original state to undergo the desired reaction. The rechargeable batteries on the other hand have reasonably longer life span and they can last for several cycles of charging and discharging. But in these devices also some unstoppable processes occur which cause the predicted cycle life to get shorten. The factors causing these unwelcoming outcomes are:

2.9.1 Aging: Though aging is undeniable and would affect the performance of the battery but there are certain practices that can lead to faster aging and capacity fade. In a battery, the total energy present or the total capacity it can deliver can be divided into three regions- the empty zone, the available energy region and the rock content.
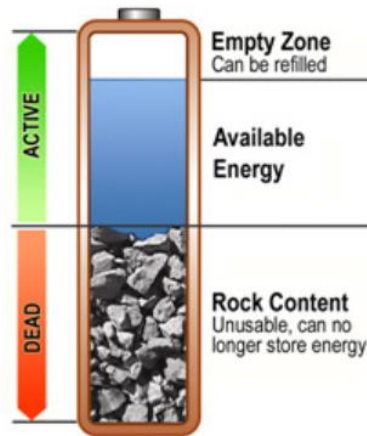
Figure 12. Battery energy utilization zones. Reproduced with the courtesy of Isidor Buchmann, Battery University. www.batteryuniversity.com.

The empty zone can be refilled but the rock content which increases as the battery ages can't be revived. This part is no longer active and the contents become dead and cannot store energy.

2.9.2 Internal resistance: The internal resistance is inevitable in a battery and is more in case of low conductivity materials. It governs the restriction the battery pack encounters during operation. With the increasing internal resistance the device heats up and the voltage drop increases leading to an early shutdown. The full energy cannot be utilized in such a situation and the battery needs to be charged sooner than usual.
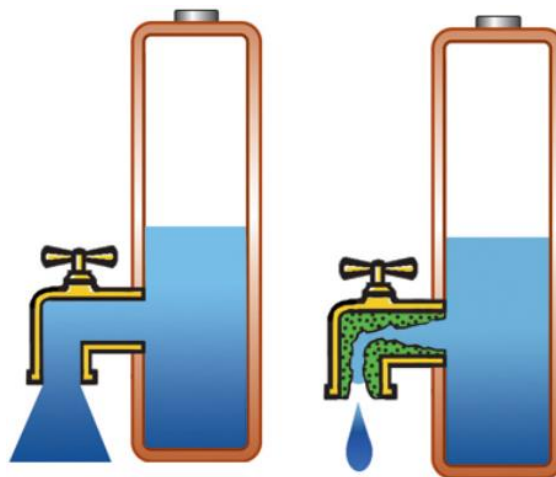
Figure 13. Illustration of internal resistance of battery. Reproduced with the courtesy of Isidor Buchmann, Battery University. www.batteryuniversity.com.

2.9.3 Self-Discharge: The self-discharge is also a phenomenon which every battery undergoes. The rate of self-discharge varies from different battery chemistries and increases with the time. The self-discharge is enhanced in elevated temperature conditions and increased reaction rates.

Figure 14. Self-discharge process in a battery. Reproduced with the courtesy of Isidor Buchmann, Battery University. www.batteryuniversity.com.

To conclude, batteries are a plausible substitute for energy dependence in future. While Li ion batteries are already matured enough and are being employed in major applications, Na ion batteries are yet to flourish and come into play. There are several parameters that need to be taken care of while designing a battery cathode or anode and while choosing a suitable electrolyte. Care should be taken that ensure long and stable battery performance and these should be followed without fail to achieve maximum output from the device.

References

[1]   N. Recham, M. Armand, L. Laffont, J.-M. Tarascon, Eco-Efficient Synthesis of LiFePO[sub 4] with Different Morphologies for Li-Ion Batteries, Electrochem. Solid-State Lett. 12 (2009) A39. doi:10.1149/1.3039090.

[2]   K. Ozawa, Lithium-ion rechargeable batteries with LiCoO2 and carbon electrodes: the LiCoO2/C system, Solid State Ionics. 69 (1994) 212–221. doi:10.1016/0167-2738(94)90411-1.

[3]   S. Choi, A. Manthiram, Synthesis and Electrochemical Properties of LiCo[sub 2]O[sub 4] Spinel Cathodes, J. Electrochem. Soc. 149 (2002) A162. doi:10.1149/1.1431574.

[4]   J. Cho, Y.J. Kim, T.J. Kim, B. Park, Zero-strain intercalation cathode for rechargeable Li-Ion cell, Angew. Chemie - Int. Ed. 40 (2001) 3367–3369. doi:10.1002/1521-3773(20010917)40:18<3367::AID-ANIE3367>3.0.CO;2-A.

[5]   I.D. Scott, Y.S. Jung, A.S. Cavanagh, Y. Yan, A.C. Dillon, S.M. George, S.H. Lee, Ultrathin coatings on nano-LiCoO2 for Li-ion vehicular applications, Nano Lett. 11 (2011) 414–418. doi:10.1021/nl1030198.

[6]   N. Nitta, F. Wu, J.T. Lee, G. Yushin, Li-ion battery materials: Present and future, Mater. Today. 18 (2015) 252–264. doi:10.1016/j.mattod.2014.10.040.

[7]   F. Amalraj, D. Kovacheva, M. Talianker, L. Zeiri, J. Grinblat, N. Leifer, G. Goobes, B. Markovsky, D. Aurbach, Publisher's Note: Synthesis of Integrated Cathode Materials xLi[sub 2]MnO[sub 3]·(1−x)LiMn[sub 1/3]Ni[sub 1/3]Co[sub 1/3]O[sub 2] (x=0.3, 0.5, 0.7) and Studies of Their Electrochemical Behavior [J. Electrochem. Soc., 157, A1121 (2010)], J. Electrochem. Soc. 157 (2010) S19. doi:10.1149/1.3491816.

[8]   C. Zhu, S. Guo, P. Wang, L. Xing, Y. Fang, S. Dong, H. Yin, S. Zhao, J. Wan, H. Tang, L. Chang, L. He, S. Yang, Y. Cai, Y. Cheng, C. V Varanasi, J. Liu, K. Xie, X. Qin, X. Wang, Y. Wang, H. Tao, Q. Wu, T.J. Welgemoed, C.F. Schutte, C. Tsouris, R. Mayes, J. Kiggans, K. Sharma, S. Yiacoumi, D. Depaoli, S. Dai, S. Tio, P. Standard, The Mendeley Support Team, F. Synthesis, S.A. Cluster, G. Hybrids, H.-P.

Oxygen, R. Reaction, M. a Shannon, P.W. Bohn, M. Elimelech, J.G. Georgiadis, B.J. Mariñas, A.M. Mayes, Y. Oren, S.J. Kim, S.H. Ko, K.H. Kang, J. Han, Y. Huajie, C.-H. Hou, C. Liang, M. Haro, G. K.S. Novoselov, S. Roth, a. K. Geim, W. Chen, S. Li, C. Chen, L. Yan, P.M. Biesheuvel, T.P. Barnett, J.C. Adam, D.P. Lettenmaier, M. a. Anderson, A.L. Cudero, J. Palma, Z. Abbas, H. Fath, T. Mezher, A. Khaled, Ref 10.Pdf, Desalination. 183 (2011) 327–340. doi:10.1016/j.desal.2005.02.054.

[9]   M. Gu, I. Belharouak, J. Zheng, H. Wu, J. Xiao, A. Genc, K. Amine, S. Thevuthasan, D.R. Baer, J.G. Zhang, N.D. Browning, J. Liu, C. Wang, Formation of the spinel phase in the layered composite cathode used in Li-Ion batteries, ACS Nano. 7 (2013) 760–767. doi:10.1021/nn305065u.

[10]   M.M. Thackeray, S.-H. Kang, C.S. Johnson, J.T. Vaughey, R. Benedek, S.A. Hackney, Li2MnO3-stabilized LiMO2 (M = Mn, Ni, Co) electrodes for lithium-ion batteries, J. Mater. Chem. 17 (2007) 3112. doi:10.1039/b702425h.

[11]   G. Ceder, Y.-M. Chiang, D.R. Sadoway, M.K. Aydinol, Y.-I. Jang, B. Huang, Identification of cathode materials for lithium batteries guided by first-principles calculations, Nature. 392 (1998) 694–696. doi:10.1038/33647.

[12]   S. Madhavi, G. V. Subba Rao, B.V.R. Chowdari, S.F.Y. Li, Effect of Cr dopant on the cathodic behavior of LiCoO2, Electrochim. Acta. 48 (2002) 219–226. doi:10.1016/S0013-4686(02)00594-7.

[13]   Y. Nishi, Past, Present and Future of Lithium-Ion Batteries. Can New Technologies Open up New Horizons?, Elsevier, 2014. doi:10.1016/B978-0-444-59513-3.00002-9.

[14]   D. Choi, D. Wang, I.T. Bae, J. Xiao, Z. Nie, W. Wang, V. V. Viswanathan, Y.J. Lee, J.G. Zhang, G.L. Graff, Z. Yang, J. Liu, LiMnPO4nanoplate grown via solid-state reaction in molten hydrocarbon for Li-ion battery cathode, Nano Lett. 10 (2010) 2799–2805. doi:10.1021/nl1007085.

[15]   J.M. Lloris, C. Pérez Vicente, J.L. Tirado, Improvement of the Electrochemical Performance of LiCoPO[sub 4] 5 V Material Using a Novel Synthesis Procedure, Electrochem. Solid-State Lett. 5 (2002) A234. doi:10.1149/1.1507941.

[16]   M.D. Levi, D. Aurbach, Diffusion Coefficients of Lithium Ions during Intercalation

into Graphite Derived from the Simultaneous Measurements and Modeling of Electrochemical Impedance and Potentiostatic Intermittent Titration Characteristics of Thin Graphite Electrodes, J. Phys. Chem. B. 101 (1997) 4641–4647. doi:10.1021/jp9701911.

[17] F. Schipper, D. Aurbach, A brief review: Past, present and future of lithium ion batteries, Russ. J. Electrochem. 52 (2016) 1095–1121. doi:10.1134/S1023193516120120.

[18] M. Broussely, P. Biensan, B. Simon, Lithium insertion into host materials: the key to success for Li ion batteries, Electrochim. Acta. 45 (1999) 3–22. doi:10.1016/S0013-4686(99)00189-9.

[19] T. Zheng, Lithium Insertion in High Capacity Carbonaceous Materials, J. Electrochem. Soc. 142 (1995) 2581. doi:10.1149/1.2050057.

[20] G.-N. Zhu, Y.-G. Wang, Y.-Y. Xia, Ti-based compounds as anode materials for Li-ion batteries, Energy Environ. Sci. 5 (2012) 6652. doi:10.1039/c2ee03410g.

[21] N. Takami, K. Hoshina, H. Inagaki, Lithium Diffusion in Li4/3Ti5/3O4 Particles during Insertion and Extraction, J. Electrochem. Soc. 158 (2011) A725. doi:10.1149/1.3574037.

[22] M.K.Y. Chan, C. Wolverton, J.P. Greeley, First principles simulations of the electrochemical lithiation and delithiation of faceted crystalline silicon, J. Am. Chem. Soc. 134 (2012) 14362–14374. doi:10.1021/ja301766z.

[23] I.A. Courtney, Electrochemical and In Situ X-Ray Diffraction Studies of the Reaction of Lithium with Tin Oxide Composites, J. Electrochem. Soc. 144 (1997) 2045. doi:10.1149/1.1837740.

[24] A. Ponrouch, M.R. Palacín, Optimisation of performance through electrode formulation in conversion materials for lithium ion batteries: Co3O4 as a case example, J. Power Sources. 212 (2012) 233–246. doi:10.1016/j.jpowsour.2012.04.005.

[25] J. Cabana, L. Monconduit, D. Larcher, M.R. Palacín, Beyond intercalation-based Li-ion batteries: The state of the art and challenges of electrode materials reacting

through conversion reactions, Adv. Mater. 22 (2010) 170–192. doi:10.1002/adma.201000717.

[26] Y. Oumellal, A. Rougier, G.A. Nazri, J.M. Tarascon, L. Aymard, Metal hydrides for lithium-ion batteries, Nat. Mater. 7 (2008) 916–921. doi:10.1038/nmat2288.

[27] P.G. Bruce, B. Scrosati, J.M. Tarascon, Nanomaterials for rechargeable lithium batteries, Angew. Chemie - Int. Ed. 47 (2008) 2930–2946. doi:10.1002/anie.200702505.

[28] H.D. Yoo, E. Markevich, G. Salitra, D. Sharon, D. Aurbach, On the challenge of developing advanced technologies for electrochemical energy storage and conversion, Mater. Today. 17 (2014) 110–121. doi:10.1016/j.mattod.2014.02.014.

[29] A. Ponrouch, P.L. Taberna, P. Simon, M.R. Palacín, On the origin of the extra capacity at low potential in materials for Li batteries reacting through conversion reaction, Electrochim. Acta. 61 (2012) 13–18. doi:10.1016/j.electacta.2011.11.029.

[30] A. Ponrouch, E. Marchante, M. Courty, J.M. Tarascon, M.R. Palac??n, In search of an optimized electrolyte for Na-ion batteries, Energy Environ. Sci. 5 (2012) 8572–8583. doi:10.1039/c2ee22258b.

[31] Q. Li, J. Chen, L. Fan, X. Kong, Y. Lu, Progress in electrolytes for rechargeable Li-based batteries and beyond, Green Energy Environ. 1 (2016) 18–42. doi:10.1016/j.gee.2016.04.006.

[32] E.S. Nimon, A. V. Churikov, Electrochemical behaviour of Li-Sn, Li-Cd and Li-Sn-Cd alloys in propylene carbonate solution, Electrochim. Acta. 41 (1996) 1455–1464. doi:10.1016/0013-4686(95)00394-0.

[33] D. Aurbach, H. Gottlieb, The electrochemical behavior of selected polar aprotic systems, Electrochim. Acta. 34 (1989) 141–156. doi:10.1016/0013-4686(89)87079-3.

[34] J.M. Tarascon, D. Guyomard, New electrolyte compositions stable over the 0 to 5 V voltage range and compatible with the Li1+xMn2O4/carbon Li-ion cells, Solid State Ionics. 69 (1994) 293–305. doi:10.1016/0167-2738(94)90418-9.

[35] M. Dahbi, F. Ghamouss, F. Tran-Van, D. Lemordant, M. Anouti, Comparative study

of EC/DMC LiTFSI and LiPF6 electrolytes for electrochemical storage, J. Power Sources. 196 (2011) 9743–9750. doi:10.1016/j.jpowsour.2011.07.071.

[36] L. Chen, X. Xie, J. Xie, K. Wang, J. Yang, Binder effect on cycling performance of silicon/carbon composite anodes for lithium ion batteries, J. Appl. Electrochem. 36 (2006) 1099–1104. doi:10.1007/s10800-006-9191-2.

[37] W.-R. Liu, M.-H. Yang, H.-C. Wu, S.M. Chiao, N.-L. Wu, Enhanced Cycle Life of Si Anode for Li-Ion Batteries by Using Modified Elastomeric Binder, Electrochem. Solid-State Lett. 8 (2005) A100. doi:10.1149/1.1847685.

[38] H. Buqa, M. Holzapfel, F. Krumeich, C. Veit, P. Novák, Study of styrene butadiene rubber and sodium methyl cellulose as binder for negative electrodes in lithium-ion batteries, J. Power Sources. 161 (2006) 617–622. doi:10.1016/j.jpowsour.2006.03.073.

[39] J.H. Chae, K.C. Ng, G.Z. Chen, Nanostructured materials for the construction of asymmetrical supercapacitors, Proc. Inst. Mech. Eng. Part A J. Power Energy. 224 (2010) 479–503. doi:10.1243/09576509JPE861.

[40] P. Adelhelm, P. Hartmann, C.L. Bender, M. Busche, C. Eufinger, J. Janek, From lithium to sodium: Cell chemistry of room temperature sodium-air and sodium-sulfur batteries, Beilstein J. Nanotechnol. 6 (2015) 1016–1055. doi:10.3762/bjnano.6.105.

[41] M.D. Slater, D. Kim, E. Lee, C.S. Johnson, Sodium-ion batteries, Adv. Funct. Mater. 23 (2013) 947–958. doi:10.1002/adfm.201200691.

[42] K. Kubota, S. Komaba, Review—Practical Issues and Future Perspective for Na-Ion Batteries, J. Electrochem. Soc. 162 (2015) A2538–A2550. doi:10.1149/2.0151514jes.

[43] J.-Y. Hwang, S.-T. Myung, Y.-K. Sun, Sodium-ion batteries: present and future, Chem. Soc. Rev. 46 (2017) 3529–3614. doi:10.1039/C6CS00776G.

[44] P.K. Nayak, L. Yang, W. Brehm, P. Adelhelm, From Lithium-Ion to Sodium-Ion Batteries: Advantages, Challenges, and Surprises, Angew. Chemie - Int. Ed. 57 (2018) 102–120. doi:10.1002/anie.201703772.

[45] S.W. Kim, D.H. Seo, X. Ma, G. Ceder, K. Kang, Electrode materials for rechargeable

sodium-ion batteries: Potential alternatives to current lithium-ion batteries, Adv. Energy Mater. 2 (2012) 710–721. doi:10.1002/aenm.201200026.

[46] E. De La Llave, V. Borgel, K.J. Park, J.Y. Hwang, Y.K. Sun, P. Hartmann, F.F. Chesneau, D. Aurbach, Comparison between Na-Ion and Li-Ion Cells: Understanding the Critical Role of the Cathodes Stability and the Anodes Pretreatment on the Cells Behavior, ACS Appl. Mater. Interfaces. 8 (2016) 1867–1875. doi:10.1021/acsami.5b09835.

[47] C. Vaalma, D. Buchholz, M. Weil, S. Passerini, A cost and resource analysis of sodium-ion batteries - Supplementary Information, (2018).

[48] M. Meeus, G. Pace, Current and future development of battery technology and its suitability within smart grids, (2013).

[49] G. Ramos-Sanchez, F.A. Soto, J.M. Martinez de la Hoz, Z. Liu, P.P. Mukherjee, F. El-Mellouhi, J.M. Seminario, P.B. Balbuena, Computational Studies of Interfacial Reactions at Anode Materials: Initial Stages of the Solid-Electrolyte-Interphase Layer Formation, J. Electrochem. Energy Convers. Storage. 13 (2016) 031002. doi:10.1115/1.4034412.

[50] G. Fitzgerald, J. DeJoannis, M. Meunier, Multiscale modeling of nanomaterials: Recent developments and future prospects, Elsevier Ltd., 2015. doi:10.1016/B978-1-78242-228-0.00001-6.

[51] P. Verma, P. Maire, P. Novák, A review of the features and analyses of the solid electrolyte interphase in Li-ion batteries, Electrochim. Acta. 55 (2010) 6332–6341. doi:10.1016/j.electacta.2010.05.072.

[52] S. Kumar, P. Bhushan, S. Bhattacharya, Diagnosis of communicable diseases using papepr microfluidic platforms, 2017. doi:10.5599/obp.11.2.

[53] A.I. Zia, S.C. Mukhopadhyay, Electrochemical Sensing: Carcinogens in Beverages, 20 (2016). doi:10.1007/978-3-319-32655-9.

Chapter 3.

Nanotubular hard carbon derived from renewable natural seed gel as high performance sodium-ion battery anode

Abstract

Na-ion battery has been attracting significant attention lately due to the concerns about the limited reserves and high cost of Li. Hard carbon is recognized as a good anode material for Na-battery. In this work we present a novel approach to synthesize hard carbon with peculiar nanotubular morphology from a renewable resource in the form of natural gel derived from the commonly used Basil seeds (*Osimum Basilicum*) which swell over 30 times their weight by absorbing water. The natural gel derived hard carbon (NGHC) obtained by controlled pyrolysis of the freeze-dried mucilage possesses nanotubular morphology decorated with desirable surface defects attributed to the presence of oxygen functionalities. This hard carbon shows a good reversible capacity of 195 mAh g^{-1} at 100 mA g^{-1} with an impressive ~91% retention of initial capacity after 300 cycles and >96% Coulombic efficiency (CE) throughout. The comparison with commercial hard carbon also proves the better performance of NGHC over HC.

The following paper has been published based on the work presented in this chapter.

3.1 Introduction

Clean and renewable energy is the most intensely researched field today in view of its significant implications for our environment and hence our future. There are three major domains of activity in this field, namely energy conversion, storage and conservation. Amongst these, the area of energy storage is attracting most attention because the costs of electrical energy storage devices are currently extremely high and the availability of materials employed in such devices is scarce for large scale implementation of such devices for products ranging from portable electronics to pollution free electric vehicles. Researchers are therefore looking for low cost, earth abundant, and preferably renewable precursor materials for electrodes of storage devices such as batteries and supercapacitors. [1,2] Realization of high energy and power densities, and good cycling stability is the cherished goal of this research.

Among the rechargeable batteries, as mentioned at length in previous chapters, although the Li-ion battery continues to be the main player, Sodium (Na) ion battery (NIB) has gained a huge attention lately due to the many-fold higher abundance of Na over Li, and the expected similarities in the basic Li and Na chemistry (belonging to same group etc.). [3,4] Indeed, this alluring alternative has already shown promise to compete with its well established and famous adversary.[5] However, NIBs are yet to be commercialized due to some basic problems that arise due to the variance factors between Li and Na. These include the ionic radii difference between Li and Na, irreversible trapping of Na into the pores leading to higher extraction voltages for Na than Li, electroplating of Na at low insertion voltage etc. [6] Due to the aforementioned reasons, extensive research is being carried out to explore new materials and morphologies that allow better insertion and de-insertion of Na in spite of its bulky size without destabilizing the electrodes.

Amid the numerous electrode materials, carbonaceous materials have been extensively explored as anode in both the LIBs and NIBs owing to their chemical stability, adequate structural and morphological parameters for insertion of alkali metals, and availability of low cost precursors.[7,8] Graphite forms LiC_6 as the intercalated compound with Li and has most quality factors that suit very well for LIBs. Unfortunately, with its interplanar spacing of 0.335 nm graphite is not suitable as an insertion anode for Na-

battery because of the higher ionic radius of Na (0.102 nm) as compared to that of Li (0.77 nm).

On the other hand, hard carbons are considered to be adequate for Na insertion[9] since the corresponding d-spacing is higher and process tunable (0.37 nm and above) due to the dislocation of planes and presence of cross-linking sp^3 carbons providing better insertion space for the Na ions at low voltage.

Till date many cheap and naturally occurring carbon precursors have been exploited as sources for synthesizing porous carbons for NIBs. These include banana peels,[10] wood,[11] oatmeal [12] etc. These precursors provide hard, low surface area carbon having more interlayer spacing than graphite. Mitlin and co-workers [10] employed banana peels to obtain hard carbon showing a good reversible capacity of 330 mAh g⁻¹ at 50 mA g⁻¹ with 88% of capacity retention over 290 cycles. Sun et al.[13] reported use of shaddock peels to get hard carbon with reversible capacity of 350 mAh g⁻¹ at 50 mA g⁻¹ with first cycle Coulombic efficiency (CE) as 69%. Li et al.[14] used hard carbon micro-spherules obtained by sucrose hydrothermal treatment and pyrolysis giving specific capacity of 300 mAh g⁻¹ at 30 mA g⁻¹. The holly-leaf derived lamellar carbon reported by Guo and co-workers [15] showed a reversible capacity of 254 mAh g⁻¹ at 20 mA g⁻¹ attributed to the enlarged nano- and meso-pores of the lamellar carbon. Recently, Zhao and co-workers reported successful use of carbon nanoparticles (CNPs) derived by burning coconut oil for Na ion battery.[16] The soot obtained was treated with piranha solution to get carboxylated CNPs which showed specific capacity of 200 mAh g⁻¹ at 100 mA g⁻¹ after 200 cycles. In their interesting and informative article on biohydrogels such as chitosan, chitin etc., Armelin et al.[17] have discussed their use as electrolytes in charge storage applications. However, to the best of our knowledge, there is no report on the use of functional carbon material obtained by the pyrolysis of natural hydrogels for obtaining battery anode.

Herein, we report the synthesis of hard carbon with peculiar nanotubular morphology by controlled pyrolysis of freeze-dried renewable natural seed gel, with property features that are most suitable for a robust Na battery anode. In the following, we refer to this carbon as Natural Gel Derived Hard carbon (NGHC). We have not used any activation agent, and the process is simple, cost effective, and readily scalable; a first of its kind. The source of carbon is the mucilage (gel) extracted from the commonly

used Ocimum Basilicum or Basil seeds rich in polysaccharides and lipids. The readily available Basil is known for pharmaceutical applications and is used as an herb to cure ulcer and diarrhoea [18]. It is also widely used in beverages in Asian countries.

The composition of the mucilage reported by Tharanathan et al. [19,20] is given in Table 1†. The components consist of carboxylic acid and hydroxyl groups. Their presence in the carbon forming precursor can potentially lead to the enhancement of the adsorption sites for Na by inducing surface defects in carbon. As stated by Han et al. [21] the presence of functional groups is very crucial for Na ion insertion. The NGHC obtained after the pyrolysis of Basil seed mucilage gives a good reversible capacity of 195 mAh g^{-1} at the current density of 100 mA g^{-1} with 91.2% retention of its first cycle specific capacity even after 300 cycles.

3.2 Experimental Section

3.2.1 Material Synthesis

The synthesis protocol for NGHC is shown in Scheme 1. Briefly, the seeds of Ocimum Basilicum or Basil were soaked in DI water overnight. They absorb significant quantity of water (over 30 times own weight), swell, and form a gel. The seed mucilage was extracted by removing the seed nucleus and kept for freeze drying. The gel or mucilage forms white flakes which are cotton like, extremely light weight and soft. The freeze dried flakes were pyrolyzed at 1000°C for 6 hours under continuous Argon flow at a heating rate of 5°C min^{-1}. The yield is approximately 10% w/w from the starting material. The obtained carbon was treated with 1M HCl to wash off impurities. The material was washed several times with aliquots of DI water till the pH was neutral. Then it was dried overnight at 80 °C and used for all the characterizations and further work on battery anode.

3.2.2 Material Characterization

Powder X-Ray diffraction was done using Bruker D8-Advance X-ray Diffractometer (Germany) with Cu kα (wavelength = 1.5418 Å). The RAMAN study was performed using LABRAM HR800 from Jobin Yvon Horiba. Scanning electron microscopy (SEM) was done using FEI Nova Nano 450 SEM. The High-resolution transmission electron (TEM) microscopy was performed with FEI, Tecnai F30, FEG system with
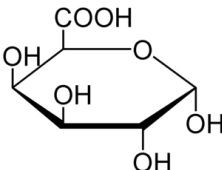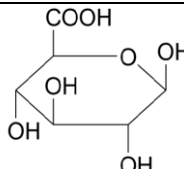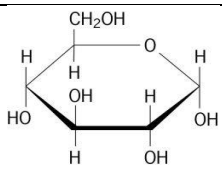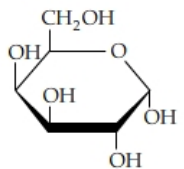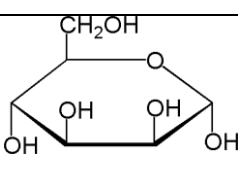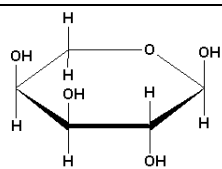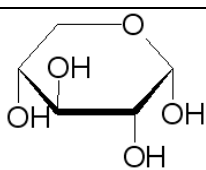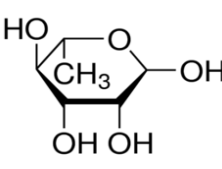
Component	Structure	% fraction
D-galacturonic acid		6.1
D-mannuronic acid		3.3
D-glucose		25.0
D-galactose		24.4
D-mannose		10.0
L-arabinose		12.4
D-xylose		7.5
L-rhamnose		7.0

Table 1. Chemical composition of basil seed mucilage.
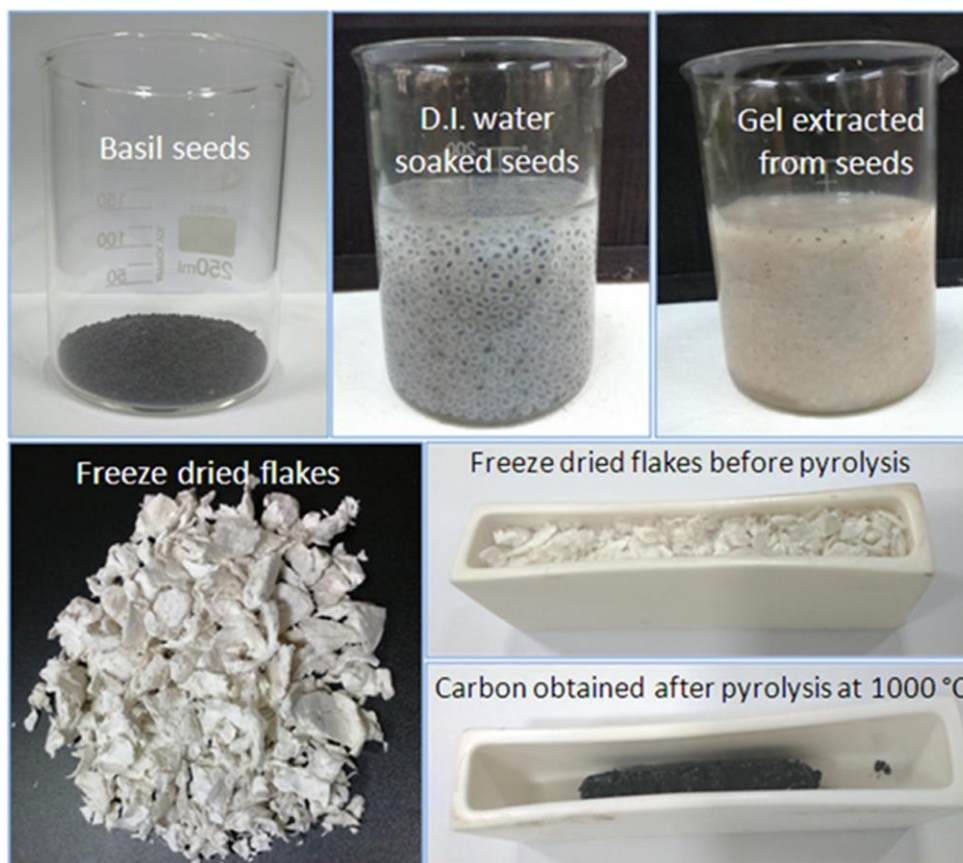
Scheme 1. Synthesis protocol of NGHC.

300 kV. The Brunauer-Emmett-Teller (BET) adsorption measurements for surface area calculation were done using Quadrasorb automatic volumetric instrument. X-ray Photoelectron Spectroscopy (XPS) study was performed using a PHI 5000 Versa Probe II equipped with a mono-chromatic Al Ka (1486.6 eV), a X-ray source and a hemispherical analyzer. The Fourier transform infrared spectroscopy (FTIR) was done using a NICOLET 6700 FTIR spectrophotometer.

3.2.3 Electrochemical Measurements

The electrodes were prepared by making slurry of NGHC, conducting carbon, and PVDF binder in the weight ratio 85:10:5 using NMP as solvent. The slurry was coated onto a Cu foil and the foil was kept for drying overnight at 80 °C. The foil was then punched into 1 cm2 circular discs. The CR 2032 coin cells were assembled using NGHC as working electrode and Na metal as reference electrode. The microporous glass fiber separator (Whatman, UK) was used as the separator and 1M NaClO4 in EC: DMC (1:1 volume) was used as the electrolyte. Galvanostatic charge discharge measurements were done with BTS-Neware (China) 5V, 10mA battery tester. The

impedance and cyclic voltammetry were done with VMP3 biologic system equipped with potentiostat and galvanostat channels.

3.3 Results and discussion

3.3.1 Physical Characterizations: The freeze dried gel composition was investigated using Fourier Transform Infra-red spectroscopy (FTIR) and has been discussed in Figure 1. To study the properties of the freeze dried and pyrolyzed NGHC, various characterization techniques were employed which have been discussed in this section.

The powder X-ray analysis in Figure 2(a) of NGHC shows the characteristic peaks of amorphous carbon. The two broad peaks having 2θ at $23.57°$ and $43.64°$ correspond to the (002) and (100) planes of the disordered carbon.[22] The (002) plane depicts the layered graphitic structure i.e. the stacking of 2D graphite sheets, whereas the (100) plane is known to be the graphite diffraction plane. The sample exhibits a certain number of sharp peaks appearing along with the characteristic carbonaceous broad peaks shown in the plot which can be attributed to the metal impurities. After acid treatment these features disappear as indicated by the comparison plot. The interlayer distance from Bragg's diffraction law is 0.38nm. This shows that the hard carbon thus obtained flaunts more interlayer spacing than pure graphite (0.335nm) and can easily accommodate Na ions efficiently serving the purpose of an anode.
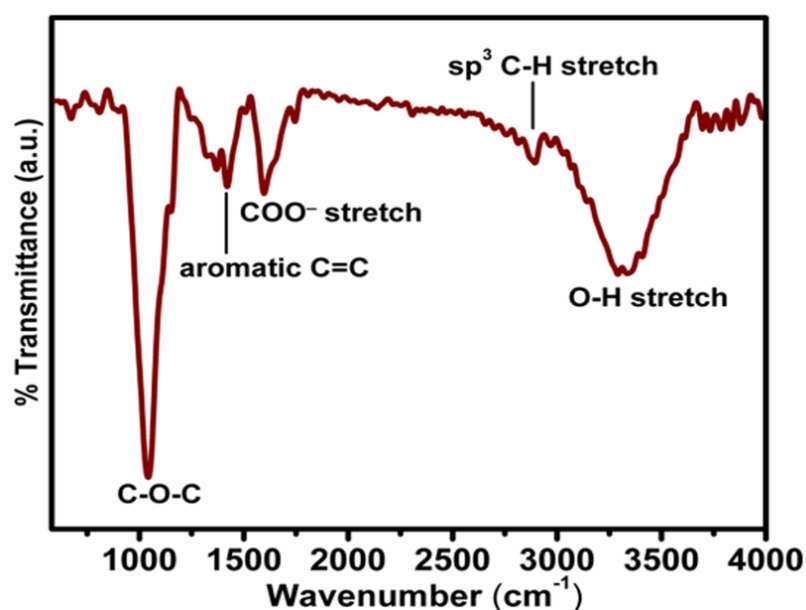
Figure 1. FTIR of freeze dried mucilage.
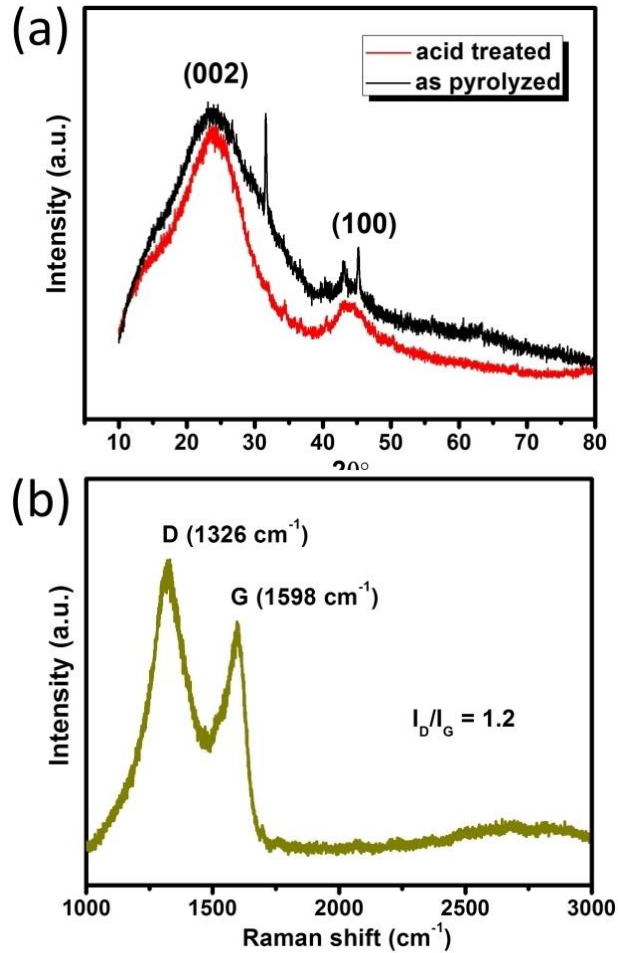
Figure 2. (a) PXRD patterns of as pyrolyzed and acid treated NGHC (b) RAMAN of NGHC.

Figure 2(b) depicts the typical Raman spectrum of NGHC. The D-band at 1326 cm^{-1} refers to the disordered structure resulting from the A_{1g} phonons breathing mode vibrations of sp^3 hybridized carbon. [21,23] The G-band at 1598 cm^{-1} arises due to the stacking of sp^2 bonded carbon atom planar sheets in graphite like materials.[24] This implies that the carbon has graphite like planar geometry but the planes are randomly oriented which in turn leads to more interlayer spacing. The intensity ratio of the D-band and G-band is 1.2, more than that of graphite (< 1) which means the carbon obtained is defective in nature.The defects can be credited to the oxygen containing groups present in the carbon as discussed earlier. This is a desirable attribute in the context of the charge storage application at hand.

The scanning electron microscopy (SEM) images of NGHC primarily exhibit the presence of fibrous or nanotubular structures as shown in Figure 3 (a), (b) with

occasional sheets with nanocurls. As is well known, the curling of graphene-like sheet occurs due to geometrical defects. As stated above, in our case the surface functionalities in the precursor are responsible for defect formation and are therefore also the reason for the curling of the evolving graphene-like sheets leading to nanotubule formation. The nanotubes are typically in the diameter range of 100-200 nm, as shown in the images, although a hierarchical distribution in nanotubule diameter can be easily noted.
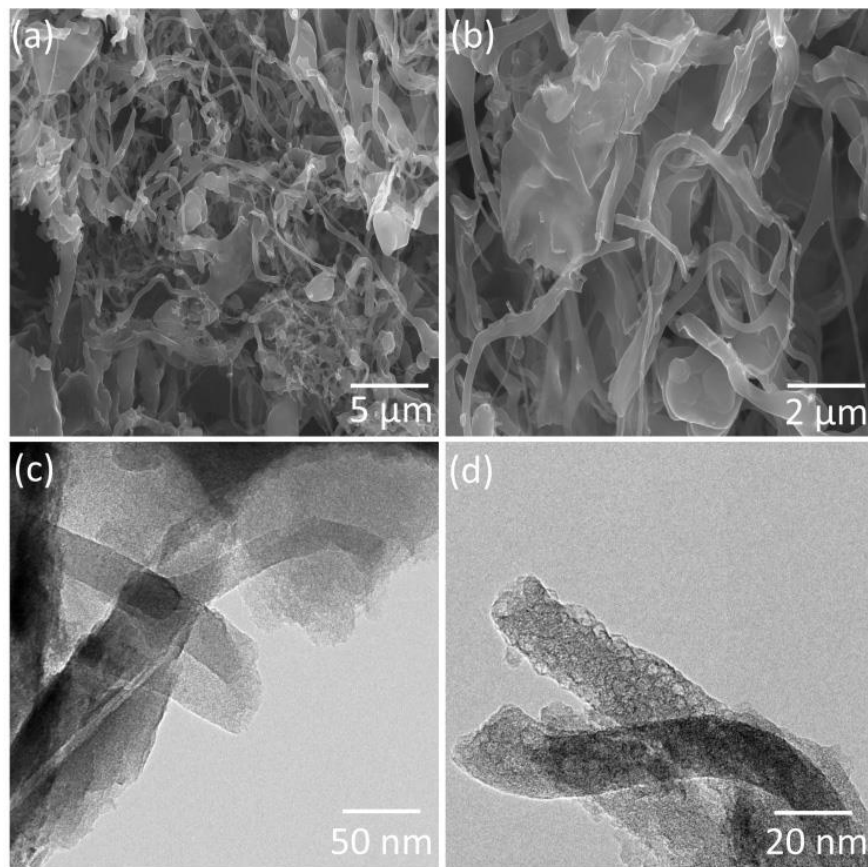
Figure 3. (a),(b) SEM and (c),(d) HRTEM images of NGHC.

These tubules can facilitate the transport of Na ions leading them to the adsorption sites [25] activated by local defects, which can render additional storage capacity to the hard carbon. The transmission electron microscopy (TEM) images shown in Figure 3 (c), (d) also reveal the microstructure of the nanotubular structures more clearly. The tubular structures can be seen to be having pores which contribute to the porosity in NGHC giving rise to the adsorption of Na metal at a low potential. [26] The absence of long range order also implies that it is an amorphous carbon. Thus, the structural features

seen from the SEM and TEM images corroborate the hard carbon nature of NGHC with a peculiar nanotubular morphology.

The N2 adsorption isotherm shown in Figure 4a obtained by BET analysis exhibits Type-IV nature which indicates the multilayer adsorption due to capillary condensation.[27] This is favorable for the battery application as different adsorption sites are available for the ions to get inserted or adsorbed.

The surface area of NGHC is 40 m^2 g^{-1}; an expected and desired valued for a typical hard carbon. The pore size distribution proclaims the mesoporosity of NGHC as the average pore size is 3 nm shown in Figure 3b. These statistics follow well with the broad characteristics of the hard carbon derived from biomass or natural precursors.

The X-ray photoelectron spectra were recorded to understand the chemical states of carbon and oxygen in NGHC. The C 1s and O 1s spectra are shown in Fig. 3. The XPS spectrum for C 1s in Fig. 3c is de-convoluted into four peaks. The peak at 284.79 eV represents the sp3 bonded carbon atoms supporting the graphene sheet edges.[28,29]
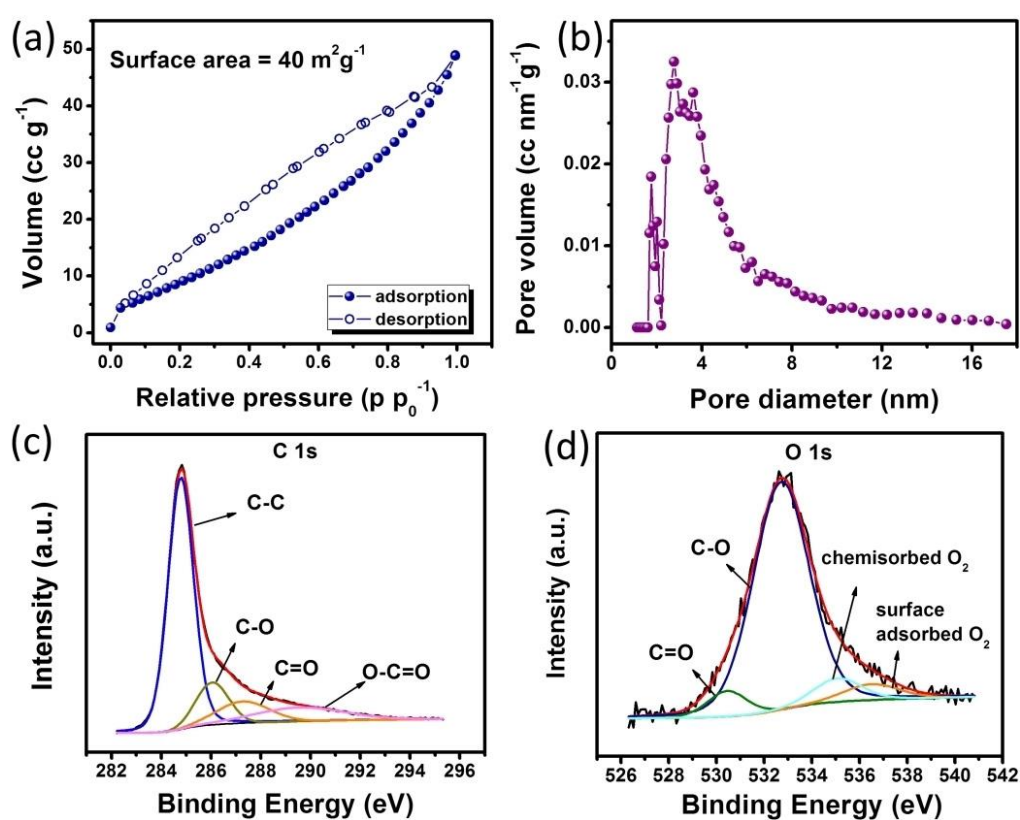
Figure 4. (a) N2 adsorption desorption isotherms; (b) pore size distribution of NGHC and X-ray photoelectron spectra (XPS) for (c) C 1s; (d) O 1s of NGHC.

The presence of hydroxyl and epoxy functional groups is evident from the C-O peak at 286.05 eV and C=O peak at 287.27 eV. A small carboxylate peak at 289.54 eV is also seen in the spectrum.[30] The O 1s spectrum in Fig. 3d exhibit C=O and C-O peaks at 530.44 eV and 532.72 eV, respectively. The peaks at 535.07 eV and 536.5 eV mark the chemisorbed and surface adsorbed oxygen [31,32] in NGHC owing to the components present in the gel. Thus the XPS analysis gives the evidence of the presence of surface functionalities in NGHC which could serve as the additional adsorption sites helpful for capacity enhancement.

3.3.2 Electrochemical performance

The cyclic voltammograms were recorded from 0.01 to 3 V at the scan rate of 0.1 mV s-1 against Na/Na+. As seen in Figure 5 (a), the first cathodic scan shows a broad peak from 1.3 to 0.3 V which is the characteristic SEI layer formation [33] in carbonaceous materials and it disappears in the next cycles. The second peak in the cathodic scan is at 0.09 V which depicts the insertion of Na into hard carbon. The subsequent peak in the anodic scan appears at 0.14 V giving the de-insertion of Na ions.[34] The pair of redox peaks is reproduced in further cycles with slight shift in the potential. The CV is stable up to 15 cycles with both peaks intact in nature. In order to study the change in the impedance at different interfaces, electrochemical impedance spectroscopy was performed after 5th, 10th and 15th cycles of CV given in Figure 4(b). The obtained Nyquist plot was fitted to an equivalent circuit as shown in Figure 6.
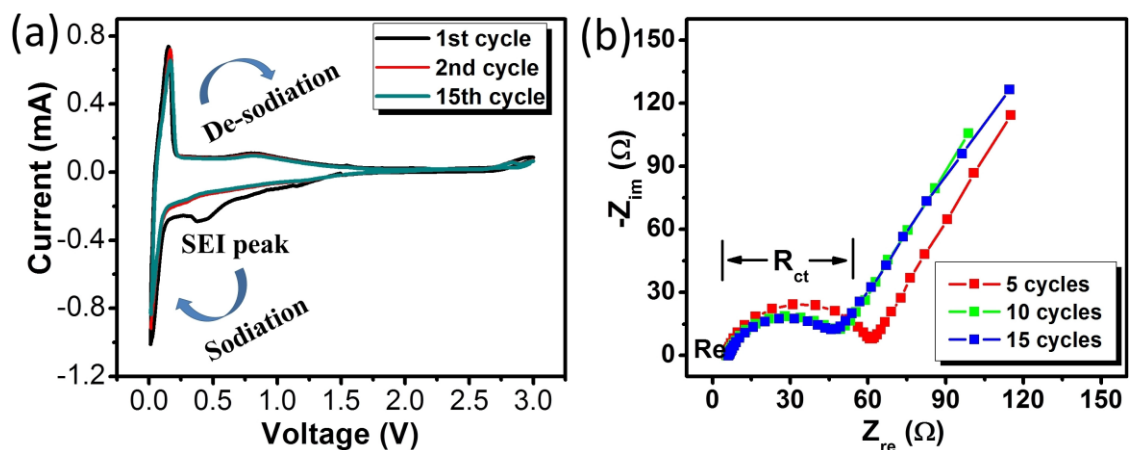
Figure 5. (a) CV curves in the range 0.01-3 V vs. Na/Na$^+$ at scan rate of 0.1 mV s^{-1} and (b) Nyquist plot of NGHC.

The Nyquist plot consists of semicircle region at high frequency region and straight line in low frequency region. The circuit consists of R_e, the total resistance of the electrolyte, electrode and separator; CPE 1 (C1 in Figure 6) and R_f belongs to capacitance at the surface film and impedance faced by Na ions in the SEI bulk; CPE 2 (C2 in Figure 6)and R_{ct} are the double layer capacitance and charge transfer resistance, respectively; Z_w is the Warburg impedance related to Na ion diffusion in the carbon electrode; C3 is the capacitance related to Na ion insertion into the sites of hard carbon.[35] It is clear from the figure that as the number of cycles increases the diameter of the semicircle decreases along with a depression in Z_{im}. The important kinetic parameters are listed in Table S2. There is no considerable change in the R_e value. The R_{ct} value calculated from the fit decreases with the number of cycles indicating that the Na ions do pass through SEI easily. Collectively, it could be inferred that the compactness of SEI increases with the number of cycles. No significant change is observed in the other parameters Z_w and C3.
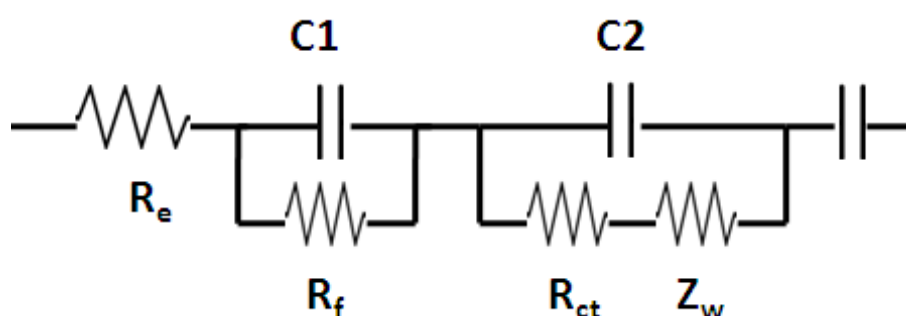
Figure 6. Equivalent circuit of Nyquist plot.

R_e	R_{ct}	C3
5.8 (After 5cycles)	49.25	0.018
5.9 (After 10cycles)	33.58	0.015
6.4 (After 15cycles)	31.24	0.019

Table 2. Different resistance values from Nyquist plot.

The galvanostatic charge discharge measurements carried out at the current density of 100 mA g^{-1} are shown in Figure 7 (a). It shows an initial discharge capacity of 378 mAh g^{-1}. There is a sloping region from 1.5 V to 0.3 V which is due to the formation of solid electrolyte interphase [36] layer on the surface of the anode mainly from the electrolyte decomposition and/or other side reactions taking place on the surface due to the presence of defects. This leads to the irreversible loss in the specific capacity of the anode. Depending upon the material and the surface reactions, this loss can be huge or less. Importantly, NGHC has a reversible specific capacity of 214 mAh g^{-1} and thus a relatively low irreversible capacity loss. The curves evince typical insertion nature and can be divided into two regions. One is the sloping voltage region from 1.0 V to 0.02 V arising due to the randomly oriented graphitic planes of hard carbon. The Na insertion potential varies for different insertion sites resulting into a slope in the curve. The second is the low potential plateau region near 0.01 V which marks the onset of pore filling or adsorption of metal into nano-porosity regions in the carbon. The Na metal gets inserted into the sites having a potential coinciding with the metal itself.[37] This leads to a voltage close to 0 V and a well-defined plateau. This refers to the turbostratic nature of NGHC facilitating Na ion insertion. The specific capacity and nature of the curve are maintained well in the subsequent cycles.

The carbon anode was tested at different current densities ranging from 50 mA g^{-1} to 2000 mA g^{-1}. The rate performance of NGHC is shown in Figure 7 (b). The specific capacity values were 250 mAh g^{-1}, 226 mAh g^{-1}, 198 mAh g^{-1}, 170 mAh g^{-1}, 143 mAh g^{-1}, 124 mAh g^{-1}, 102 mAh g^{-1} and 95 mAh g^{-1} for 50 mA g^{-1}, 100 mA g^{-1}, 200 mA g^{-1}, 500 mA g^{-1}, 750 mA g^{-1}, 1000 mA g^{-1}, 1500 mA g^{-1} and 2000 mA g^{-1}, respectively. When the current density was reduced from 2000 mA g^{-1} to 200 mA g^{-1}, 95% of the initial capacity was recovered. This elucidates the excellent sustainability of NGHC electrode towards the higher current densities.

The NGHC has splendid cyclic performance as evident from Figure 7 (c). The carbon retains a high specific capacity of 195 mAh g^{-1} at 0.1 A g^{-1} after 300 cycles showing only 8.8% loss of its initial capacity. The first cycle Coulombic efficiency (CE) for the NGHC is 58% and rises to 99% in the second cycle and varies between 96 , CE , 100 throughout the cycling. Thus the carbon obtained shows very impressive cycling stability and Coulombic efficiency. With these performance features our NGHC stands
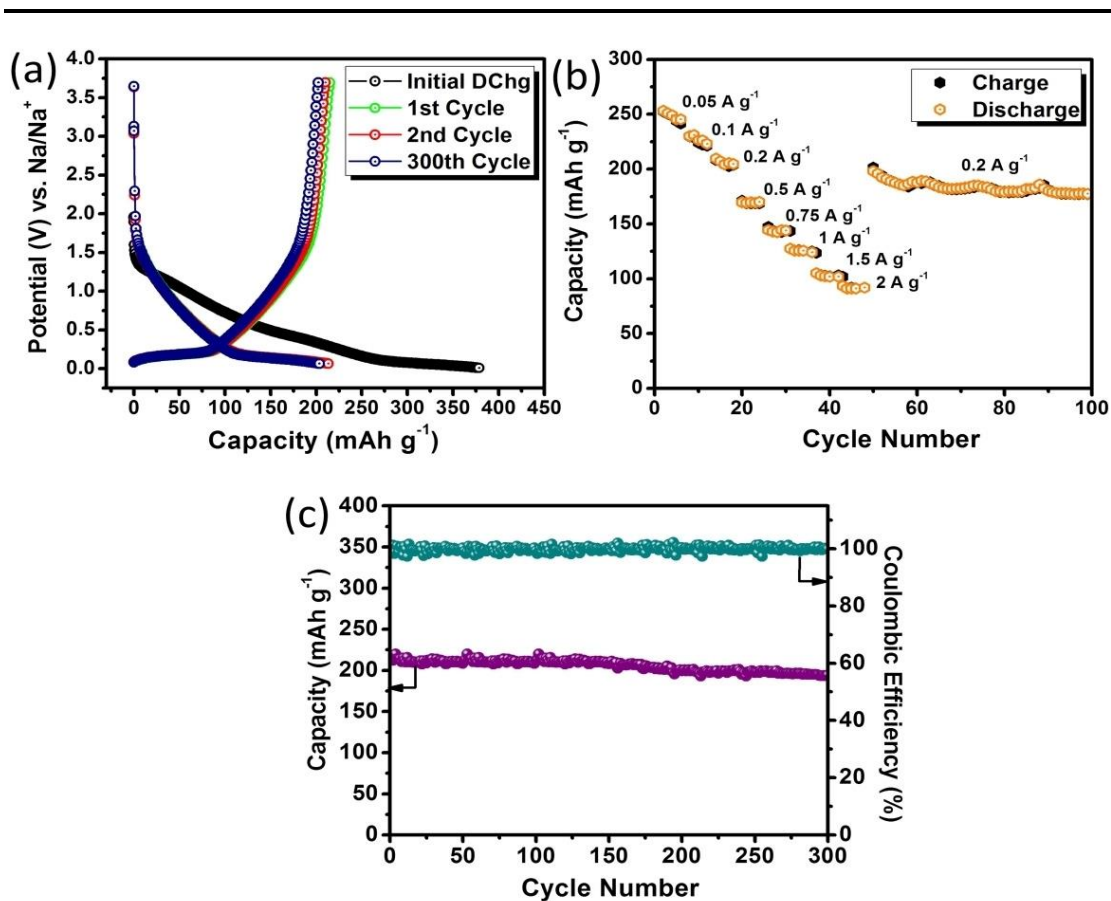
Figure 7. (a) Charge discharge curves at 0.1 A g^{-1}; (b) Rate performance at different current densities of NGHC; (c) Cycling stability and Coulombic efficiency plot of NGHC.

out fairly well in the family of biomass derived carbons reported by previous interesting studies, especially in respect of good specific capacity along with high cycling stability at a high current density of 0.1A g^{-1} and high Coulombic efficiency (>97% throughout).

Figure 8 (a) shows the charge discharge curve nature comparison of NGHC and commercial hard carbon (HC). It is seen that NGHC has a well-defined plateau in low voltage region similar to HC which is a good characteristic of any material to be used in battery. Figure 8 (b) demonstrates the rate performance comparison of NGHC and commercially available HC. It is evident from the plot that though the commercial HC delivers higher capacity at low current density of 0.05 A g^{-1} (which is too low for practical applications), but it can't withstand high current densities above 0.1A g^{-1} and the value drops drastically whereas NGHC performs fairly well under high current rates. Thus, NGHC if seen from commercial point of view has the capability to deliver good capacity at high rates. A table of comparison among various biomass derived hard
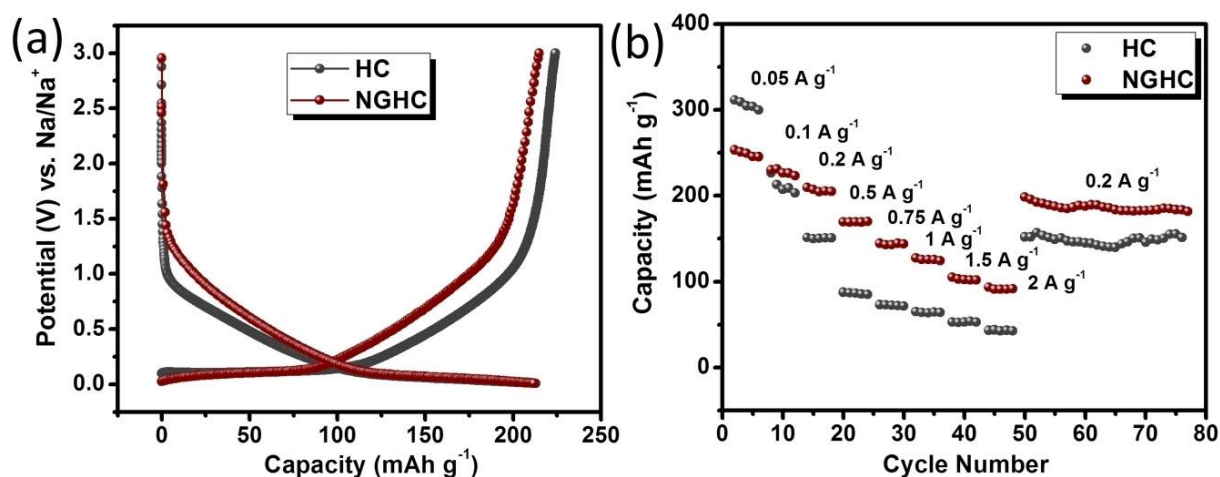
Figure 8. (a) Charge discharge curves of NGHC and HC at 0.1 A g^{-1}; (b) Comparison of Rate performance at different current densities of NGHC and HC.

carbons from different sources with NGHC is provided to analyze where NGHC stands in terms of performance when compared with literature.

3.4 Conclusions

A novel approach is presented to synthesize high quality hard carbon for Na ion battery anode by controlled pyrolysis of a natural gel derived from the commonly used Basil seeds (Ocimum Basilicum) which swell by absorbing water over 30 times their weight. The hard carbon obtained by pyrolysis of the freeze-dried mucilage possesses peculiar sheet-like and tubular morphology decorated with oxygen-related surface defects originating from oxygen containing functionalities namely polysaccharides and lipids present in the gel. The NGHC thus synthesized shows a very good reversible capacity of 195 mAh g^{-1} at a current density of 0.1 A g^{-1} and excellent rate performance with specific capacity of 95 mAh g^{-1} even at a very high current density of 2 A g^{-1}. Moreover, when the current density is reduced to 0.2 A g^{-1}, the NGHC shows 95% retention of its initial capacity. The cycling stability of NGHC is also very good and it retains 91.2% of its first cycle capacity (214 mAh g^{-1}) after 300 cycles, with >97% Coulombic efficiency throughout. We believe that NGHC derived from the Basil seed mucilage stands out as a good anode material in the category of biomass derived hard carbons and thus can be commercialized as a Na ion battery anode as illustrated by comparing it with commercial hard carbon. Thus, NGHC if seen from commercial point of view has the capability to deliver good capacity at high rates.

Source of carbon	Process	Type of carbon obtained	Specific capacity (mAh g^{-1})	Current density	Cycles
Coconut oil	Burning oil wick collecting soot	Carbon nano particles	200	100	200
Peat moss	Pyrolysis and KOH treatment	Carbon nano sheets	255	100	200
Sucrose	Pyrolysis with GO	G-Hard Carbon Only HC	274 85	20 20	200 200
Shaddock peels	Pyrolysis	Hard Carbon	352	50	200
Banana Peels	Pyrolysis	Hard Carbon	330	50	50
Wood	Pyrolysis	Hard Carbon		10	
Ramie Fibres	Pyrolysis	3D-carbon micro structure	122	100	100
Corncobs	Pyrolysis	2D-carbon sheets	139	100	100
Pomelo peels	H3PO4 treatment and pyrolysis	Hard carbon	181	200	220
Sucrose	Hydrothermal and pyrolysis	Hard carbon micro spherules	300	30	100
Blue green algae	Pyrolysis	Carbon	230	20	60
Peanut skin	KOH treatment and pyrolysis	Hierarchical porous carbon	148	500	200
Holly leaf	Hydrothermal and pyrolysis	Lamellar hard carbon	254	20	100
Oatmeal	Hydrothermal and pyrolysis	N-doped carbon microspheres	336	50	50
This work	**Pyrolysis**	**Hard Carbon**	**200**	**100**	**210**

Table 3. Comparison of specific capacities of different biomass derived carbons.

References

[1]   L. Xiao, Y. Cao, W.Henderson, M. L.Sushko, Y. Shao, J. Xiao, W. Wang, M.H.Engelhard, Z. Niec and J. Liu, Nano Energy 19 (2016) 279-288.

[2]   M. D. Slater, D. Kim , E. Lee M. Doeff and C. S. Johnson, Adv. Funct. Mater. 23 (2012) 947-958.

[3]   E. Irisarri, A. Ponrouch and M. R. Palacin, J. Electro . Soc. 162 (2015) A2476-A2482.

[4]   S. Peng , X. Han, L. Li, Z. Zhu, F. Cheng, M. Srinivansan, S. Adams and S. Ramakrishna, Small 12 (2016) 1359-1368.

[5]   S. Komaba, W. Murata, T. Ishikawa, N. Yabuuchi, T. Ozeki ,T. Nakayama, A. Ogata, K. Gotoh and K. Fujiwara, Adv. Funct. Mater. 21 (2011) 3859-3867.

[6]   G. Hasegawa, K. Kanamori, N. Kannari, J. Ozaki, K. Nakanishi and T. Abe, Chem. Electro. Chem. 2 (2015) 1917-1920.

[7]   M. Wang , Z. Yang , W. Li , L. Gu and Y. Yu, Small 12 (2016) 2559-2566.

[8]   D. Zhou, M. Peer, Z. Yang, V. G. Pol, F. D. Key, J. Jorne, H. C. Foley and C. S. Johnson, J. Mater. Chem. A 4 (2016) 6271-6275.

[9]   J. Sun, H.W. Lee, M. Pasta, H. Yuan, G. Zheng, Y. Sun, Y. Li and Y. Cui, Nature Nanotechnology 10 (2015) 980-985.

[10]   E. M. Lotfabad, J. Ding, K. Cui, A. Kohandehghan, W. P. Kalisvaart, M. Hazelton and D. Mitlin, ACS Nano 8 (2014) 7115-7129.

[11]   F. Shen, W. Luo, J. Dai, Y. Yao, M. Zhu, E. Hitz, Y. Tang, Y. Chen, V. L. Sprenkle, X. Li and L. Hu, Adv. Energy Mater. 6 (2016) 1600377-1600384.

[12]   D. Yan, C. Yu, X. Zhang, W. Qin, T. Lu, B. Hu, H. Li and L. Pan, Electrochimica Acta 191 (2016) 385-.391

[13]   N. Sun, H. Liu and B. Xu, J. Mater. Chem. A 3 (2015) 20560-20566.

[14]   Y. Li, S. Xu, X. Wu, J. Yu, Y. Wang, Y. S. Hu, H. Li, L. Chen and X. Huang, J. Mater. Chem. A 3 (2015) 71-77.

[15]   P. Zheng, T. Liu, X. Yuan, L. Zhang, Y. Liu, J. Huang, S.Guo, Sci. Rep. 6 (2016) 26246-26255.

[16]   R. R. Gaddam, D. Yang, R. Narayan, KVSN Raju, N. A. Kumar, X. S. Zhao, Nano Energy 26 (2016) 346-352.

[17]   E. Armelin, M. M. P´erez-Madrigal, C. Alem´an and D. D´. D´ıaz, J. Mater. Chem. A 4 (2016) 8952-8968.

[18]   M. Biswal, K. Bhardwaj, P. K. Singh, P. Singh, P. Yadav, A. Prabhune, C. V. Rode and S. B. Ogale , RSC Advances 3 (2013) 2288-2295.

[19]   Y. V. Anjaneyalu and R. N. Tharanthan, Aust. J. Chem. 24 (1971) 1501-1507.

[20]   R. N. Tharanthan and Y. V. Anjaneyalu, Aust. J. Chem. 28 (1975) 1345-1350.

[21]   Y. J. Kang, S. C. Jung, J. W. Choi and Y. K. Han, Chem. Mat. 27 (2015) 5402-5406.

[22]   R. Alcántara, P. Lavela, G. F. Ortiz and J. L. Tirado, Elec. S. State Lett. 8 (2005) A222-A225.

[23]   J. R. Dennison, M. Holtz and G. Swain, Spectroscopy 11 (1996) 38-45.

[24]   K. Hong, L. Qie, R. Zeng, Z. Yi, W. Zhang, D. Wang, W. Yin, C. Wu, Q. Fan, W. Zhang and Y. Huang, J. Mater. Chem. A 2 (2014) 12733-.

[25]   D. S. Su and R. Schlçgl, Chem. Sus. Chem. 3 (2010) 136-168.

[26]   W. Luo, Z. Jian, Z. Xing, W. Wang, C. Bommier, M. M. Lerner and X. Ji, ACS Cent. Sci. 1 (2015) 516-522.

[27]   A. Grosman and C. Ortega, Langmuir 24 (2008) 3977-3986.

[28]   K. Yuan , Y. Xu , J. Uihlein , G. Brunklaus , L. Shi , R.Heiderhoff, M. Que, M. Forster, T. Chassé, T. Pichler, T. Riedl, Y. Chen and U. Scherf, Adv. Mater. 27 (2015) 6714-6721.

[29]   L. Ren, F. Yang, C. Wang, Y. Li, H. Liu, Z. Tu, L. Zhang, Z. Liu, J. Gaoa and C. Xua, RSC Adv. 4 (2014) 63048-63054.

[30]   D. H. Wang, Y. Hu, J. J. Zhao,L. L. Zeng, X. M. Tao and W. Chen, J. Mater. Chem. A 2 (2014) 17415-17420.

[31]   Y. J. Oh, J. J. Yoo, Y. I. Kima, J. K. Yoon, H. N. Yoon, J.-H. Kim and S. B. Park, Electro. Acta. 116 (2014) 118-128.

[32]   L.N. Mazalov, S.V. Tribuna, N. A. Kryuchkova, O. A. Tarasenko,S. V. Trubin and G. I. Zharkova, J. Struct. Chem. 48 (2007) 253-261.

[33]   X. Li, Y. Hu, J. Liu, A. Lushington, R. Li and X. Sun, Nanoscale 5 (2013) 12607-12615.

[34]   J.Ding, H. Wang, Z. Li, A. Kohandehghan, K. Cui, Z. Xu, B. Zahiri, X. Tan, E. M. Lotfabad, B. C. Olsen and David Mitlin, ACS Nano 7 (2013) 11004-11015.

[35]   D. Andrea, M. Meilera, K. Steinera, Ch. Wimmera, T. Soczka-Gutha and D.U. Sauer, J. P. Sources 196 (2011) 5334-5341.

[36]   D. A. Stevens and J. R. Dahn, J. Electrochem. Soc. 147 (2000) 1271-1273.

[37]   M.M. Doeff, Y. Ma, S. J. Visco and L. Jonghe, J. Electrochem. Soc. 140 (1993) L169-L170.

Chapter 4.

Carbon caged Si nanoparticles with high capacity and cycling stability for Li-ion battery anode

Abstract

Si-nanoparticles caged by carbon are synthesized by uniform loading of Si NPs in the natural gel during swelling, followed by high temperature pyrolysis of the freeze dried gel. The Si-GDC (gel derived carbon) renders an impressive specific capacity of 1460 mAh g^{-1} at 1 A g^{-1} with only a small irreversible capacity loss. It is highly stable even up to 250 cycles and exhibits an impressive value of 700 mAh g^{-1} even at a high rate of 2 A g^{-1}. Post cycling SEM images of Si-GDC confirm robust carbon encapsulation upon cycling and uniform SEI layer formation providing high stability.

Declaration: This is the original work and has not yet been published anywhere.

4.1 Introduction

As described in chapter 2, though Na ion batteries are a potential candidate to act as a replacement for Li ion batteries still there are many loop holes which need to be filled before the community starts relying on them completely. For that reason, Li ion battery research is being carried out in the context of Li-ion batteries have been playing a central role in the field of energy storage with diverse applications in areas such as portable electronics, electric mobility, and grid storage systems.[1],[2] While the cathodes are primarily composed of some multi-component metal oxide systems and organic compounds[3], there are many possible choices of anode materials belonging to the intercalation, alloying and conversion categories, with different strengths and weaknesses.[4],[5] Generally, graphite is used as anode mainly because of its high stability, safe operating potential, and good specific capacity.[6] Yet it is not found to be suitable for the emerging class of high energy applications.[7],[8] To enhance the power and energy density of the Li-ion battery, one ought to use anodes with high specific capacity.[9] The anode should have high power and energy density, cycling stability and should be environmental friendly with ease of synthesis. Needless to say that concurrent effort on enhancing the performance parameters of cathode materials is also equally important.[10] An important factor electrolyte which plays a vital role in battery performance has also been investigated experimentally as well as theoretically to check their viability in various environments.[11]

Silicon (Si) is an earth abundant material with an ability to form high-Li-alloy and therefore to render a high specific capacity. It is known to incorporate 4.4 Li atoms while reacting with Li which results into its high theoretical capacity of 4200 mAh g^{-1}.[12] Unfortunately the silicon-based anodes have an intrinsic issue of huge volume expansion (~300%) upon lithiation causing cracks and de-lamination of material from electrode during de-lithiation.[13],[14] This leads to a rapid capacity fade making it unsuitable for commercial applications. Si nanostructures like nanowires, nanotubes etc. have been proposed to mitigate this problem because such nanostructures the smaller particles reduce the overall size of Li-Si alloy minimizing volume expansion.[15],[16] Yi Cui and co-workers have published many seminar contributions describing the origin and minimization of the volume expansion of Si in a Li-ion battery anode.

In one of their papers it was demonstrated that use of Si nanowires instead of bulk Si shows 60% capacity retention after 50 cycles at 800 mA g^{-1}.[17] There are several interesting subsequent reports by Y. Cui group on the use of different nanostructures of Si for Li ion battery application.[18],[19] Another approach to address this complication is using a matrix framework to incorporate Si and allowing the Si expansion to occur within the confines of such matrix during cycling to avoid delamination of the material.[20] Carbonaceous materials like carbon nanofibers (CNFs), carbon nanotubes (CNTs), graphene sheets, core shell coating on Si particles have been employed.[21],[22] The coating or covering of carbonaceous materials protects Si particles from breaking apart and maintains the integrity of the electrode.[23] The efforts are currently directed towards developing a composite which is easy to synthesize, has the right set of properties, and involves environmentally friendly methods and compounds.[24]

In this work we report a facile, cheap and eco-friendly pyrolytic synthesis of conducting carbon coated Si nanoparticles (Si NPs) from a natural gel (basil seed derived) as a Li ion battery anode. The Si-gel derived carbon (Si-GDC) is synthesized by simple pyrolysis of freeze-dried Si NPs loaded basil seed gel to obtain Si NPs bunches embedded in carbon.
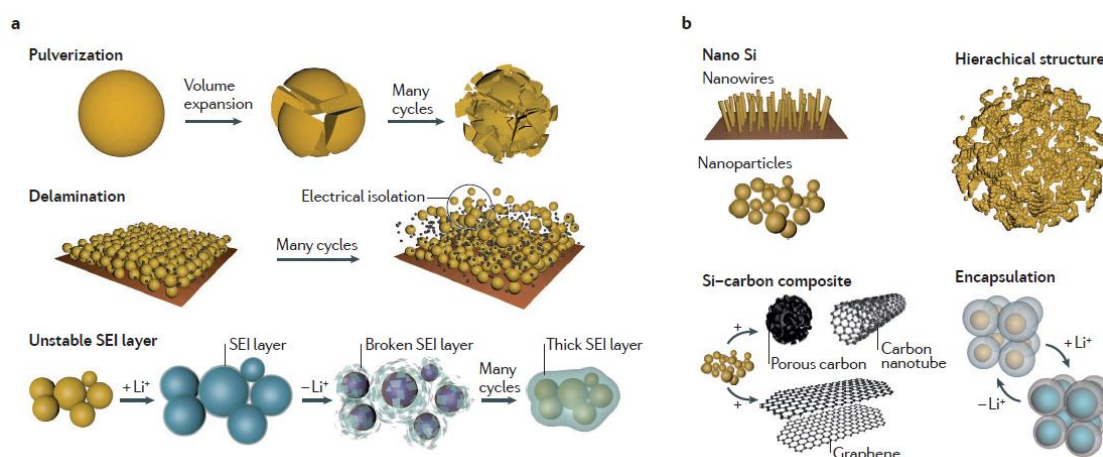
Figure 1. (a) Volume expansion in Si and (b) proposed methodologies to minimize it by growing nanostructures and encapsulation with carbonaceous materials. Copyright Springer Nature. Reproduced with permission of Ref [25].
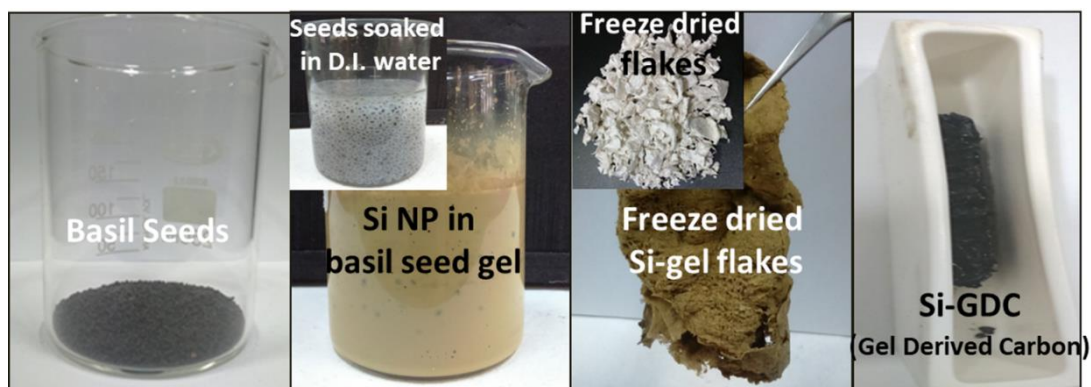
Figure 2. Synthesis protocol of Si-GDC.

The Si-GDC composite is remarkable as a Li-ion battery anode with specific capacity of 1460 mAh g^{-1} at high current density of 1A g^{-1} with superior cycling stability up to 250 cycles and a superior rate performance.

4.2 Experimental Section

4.2.1 Material Synthesis

Si NPs were procured form Global Nanotech with size of 70-80 nm. The synthesis protocol for Si-GDC is shown in Figure 2 as per our previuos report.[26] Briefly, the Si NPs were dispersed in DI water by sonication. The seeds of Basil (*Ocimum Basilicum)* were soaked in pre-sonicated Si NPs aqueous dispersion and kept overnight. The seed mucilage was extracted by removing the seed nucleus and kept for freeze drying. The freeze dried flakes were pyrolyzed at 1000 °C for 6 hours under continuous Ar flow at a heating rate of 5 °C min^{-1}. The obtained Si-GDC (Si-Gel derived carbon) with Si: C ratio to be 2:1 was used as synthesized.

4.2.2 Characterizations

Powder X-Ray diffraction was done using Bruker D8-Advance X-ray Diffractometer (Germany) with Cu kα (wavelength 1.5418 Å). The Raman study was performed using a Renishaw InVia microscope Raman system with a laser wavelength of 532 nm in the back scattering geometry laser power on the sample was 5 mW with a laser spot size 1 μm. Scanning electron microscopy (SEM) was done using FEI Nova Nano 450 SEM.

The High-resolution transmission electron (TEM) microscopy was performed using TEM (Model: TECNAI G2 20) instrument equipped with EDS attachment, operated at an accelerating voltage of 200 kV. The Brunauer-Emmett-Teller (BET) adsorption measurements for surface area calculation were done using Quadrasorb automatic volumetric instrument.

4.2.3 Electrochemical Measurements

The electrodes were prepared by making slurry of Si-GDC or Si NPs, conducting carbon, and CMC binder in the weight ratio 70:20:10 in DI water. The slurry was coated onto a Cu foil and the foil was kept for drying overnight at 80 °C and punched into 1 cm^2 circular discs. The CR 2032 coin cells were assembled with Li metal as reference electrode. Celgard 2500 was used as the separator and a commercial electrolyte with 1M LiPF$_6$ in EC: DMC (1:1 volume) was used with 10 % FEC as an additive. Galvanostatic charge discharge measurements were performed with BTS-Neware (China) 5V-10mA battery tester. The calculations were done considering only the Si weight in the electrode as in previous reports[27] with weight of the active material being 1.2-1.5 mg. The impedance and cyclic voltammetry voltammetry were performed with VMP3 biologic system equipped with potentiostat and galvanostat channels.

4.3 Results and Discussion

4.3.1 Physical Characterization

The powder x-ray diffraction (PXRD) data for Si NPs is presented in Figure 3. The pristine Si NPs render the expected characteristic peaks at 28.6°, 47.5° and 56.3°, which correspond to the (111), (220) and (311) planes of Si, respectively.[28] In the Si-GDC composite case, the Si peaks are intact with the superimposed carbon-related features as shown in Figure 4 (a). The powder XRD of GDC shows a broad peak at 23.57° indicating the (002) plane of disordered carbon and a small peak at 43.64° representing the (100) plane of carbon.[29] Although the (002) peak is clearly retained in the composite, the diminished (100) peak signifies the reduced in-plane ordering or smaller lateral crystallite size L$_a$ of the disordered carbon.[30]
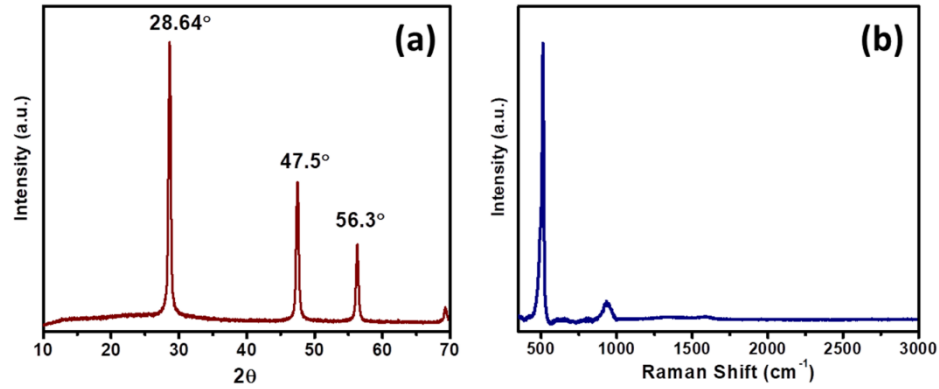
Figure 3. (a) PXRD and (b) RAMAN of pristine Si NPs.

The Raman spectrum of Si NPs in Figure 3(b) consists of bulk crystalline Si features also reflected in Si-GDC composite as seen from Figure 4 (b). A sharp peak at 510 cm^{-1} is ascribed to the first order phonon scattering and the Si-Si stretching vibration.[31] Also, it consists of the GDC related D-band at 1326 cm^{-1} which refers to the disordered structure resulting from the A_{1g} phonons breathing mode vibrations of sp^3 hybridized carbon and the G-band at 1598 cm^{-1} due to the stacking of sp^2 bonded carbon atom planar sheets in graphite like materials.[32]

The high I_D/I_G ratio in GDC is due to the reduced sp^3 content and increased ordered ring clusters which occurs in carbon with nanocrystalline graphitic domains according to the Ferrari and Robertson model.[33]
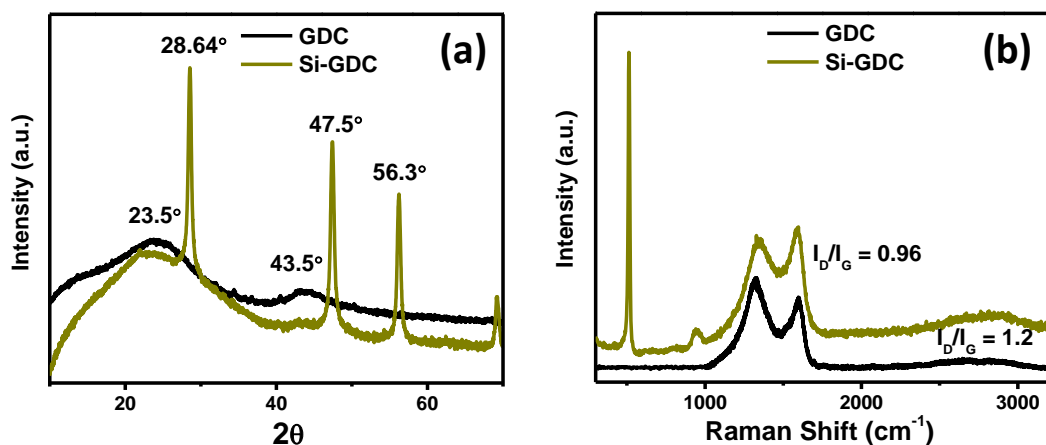
Figure 4. (a) PXRD pattern of GDC and Si-GDC; (b) Raman spectra of GDC and Si-GDC.
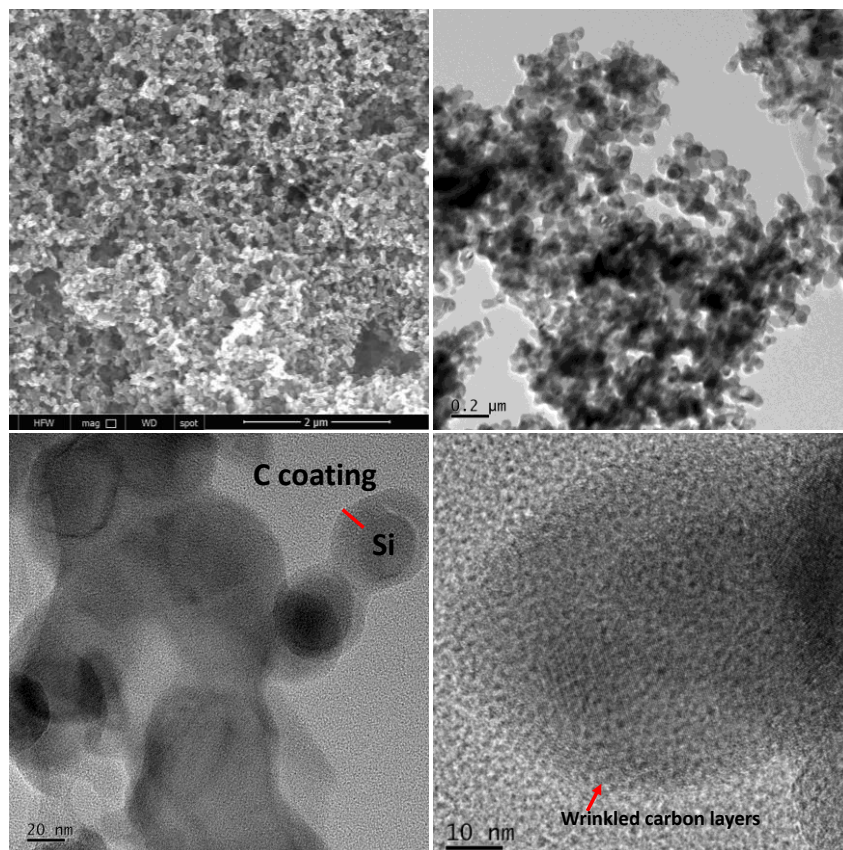
Figure 5. (a) SEM image; (b-d) HRTEM images of Si-GDC (inset- SAED pattern).

On the contrary, the lower I_D/I_G ratio in Si-GDC suggests significant reduction in defect density due to heterogeneous nucleation on the surface of Si NPs during the pyrolysis process. This would concurrently render better conductivity to the carbon which is desirable for the battery electrode application.

The optical micrographs of Si-GDC have been provided in Figure 5. The Si NPs bunches embedded into the carbon are evident from the SEM. The TEM images also reveal the same with the Si NPs completely engulfed into the conducting carbon layers. The wrinkled layers in Figure 4(d) signify the turbostratic nature of carbon.[34] This configuration could be quite helpful for the Li incorporation into Si NPs with the outer covering of carbon which prevents the cracking of the particles due to volume expansion during lithiation or de-lithiation. The N_2 adsorption isotherms for GDC and Si-GDC obtained by BET analysis are compared in Figure 6. The isotherms exhibit Type-IV nature which indicates multilayer adsorption due to capillary condensation. The surface area of GDC is 40 $m^2 g^{-1}$.
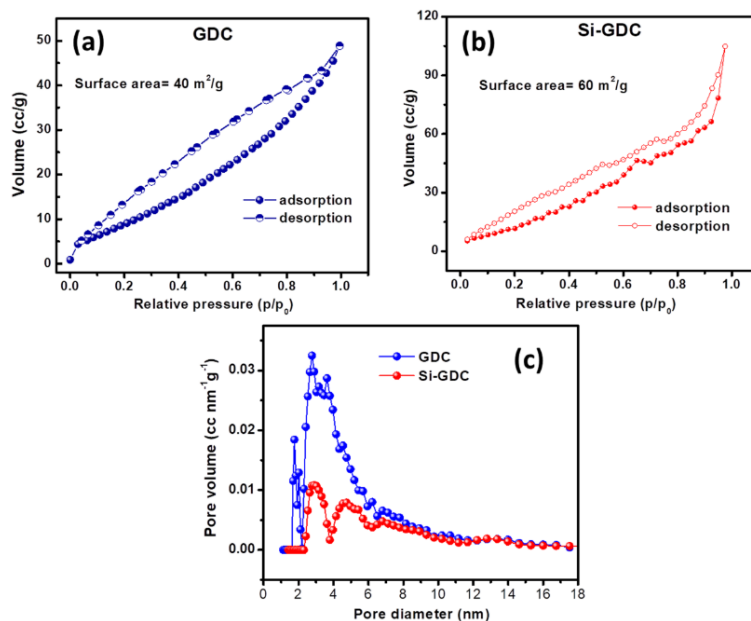
Figure 6. N2 adsorption isotherms of (a) GDC (Reprinted with permission from John Wiley and Sons[1]); (b) Si-GDC; (c) Pore size distribution of GDC and Si-GDC.

The same trend is observed for the isotherm of Si-GDC and but with a higher surface area of 60 $m^2 g^{-1}$. This means that the Si NPs are not simply adsorbed onto the carbon but are embedded in the carbon. The pore size distribution is bimodal[35] with the pores in mesoporous regime.[36]

4.3.2 Electrochemical data

4.3.2.1 Impedance spectroscopy: The potentiostatic electrochemical impedance spectroscopy (PEIS) data for Si NPS and Si-GDC composite are presented in Figure 7 (a) and 7 (b) for the fresh cells and the cells after cycling, respectively. Pristine Si NPs anode possesses very low series resistance due to the smaller size of nanoparticles which facilitates quick electrolyte dispensation and contact on the electrode surface. The Si-GDC anode also has negligible series resistance due to the high conductivity of the carbon. The charge transfer resistance of pristine Si NPs anode is very high as the Si NPs are non-conducting in nature.[37] On the other hand, the Si-GDC anode shows considerably less charge transfer resistance than Si NPs and this enables fast ion transport through the anode. After 5 cycles, the series resistance of electrodes remains almost the same but the charge transfer resistance changes considerably. The charge

transfer resistance in the case of Si-GDC reduces very significantly whereas Si NPs possess much higher value than Si NPs.
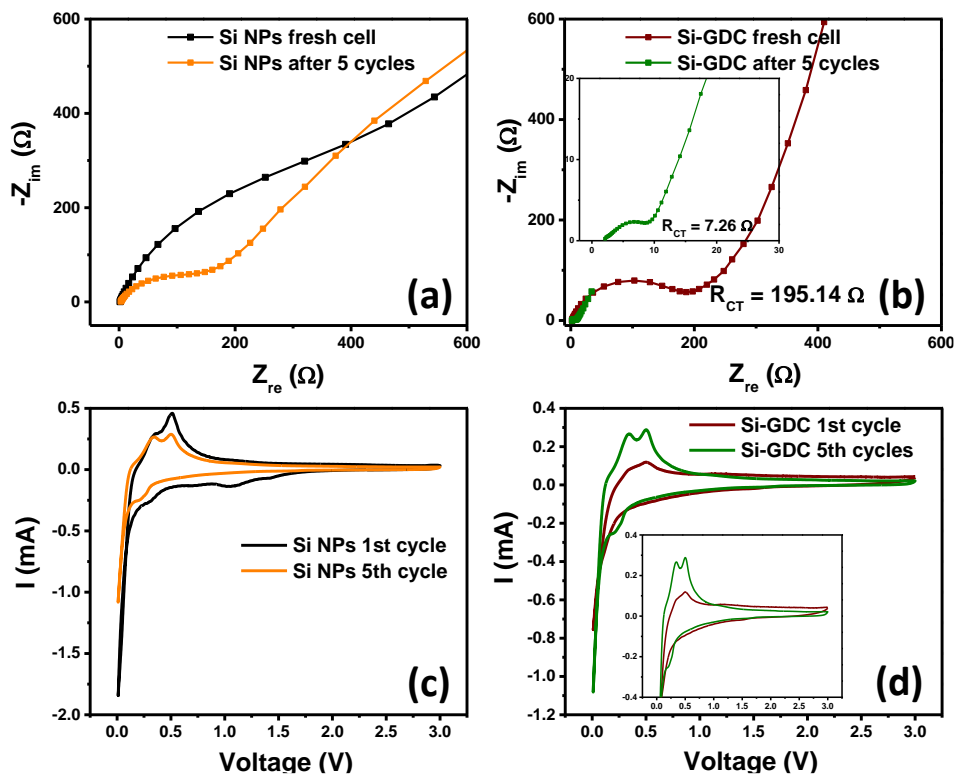
Figure 7. (a) Nyquist plots of Si NPs and (b) Si-GDC respectively; (c) and (d) Cyclic Voltammograms of Si NPs and Si-GDC.

This can be attributed to the high conductivity of carbon and the ease of electrolyte percolation through carbon channels enabling the fast charge transfer rate.

4.3.2.2 Cyclic Voltammetry: The typical CV curves for different anodes were obtained by scanning in the range 0.01 – 3 V with scan rate of 0.1 mV s^{-1} and the data are shown in Figure 7 (c) and 7 (d) for Si NPs and Si-GDC respectively. The broad peak at 1.0 V in Si NPs anode cathodic scan is due to the SEI formation arising due to the electrolyte decomposition at the electrode surface which is the same for the Si-GDC anode. The SEI formation in GDC occurs in the range of 1.5 V to 0.7 V (Figure S4†).[38] The subsequent cycles show peak at 0.19 V in the cathodic part indicative of the Li-Si alloy formation during lithiation. Additionally, Si-GDC has low intercalation and de-intercalation peaks close to 0.01 V for the carbon. During the anodic scan, the peaks appearing at 0.3 V and 0.48 V correspond to the de-lithiation of Li-Si alloys.[22] It is to

be noted that the peak intensity in Si NPs anode case reduces during cycling due to the cracking of anode during cycling. This does not happen in the case of Si-GDC anode as evident from Figure 6 (d).
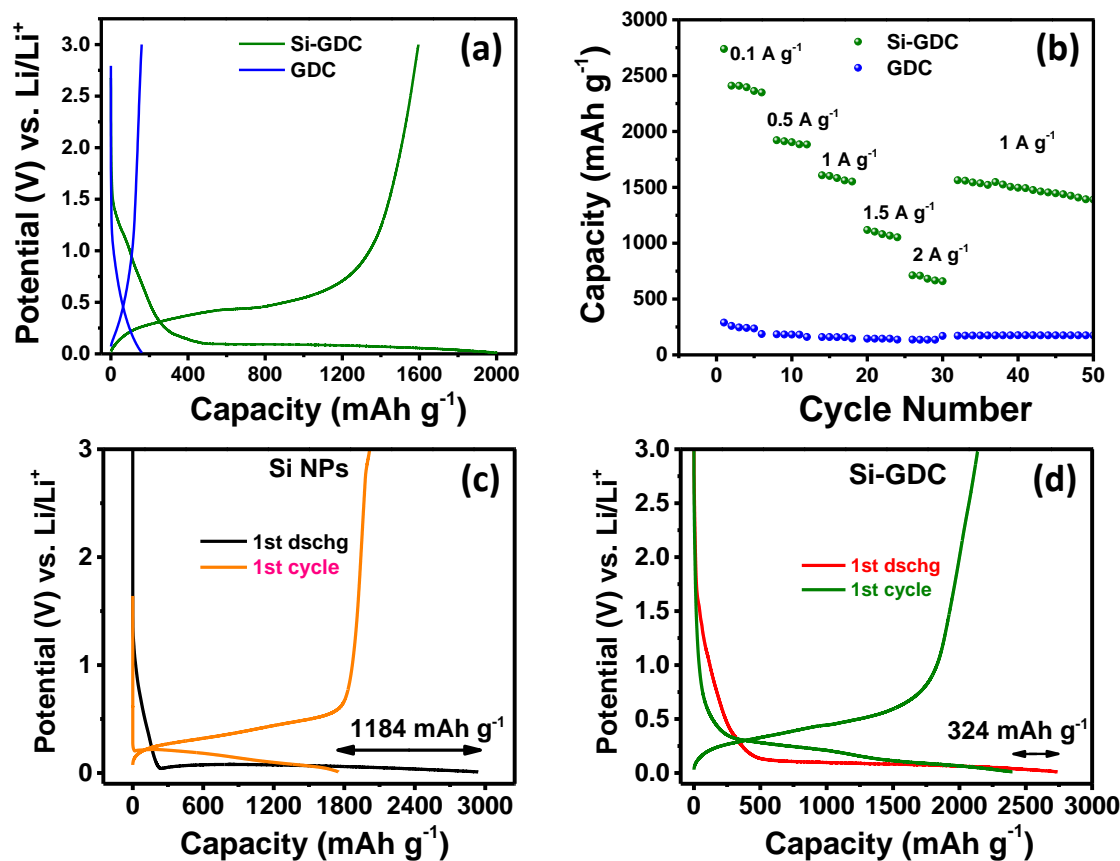
Figure 8. (a) Charge discharge curves of Si-GDC and GDC; (b) Rate performance of Si-GDC and GDC; (c) Irreversible capacity loss in Si NPs anode and (d) in Si-GDC

4.3.2.3 Charge Discharge: The Galvanostatic charge discharge measurements of Si-based anodes were carried out from 0.01 V to 3.0 V. The electrodes were cycled at a current density of 100 mA g^{-1} for the first few cycles before subjecting them to high current density. Later the charge discharge measurements were done at 1 A g^{-1}. The nature of the charge discharge curves for Si-GDC anode is similar to that of Si as seen in Figure 8 (a). The Li insertion and de-insertion in Si occurs from 0.5 V to 0.2 V. To differentiate, the curves for GDC are also shown which possess a typical turbostratic carbon nature with a lower potential plateau for Li insertion close to 0.01 V. The rate performance was also done from 0.1 A g^{-1} to 2 A g^{-1} as seen in Figure 8 (b). The Si-GDC anode shows a reversible capacity of 2400 mAh g^{-1}, 1800 mAh g^{-1}, 1500 mAh g^{-}

^{1}, 1000 mAh g^{-1}, 700 mAh g^{-1} at 0.1 A g^{-1}, 0.5 A g^{-1}, 1A g^{-1}, 1.5A g^{-1} and 2A g^{-1} respectively.
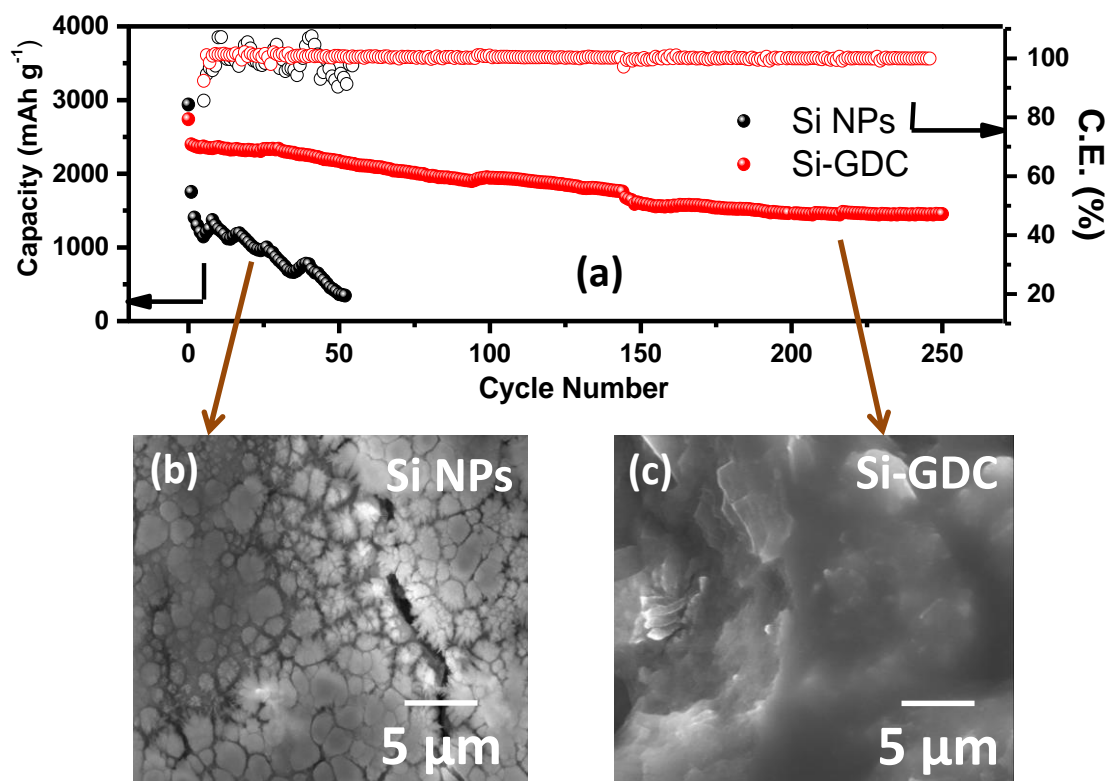
Figure 9. (a) Cycling stability and Coulombic Efficiency plots of Si NPs and Si-GDC; (b) and (c) SEM images of Si NPs and Si-GDC electrodes post cycling.

The Si-GDC attains the original value when subjected back to 1 A g^{-1}. The interesting fact about the Si-GDC is that it exhibits very less irreversible capacity loss of 324 mAh g^{-1} as compared to the huge loss of 1184 mAh g^{-1} observed for bare Si NPs anode, as seen from Figure 8 (c) and 8 (d). This imparts high stability to the Si-GDC anode clearly proven in Figure 9 (a) where the anode sustains volume expansion and shows a high reversible capacity of 1460 mAh g^{-1} at high current density of 1 A g^{-1} even after 250 charge discharge cycles with 75% capacity retention from first cycle capacity. The pristine Si NPs undergo cracking and delamination from the electrode surface as a result of volume expansion caused by Li-Si alloy formation as shown in post cycling SEM images Figure 9 (b) and 9 (c) where Si NPs anode develops cracks due to rupturing and volume expansion whereas Si-GDC retains a robust SEI layer preventing the delamination and cracking of particles. The Si NPs anode starts degrading after the first few cycles and goes less than 90 mAh g^{-1} after mere 50 cycles.

Moreover, the Coulombic Efficiency is improved as well in Si-GDC anode as compared to the pristine Si NPs. Hence, the carbon coating indeed provides long term stability to the Si-GDC as compared to pristine Si NPs. A comparison table of Si-GDC composite with existing literature os provided in Appendix B.

4.4 Conclusions

A facile natural gel-based approach is demonstrated to synthesize conducing carbon encapsulated Si NPs to serve as an anode material for Li-ion battery with high capacity and cycling stability. A very high reversible capacity of 1460 mAh g^{-1} is realized at a high rate of 1 A g^{-1} which is stable up to 250 cycles over which the performance was measured. The post cycling electrode SEM images show that Si-GDC presents itself as a robust anode material with uniform SEI layer formation.

References

[1]   J.B. Goodenough, K. Park, The Li-ion Rechargeable Battery : A Perspective The Li-ion Rechargeable Battery : A Perspective, (2013).

[2]   P.S. Attidekou, S. Lambert, M. Armstrong, J. Widmer, K. Scott, P.A. Christensen, A study of 40 Ah lithium ion batteries at zero percent state of charge as a function of temperature, J. Power Sources. 269 (2014) 694–703. doi:10.1016/j.jpowsour.2014.06.064.

[3]   M. Miroshnikov, K.P. Divya, G. Babu, A. Meiyazhagan, L.M. Reddy Arava, P.M. Ajayan, G. John, Power from nature: Designing green battery materials from electroactive quinone derivatives and organic polymers, J. Mater. Chem. A. 4 (2016) 12370–12386. doi:10.1039/c6ta03166h.

[4]   J.M. Tarascon, M. Armand, Issues and challenges facing rechargeable lithium batteries., Nature. 414 (2001) 359–67. doi:10.1038/35104644.

[5]   G.E. Blomgren, The Development and Future of Lithium Ion Batteries, J. Electrochem. Soc. 164 (2017) A5019–A5025. doi:10.1149/2.0251701jes.

[6]   R. Marom, S.F. Amalraj, N. Leifer, D. Jacob, D. Aurbach, A review of advanced and practical lithium battery materials, J. Mater. Chem. 21 (2011) 9938. doi:10.1039/c0jm04225k.

[7]   J.W. Long, B. Dunn, D.R. Rolison, H.S. White, Three-dimensional battery architectures, Chem. Rev. 104 (2004) 4463–4492. doi:10.1021/cr020740l.

[8]   J.B. Goodenough, Y. Kim, Challenges for rechargeable Li batteries, Chem. Mater. 22 (2010) 587–603. doi:10.1021/cm901452z.

[9]   M. Armand, J.-M. Tarascon, Building better batteries, Nature. 451 (2008) 652–657. doi:10.1038/451652a.

[10]   P.G. Bruce, B. Scrosati, J.-M. Tarascon, Nanomaterials for Rechargeable Lithium Batteries, Angew. Chemie Int. Ed. 47 (2008) 2930–2946. doi:10.1002/anie.200702505.

[11]   P. Prakash, J. Aguirre, M.M. Van Vliet, P.R. Chinnam, D.A. Dikin, M.J. Zdilla, S.L.

Wunder, A. Venkatnathan, Unravelling the structural and dynamical complexity of the equilibrium liquid grain-binding layer in highly conductive organic crystalline electrolytes, J. Mater. Chem. A. 6 (2018) 4394–4404. doi:10.1039/c7ta10367k.

[12] U. Kasavajjula, C. Wang, A.J. Appleby, Nano- and bulk-silicon-based insertion anodes for lithium-ion secondary cells, J. Power Sources. 163 (2007) 1003–1039. doi:10.1016/j.jpowsour.2006.09.084.

[13] M.T. McDowell, S.W. Lee, W.D. Nix, Y. Cui, 25th anniversary article: Understanding the lithiation of silicon and other alloying anodes for lithium-ion batteries, Adv. Mater. 25 (2013) 4966–4985. doi:10.1002/adma.201301795.

[14] W.J. Zhang, Lithium insertion/extraction mechanism in alloy anodes for lithium-ion batteries, J. Power Sources. 196 (2011) 877–885. doi:10.1016/j.jpowsour.2010.08.114.

[15] M.H. Park, M.G. Kim, J. Joo, K. Kim, J. Kim, S. Ahn, Y. Cui, J. Cho, Silicon nanotube battery anodes, Nano Lett. 9 (2009) 3844–3847. doi:10.1021/nl902058c.

[16] Y. Yang, M.T. McDowell, A. Jackson, J.J. Cha, S.S. Hong, Y. Cui, New nanostructured Li2S/Silicon rechargeable battery with high specific energy, Nano Lett. 10 (2010) 1486–1491. doi:10.1021/nl100504q.

[17] C.K. Chan, R. Ruffo, S.S. Hong, R.A. Huggins, Y. Cui, Structural and electrochemical study of the reaction of lithium with silicon nanowires, J. Power Sources. 189 (2009) 34–39. doi:10.1016/j.jpowsour.2008.12.047.

[18] Y. Sun, N. Liu, Y. Cui, Promises and challenges of nanomaterials for lithium-based rechargeable batteries, Nat. Energy. 1 (2016) 16071. doi:10.1038/nenergy.2016.71.

[19] J.W. Choi, L. Hu, L. Cui, J.R. McDonough, Y. Cui, Metal current collector-free freestanding silicon-carbon 1D nanocomposites for ultralight anodes in lithium ion batteries, J. Power Sources. 195 (2010) 8311–8316. doi:10.1016/j.jpowsour.2010.06.108.

[20] L. Hu, H. Wu, Y. Gao, A. Cao, H. Li, J. McDough, X. Xie, M. Zhou, Y. Cui, Silicon-carbon nanotube coaxial sponge as Li-ion anodes with high areal capacity, Adv. Energy Mater. 1 (2011) 523–527. doi:10.1002/aenm.201100056.

[21] S.H. Min, M.R. Jo, D.H. Song, K. song, J. Yang, Y.M. Kang, High crystalline carbon network of Si/C nanofibers obtained from the embedded pitch and its contribution to Li ion kinetics, Electrochim. Acta. 220 (2016) 511–516. doi:10.1016/j.electacta.2016.10.111.

[22] H.-C. Tao, L.-Z. Fan, X. Qu, Facile synthesis of ordered porous Si@C nanorods as anode materials for Li-ion batteries, Electrochim. Acta. 71 (2012) 194–200. doi:10.1016/j.electacta.2012.03.139.

[23] J.L. Gómez-Cámer, J. Morales, L. Sánchez, Anchoring Si nanoparticles to carbon nanofibers: an efficient procedure for improving Si performance in Li batteries, J. Mater. Chem. 21 (2011) 811–818. doi:10.1039/C0JM01811B.

[24] M. Thakur, R.B. Pernites, N. Nitta, M. Isaacson, S.L. Sinsabaugh, M.S. Wong, S.L. Biswal, Freestanding macroporous silicon and pyrolyzed polyacrylonitrile as a composite anode for lithium ion batteries, Chem. Mater. 24 (2012) 2998–3003. doi:10.1021/cm301376t.

[25] J.W. Choi, D. Aurbach, Promise and reality of post-lithium-ion batteries with high energy densities, Nat. Rev. Mater. 1 (2016) 16013. doi:10.1038/natrevmats.2016.13.

[26] N. Sharma, Y. Gawli, A. Ahmad, M. Muhammed, S. Ogale, Nanotubular Hard Carbon Derived from Renewable Natural Seed Gel for High Performance Sodium-Ion Battery Anode, ChemistrySelect. 2 (2017) 6909–6915. doi:10.1002/slct.201701123.

[27] C.K. Chan, R.N. Patel, M.J.O. Connell, B.A. Korgel, Y.C. Ḱ, Solution-Grown Silicon Nanowires for Lithium-Ion Battery Anodes, 4 (2010) 1443–1450.

[28] T. Matsumoto, M. Maeda, J. Furukawa, W.B. Kim, H. Kobayashi, Si nanoparticles fabricated from Si swarf by photochemical etching method, J. Nanoparticle Res. 16 (2014). doi:10.1007/s11051-013-2240-y.

[29] Y.X. Yin, S. Xin, L.J. Wan, C.J. Li, Y.G. Guo, Electrospray synthesis of silicon/carbon nanoporous microspheres as improved anode materials for lithium-ion batteries, J. Phys. Chem. C. 115 (2011) 14148–14154. doi:10.1021/jp204653y.

[30] T. Schott, J.L. Gómez-Cámer, P. Novák, S. Trabesinger, Relationship between the Properties and Cycle Life of Si/C Composites as Performance-Enhancing Additives to

Graphite Electrodes for Li-Ion Batteries, J. Electrochem. Soc. 164 (2017) A190–A203. doi:10.1149/2.0701702jes.

[31]   S.Y. Kim, J. Lee, B.H. Kim, Y.J. Kim, K.S. Yang, M.S. Park, Facile Synthesis of Carbon-Coated Silicon/Graphite Spherical Composites for High-Performance Lithium-Ion Batteries, ACS Appl. Mater. Interfaces. 8 (2016) 12109–12117. doi:10.1021/acsami.5b11628.

[32]   K. Hong, L. Qie, R. Zeng, Z. Yi, W. Zhang, D. Wang, W. Yin, C. Wu, Q. Fan, W. Zhang, Y. Huang, Biomass derived hard carbon used as a high performance anode material for sodium ion batteries, J. Mater. Chem. A. 2 (2014) 12733. doi:10.1039/C4TA02068E.

[33]   A.C. Ferrari, J. Robertson, Interpretation of Raman spectra of disordrred and amorphous carbon, Phys. Rev. B. 61 (2000) 14 295.

[34]   Z. Li, Z. Jian, X. Wang, I.A. Rodríguez-Pérez, C. Bommier, X. Ji, Hard carbon anodes of sodium-ion batteries: undervalued rate capability, Chem. Commun. 53 (2017) 2610–2613. doi:10.1039/C7CC00301C.

[35]   P.A. Gauden, A.P. Terzyk, M. Jaroniec, P. Kowalczyk, Bimodal pore size distributions for carbons: Experimental results and computational studies, J. Colloid Interface Sci. 310 (2007) 205–216. doi:10.1016/j.jcis.2007.01.082.

[36]   Z. Guan, H. Liu, B. Xu, X. Hao, Z. Wang, L. Chen, Gelatin-pyrolyzed mesoporous carbon as a high-performance sodium-storage material, J. Mater. Chem. A. 3 (2015) 7849–7854. doi:10.1039/C5TA01446H.

[37]   X. Xiao, W. Zhou, Y. Kim, I. Ryu, M. Gu, C. Wang, G. Liu, Z. Liu, H. Gao, Regulated breathing effect of silicon negative electrode for dramatically enhanced performance of Li-ion battery, Adv. Funct. Mater. 25 (2015) 1426–1433. doi:10.1002/adfm.201403629.

[38]   E. Irisarri, A. Ponrouch, M.R. Palacin, Review—Hard Carbon Negative Electrode Materials for Sodium-Ion Batteries, J. Electrochem. Soc. 162 (2015) A2476–A2482. doi:10.1149/2.0091514jes.

Chapter 5.

A hard carbon and $Li_4Ti_5O_{12}$ based physically mixed anode for superior Li-battery performance with significantly reduced Li content: A case of synergistic materials cooperation

Abstract

$Li_4Ti_5O_{12}$ (LTO) and hard carbon (HC) are commonly used anodes in the Li-ion batteries. LTO exhibits high-rate performance but with limited capacity. HC has high specific capacity but extremely low operating voltage. Herein, we show that a simple physical mixture of the two enhances the half-cell as well as full-cell performance through a synergistic cooperation between the materials. Specifically, the LTO−HC mixed anodes exhibit impressive performance even at high C-rates. This results from a quick internalization of Li ions by LTO followed by their distribution to HC regions via the high density of the winding internal interfaces between the two. The full cells of the LTO−HC mixed anodes with LiCoO2 (LCO) evince an enhanced operating voltage window and a well-defined plateau. The overall specific capacity of LCO/mixed anodes is better than the LCO/pristine anode full cells. Also, with the LTO−HC 20−80 anode (Li content reduced by 80%), the full cell exhibits an impressive performance when compared to pristine anodes without pre-lithiation. The LCO/mixed anode full cells have excellent cycling stability up to 500 cycles at a current density of 100 mA g^{-1}.

The following paper has been published based on the work presented in this chapter.

5.1 Introduction

Li ion batteries are the suitable choice for most of the practical applications such as portable electronics and hybrid/electric vehicles because of their durability, high power and energy density, long cycle life and low self-discharge rate.[1] There have been numerous developments made on the electrode materials appropriate for the Li ion batteries to achieve state of the art performance from the device and mitigating the problems faced during implementation on the real systems.[2],[3] For any practical or commercial application, the battery must deliver fairly high power density as well as energy density with minimal capacity fade during cycling.[4] To accomplish these requirements, various anode materials have been investigated; graphite being the most popular amongst all. An ideal anode material should have low intercalation potential for Li insertion/ de-insertion, short paths for ion diffusions leading to high rate capability, low volume expansion during lithiation and de-lithiation, low cost, and environmental friendly character.[5]

Among the various anodes investigated so far for the Li ion batteries under intercalation category, $Li_4Ti_5O_{12}$ (LTO) is well known owing to its superior characteristics. LTO exhibits a well-defined operating voltage of 1.55 V and a specific capacity of 175 mAh g^{-1} making it useful for practical applications.[6] It has high rate capability, good cycle life and importantly a negligible volume expansion during charging and discharging. LTO has the spinel structure and it transforms into the rock salt structure ($Li_7Ti_5O_{12}$) during discharging, having lattice parameters comparable to the spinel structure.[7] The process takes place by the migration of Li ions from the tetrahedral sites to the octahedral sites and the three incoming Li ions occupying the vacant tetrahedral sites and moving to octahedral sites. The overall reaction mechanism is given in the equation below:

$$3Li + Li_4Ti_5O_{12} \longleftrightarrow Li_7Ti_5O_{12} \tag{1}$$
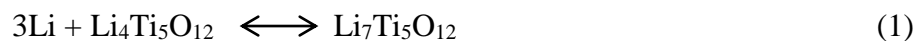
The structural transformation is reversible and is called topotactic as the final structure is similar to the parent one.[8] However, in spite of all these features, LTO has not been considered as the optimum choice as an anode material for practical devices due to some of its intrinsic limitations. Specifically, LTO has poor electronic conductivity and

owing to its low specific capacity, it is considered as a low energy density anode material.

To overcome these issues, various interesting strategies have been developed such as making LTO composites with conducting materials such as carbon or metal nanoparticles[9], making nanostructured LTO[10],[11] or coating LTO with hard or soft carbon by ball milling, CVD or pyrolysis methods.[12],[13],[14] However, these methods are expensive and elevate the overall cost of the battery including the complexity in synthesis.

Hard carbon (HC) on the other hand, is another good choice for the Li ion battery anode because of its high reversible capacity and lower Li intake potential.[15] HCs are commonly derived from biomass by simple pyrolysis treatment, thus representing a cheap material for battery application.[16] HC being non- graphitizable has its planes randomly oriented with enhanced d-spacing.[17] Though it has low surface area, still it is considered to be a high energy density material as it has high specific capacity. As proposed by J. R. Dahn,[18] hard carbon stores ions by intercalation as well as adsorption as shown in Figure 1.
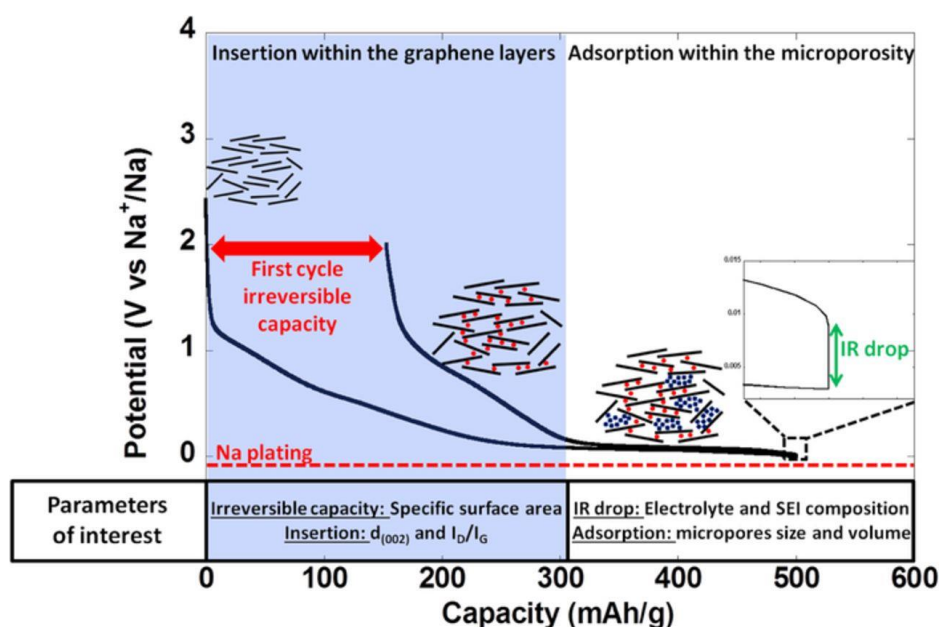

Figure 1. Storage Mechanism of hard carbon. Copyright Electrochemical Society. Reproduced with the permission of Ref [18].

The intercalation occurs in the graphitic planes of the carbon in the voltage range of 1 to 0.1 V represented by the sloping region in the discharge curve.[19] The sloping nature of the curve indicates that the voltage varies for every Li site available. The adsorption occurs at very low voltages lying close to metal plating in the micro or nano pores of the carbon where a large number of ions get trapped and can be extracted only at extremely low current densities.[20] These ions are irreversibly trapped causing huge first cycle capacity loss.[21] This limits the rate performance of the material and thereby the power density, making them inappropriate for potential use. To address this problem, hard carbons are functionalized with dopants or nanoparticles to enhance the specific capacity and operating window.[22],[23]

In this work, we propose and demonstrate that a simple physical mixture of LTO and HC as an anode renders several advantages in terms of enhanced performance factors through synergistic effects. Interestingly, due to the specific scientific reasons outlined in the course of discussion, this simple approach combines the advantages of the individual anodes and diminishes their respective shortcomings; eliminating the need to use any complex synthesis protocol. We have investigated such LTO-HC mixed anodes in half cells at various C-rates as well as at fairly high fixed values of constant current densities. Moreover, the full cells have also been tested with $LiCoO_2$ to prove that the Li content of anode can be dramatically reduced to as low as 20%, still retaining the high performance factors without any pre-lithiation process involved. Thus, this work proposes a facile methodology to gain high power as well as energy density of a full cell device without the use of any tedious procedures, thereby reducing the cost and processing complexity or time.

5.2 Experimental Section

5.2.1 Materials and methods: LTO and LCO procured from Sigma Aldrich and commercially available hard carbon were used as received. The mixed anodes were prepared by taking LTO and HC in two proportions 50-50 and 20-80 by weight respectively. The slurry was made by mixing the anode powders with super P and PVDF binder in the ratio of 80:10:10 and NMP as solvent. The slurry was coated on the Cu foil and was kept for drying overnight at 80 °C. The slurry was coated on the Cu

foil and was kept for drying overnight at 80 °C. The foil was then punched into 1 cm^2 circular discs. Powder X-Ray diffraction was done using Bruker D8-Advance X-ray Diffractometer (Germany) with Cu kα (wavelength = 1.5418 Å). Scanning electron microscopy (SEM) was done using FEI Nova Nano 450 SEM.

5.2.2 Electrochemical measurements: The 2032 coin cells were made using mixed anodes and Li metal and whatmann separator known as half-cell configuration. The full-cells were fabricated using LTO and HC mixed anodes and LCO cathode. The electrolyte used was commercial LiPF$_6$ in ethylene carbonate and dimethyl carbonate (EC: DMC in the volume ratio of 1:1). Galvanostatic charge discharge measurements were done with BTS-Neware (China) 5V, 10mA battery tester. The impedance and cyclic voltammetry were done with VMP3 biologic system equipped with potentiostat and galvanostat channels. The mass loading of the electrodes are in the range of 1.3 to 1.5 mg. The cathode to anode mass ratio is 1:1 for LTO and 1.5:1 for LTO-HC 50-50, LTO-HC 20-80 and HC. The full cell measurements were done considering the weight of both cathode and anode in all the cases.

5.3 Results and Discussion

The powder x-ray diffraction (XRD) data for LTO and HC are given in Figure 2.
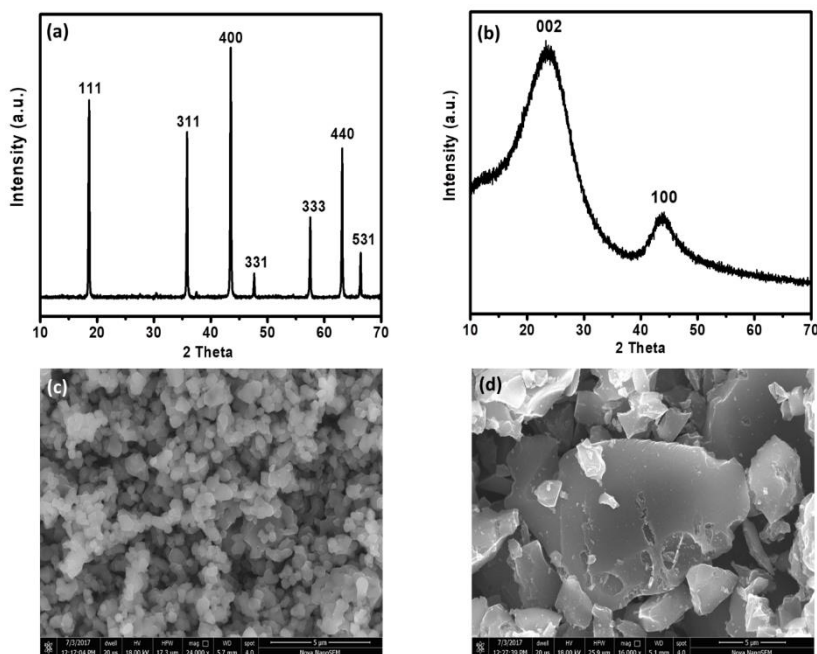
Figure 2. PXRD pattern of (a) LTO; (b) HC and SEM images of (c) LTO; (d) HC.

The XRD pattern for LTO in Figure 1 (a) can be indexed to the cubic spinel structure with space group Fd-3m according to the literature (JCPDS file no. 49-0207). The XRD for hard carbon in Figure 1 (b) consists of the broad peaks representing (002) and (100) planes of amorphous carbon at the 2θ values of 23.6° and 43.8°, respectively.[12] The morphology of both the materials is shown in Figures 1 (c) and (d). LTO is composed of small uniform sized particles whereas HC consists of big chunks.

5.3.1 Electrochemical data

5.3.1.1 Impedance spectroscopy: Figure 3 (a) illustrates the impedance spectra of all the four samples before cycling. The higher frequency regions of the Nyquist plot consist of a semi-circle which is the measure of the charge transfer resistance at the electrode surface.[24] The series resistance is found to be less in all the samples. The charge transfer resistance of the pristine LTO electrode is the lowest among all cases, in this case.

Figure 3. Impedance spectra (a) before cycling and (b) after 5 cycles and cyclic voltammograms (c) before cycling and (d) after 5 cycles of anodes.

The Nyquist plot for HC exhibits a larger semi-circle at high frequency owing to the higher charge transfer resistance at the electrode surface. At low frequencies, the Warburg component i.e. the sloping line corresponds to the diffusion process occurring in the bulk material.[25] The LTO-HC 20-80 mixed anode impedance resembles that of pristine HC whereas that of the LTO-HC 50-50 mixed anode exhibits a second semi-circle. The semi-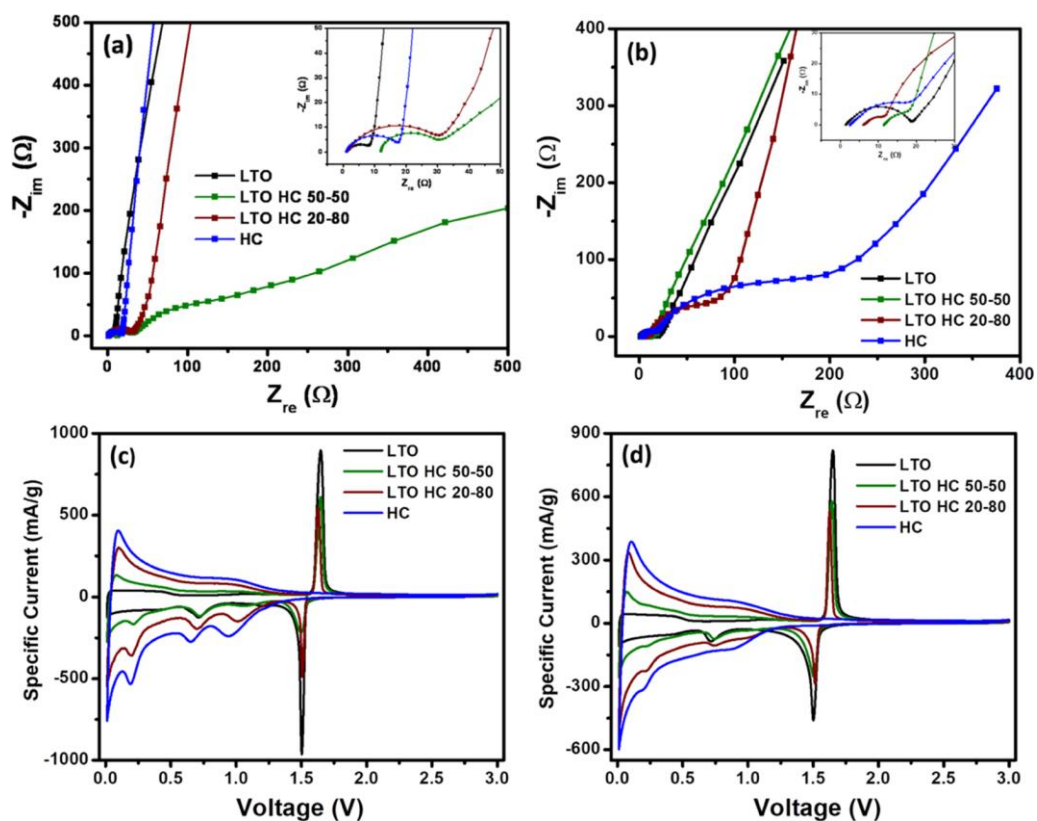circle at high frequencies corresponds to the diffusion through pores of the electrode. The mid-frequency semi-circle represents the charge transfer resistance and constant phase element (CPE) at electrode electrolyte interphase.[26] The occurrence of these two could also be attributed to the non-homogenous electrode composed of small and big particle sizes as discussed at length by Xu et al.[27] In the plot, the LTO anode shows slow diffusion and certainly invites a discussion as the reviewer has corrected asked for. As for the present case of mixed materials anodes, such type of Nyquist plot has indeed been observed in electrodes containing components having different particle sizes, big and small, and they have been studied and discussed extensively earlier.[28] The slow diffusion in such cases has been attributed to the non-homogeneity of the electrode surface, the thickness, and the difference in particle sizes of the materials.[29] When two different sized particles are present and the calendaring of the electrode is not uniform then the surface inhomogeneity leads to the development of an arc in the middle-to-low frequency region and results in the inclination of impedance curve towards real impedance axis. As LTO and HC have different particle sizes, the electrode surface will be inhomogeneous causing unequal distribution of mass that leads to a shift in the semi-circle near the low frequency regions. After 5 cycles, all electrodes exhibit a semi-circle with reduced charge transfer resistance in high frequency region and the low frequency region corresponding to bulk ion diffusion as seen from in Figure 3 (b). The 50-50 case and the pristine LTO are similar, whereas the 20-80 case is close to the pristine HC in nature.

5.3.1.2 Cyclic Voltammetry: The CV curves of the samples are presented in Figure 3 (c) and Figure 3 (d). The pristine LTO cathodic scan has intercalation peak at 1.5 V and a small peak at 0.7 V. During the anodic scan, the de-intercalation peak occurs at 1.6 V.[30] The redox peaks are consistent in the subsequent cycles. The first cycle CV for HC consists of three broad peaks along with the intercalation peak below 0.1 V in the

reverse scan.[31] The peak at 0.65 V is due to the SEI formation and disappears in the next cycle. The redox peaks at 0.93 V and 1.03 V are also present in the first cycle and can be seen in subsequent cycles with a small shift.

The peak at 0.19 V could be attributed to side reaction or irreversible ion adsorption and is absent in later cycles. The CV of the mixed anodes reveals the characteristic peaks of both LTO and HC as evident from the CV curve of LTO-HC 50-50 and LTO-HC 20-80.

5.3.1.3 Galvanostatic Charge Discharge: The half-cells were first discharged at a low current density of 50 mA g^{-1} to facilitate uniform SEI layer growth on the electrode surface. The nature of the charge discharge curves seen in Figure 4 explains the dual character of the mixed anodes when compared to the pristine ones. The LTO anode has a plateau at a high voltage of 1.55 V whereas HC has the sloping nature at high voltage but a plateau near to 0.01 V. The LTO-HC 50-50 discharge curve has the flat plateau at high voltage corresponding to Li insertion potential of LTO as well as the sloping region from 1V to 0.1 V corresponding to HC intercalation potential in the equal proportion. The LTO-HC 20-80 mixed anode partially exhibits the LTO character with the HC character dominating the charge discharge profile. The mixed anodes give high capacity as compared to the pristine anodes because of the enhanced electrochemical window from 1.55 V to 0.01 V whereas this advantage is not there in the case of individual anode materials (in LTO it is 1.55 V and in HC it is 0.1 to 0.01 V approx.). The theoretical capacities of LTO and HC are 175 mAh g^{-1} and 372 mAh g^{-1}, respectively. The calculated capacities for the mixed anodes considering the weight ratio are 273 mAh g^{-1} for LTO-HC 50-50 and 332.6 mAh g^{-1} for LTO-HC 20-80.

As seen from the curves, the realized capacity of HC is much lower than the predicted value which implies that the ion adsorption sites in HC are not accessible to Li-ions to the full extent and need very low current densities to be filled (adsorption in nano pores of HC). The reason for the excess capacity in the mixed anode cases is the quick internalization of ions facilitated by LTO and then the distribution of ions in the HC channels or the nano pores.
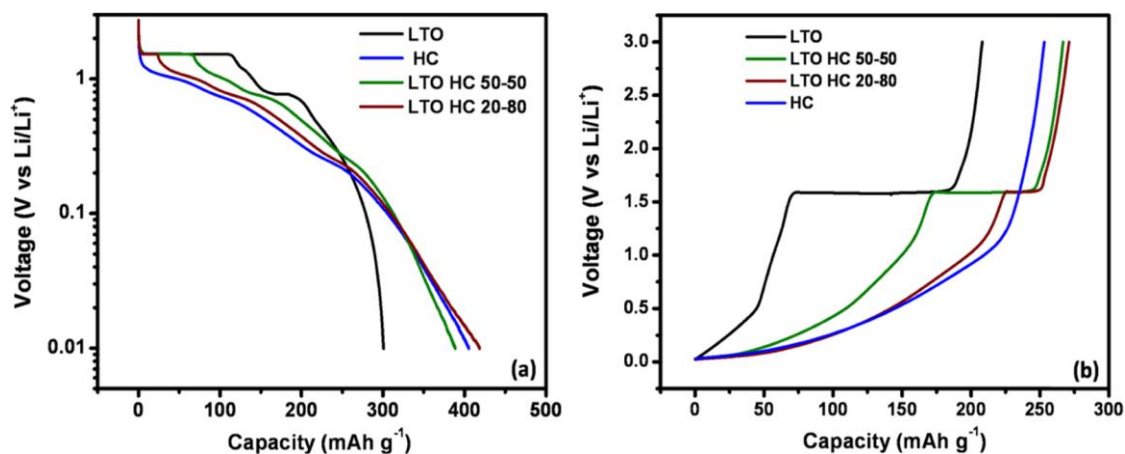
Figure 4. Charge−discharge plot nature of anodes. (a) First discharge curve of all four cases at 50 mA g^{-1} and (b) first charge curve at 50 mA g^{-1}.

The process of quick Li-ion internalization afforded by LTO thus helps these ions access more sites of HC at the same current density, hence the higher capacity reflected at that current density. This way the capacity close to the predicted value is achieved in the mixed anodes as proven by our charge discharge measurements, which is not the case with pristine HC because of its poor rate capability at the same current density. The rate performance of the samples was checked at different C-rates given in Figure 5 along with the Coulombic efficiency. The cells were cycled at high rates of 20 C. As evident, pristine LTO being the high rate capability anode, does not undergo much degradation in the specific capacity even at 20 C and gives a specific capacity value of about 145 mAh g^{-1}, whereas for the HC case the specific capacity drops down drastically when subjected to high C-rates and the specific capacity falls down to 90 mAh g^{-1}.

Interestingly, the LTO-HC mixed anodes perform superior to individual anodes at high rates and the specific capacity lies close to that of pristine LTO. Thus, the LTO-HC 50-50 mixture anode exhibits a specific capacity of 130 mAh g^{-1} at 20 C, while the LTO-HC 20-80 mixture anode gives a capacity of about 145 mAh g^{-1}. The electrodes were also cycled at constant current densities evinced in Figure 6. At high current densities of 2 A g^{-1}, and 6 A g^{-1}, the mixed anodes possess an extremely impressive performance and high cycling stability up to 3000 cycles with minimal capacity fade. In these cases as well, HC fails to withstand high current densities whereas the mixed LTO-HC electrodes function almost similar to LTO in spite of a very significant reduction in the
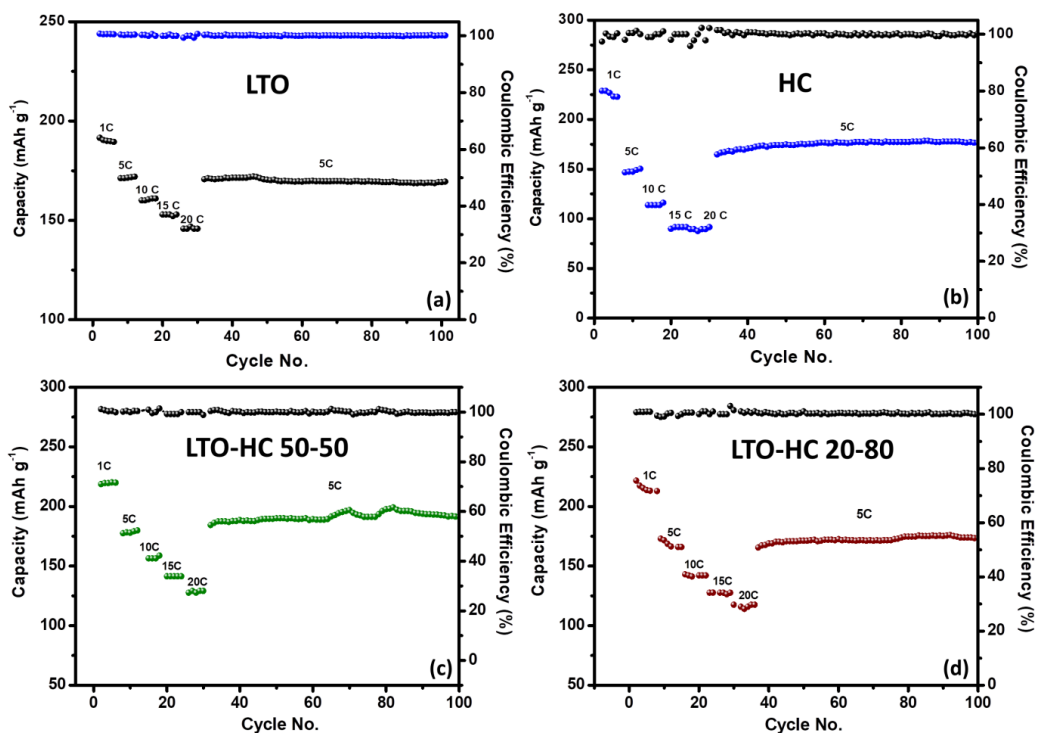
Figure 5. Rate performance at different C-rates and Coulombic Efficiency plots of (a) LTO; (b) HC; (c) LTO-HC 50-50 and (d) LTO-HC 20-80.

Li content in the anode. The possible reasons for this interesting outcome have been discussed below in the mechanism section.

5.3.2 Scanning Electron Microscopy

The SEM images in Figure 7 reveal the morphologies of the electrodes of pristine and mixed LTO-HC materials at different stages of cycling. After the first discharge, the electrodes have a uniform covering of the surface by the SEI layer. After 10 cycles, the SEI layer of LTO and HC is rather thin whereas the mixed LTO-HC electrodes have a robust SEI layer on the surface. After 200 cycles, the SEI layer on the LTO and HC surfaces ruptures at some areas of electrode, but that on the mixed LTO-HC electrodes (50-50 and 20-80 cases) reflect uniformity throughout the surface rendering good cycling stability to the mixed LTO-HC anodes. It could be anticipated that the SEI formation in mixed cases consists of two different interfaces and the layer characteristics are governed by both the anodes.

Figure 6. Cycling stability at constant current densities (a) at 2 A g^{-1} and (b) at 6 A g^{-1}.

Figure 7. SEM images of electrodes. First row: bare electrode; second row: after first discharge; third row: after 10 cycles; and fourth row: after 200 cycles.

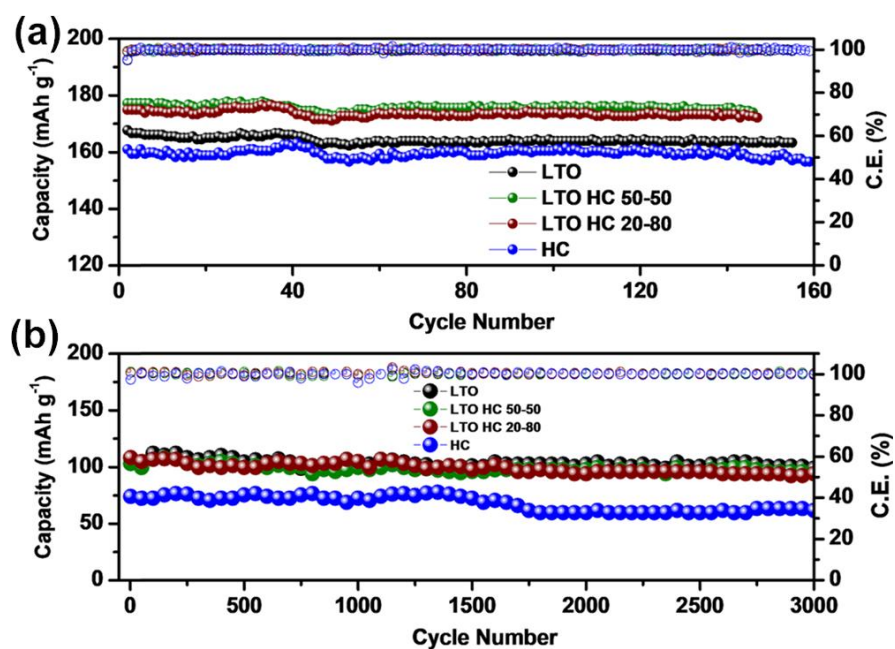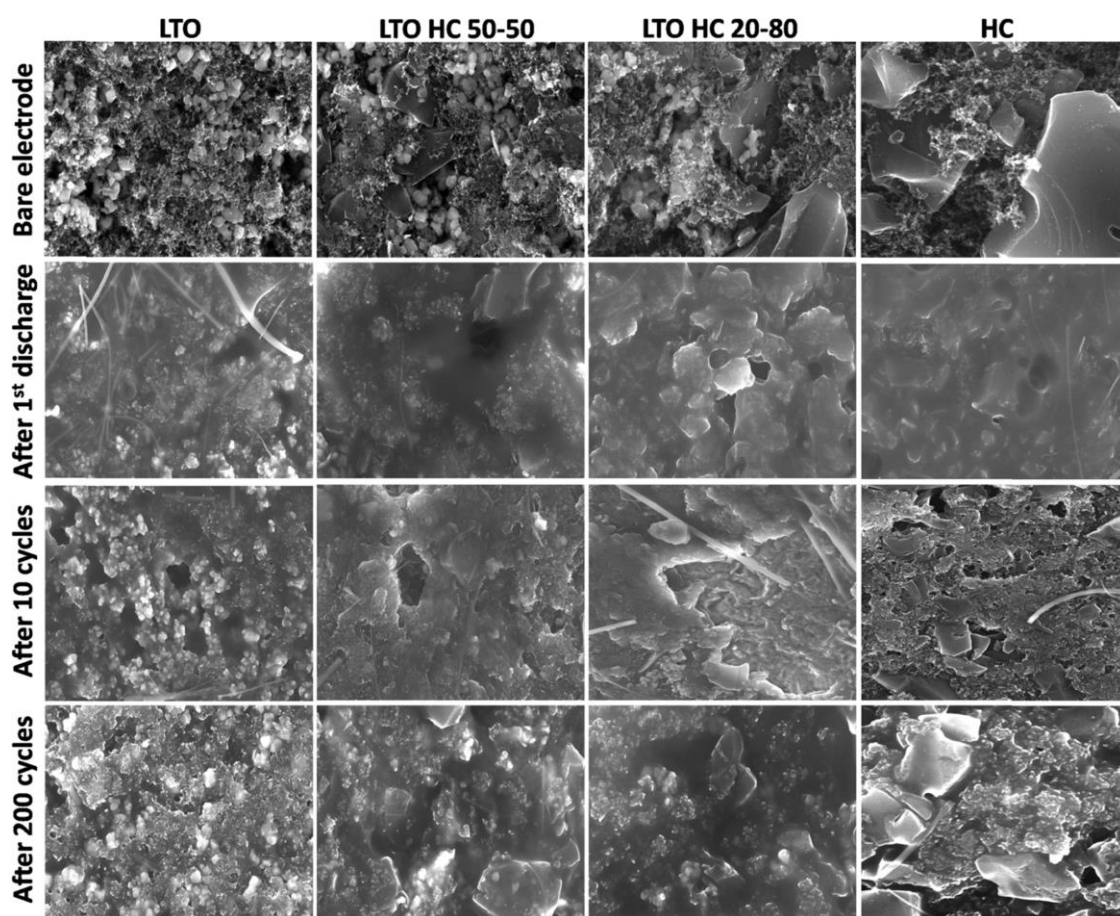This is an interesting case of laterally in-homogeneous fabric of the SEI layer and importantly the synergistic effect of individual material surfaces exposed to electrolyte leads to a better SEI formation that does not deteriorate as noted in the case of individual anodes. The synergistic effect of two SEI components clearly helps with stress relaxation and mechanical stability. This correlates very well with the good performance of the mixed electrodes during charging even at high current densities.

The uniform coverage of the electrode surface further suppresses the electrolyte decomposition and irreversible Li loss. Hence, the capacity is retained even after cycling up to 3000 cycles (as shown in Figure 5).

5.3.3 Mechanism of charge storage

Figure 8 illustrates the proposed mechanism of the Li ion storage in the case of the mixed anodes as compared to the pristine material anodes. As is well known, LTO has well defined Li insertion sites and due to small diffusion paths for ion migration from 8a tetrahedral sites to 16c octahedral sites of the spinel structure the rate capability is high, but the capacity is low because of the limited Li ion vacancies as explained in the introduction above. Due to high rate capability the LTO capacity does not drop when the current density is raised from a low to a high value. On the other hand, HC has turbostratic planes and no direct channels or sites for ions as in the LTO case. Moreover, HC consists of nano pores and thus to realize its full capacity it has to be charged at very low current densities for all pores to get filled. Thus, HC anode gives high capacity at low current densities, but very low capacity at high current densities as the Li ions are not able to access all the available sites.

As seen in the mixed anode cases, the capacity is enhanced and the rate performance is also improved due to the channelized distribution of the ions. Presence of LTO facilitates quick Li uptake even at high rates and HC provides additional sites for their localization on the surface of electrode. The synergistic effect of quick internalization of Li ions by LTO and its re-distribution to the HC across the internal effective large area winding interfaces between LTO and HC provides high power as well as energy density in the mixed materials anode case. This is true for the case where Li content is reduced even up to 80%.
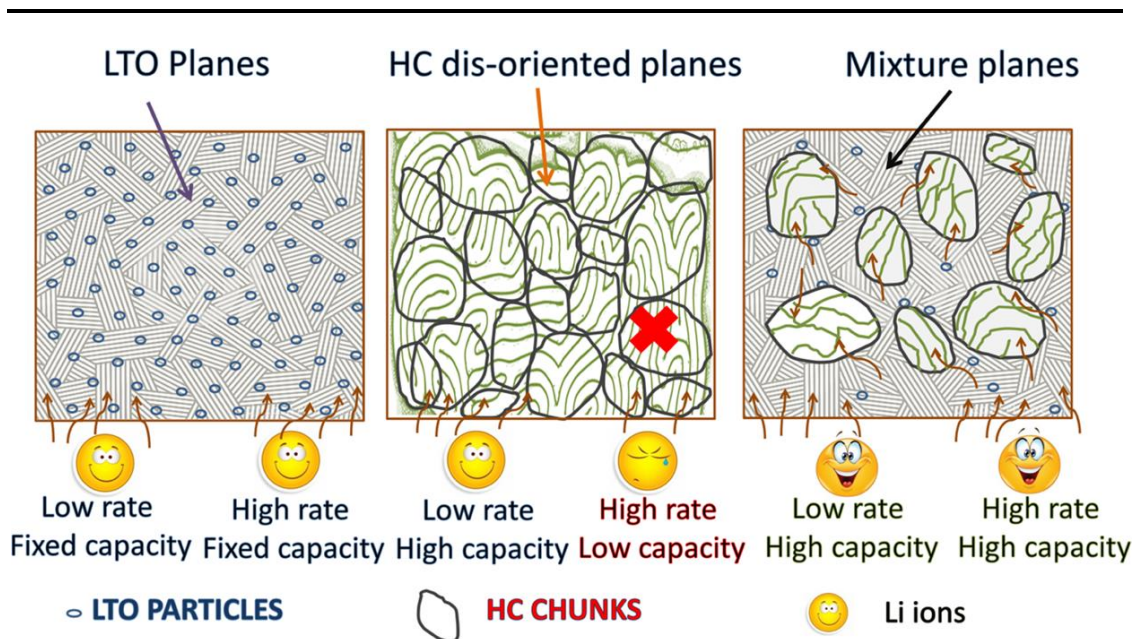
Figure 8. Mechanism of Charge Storage in the Mixed Anodes.

5.3.4 Full-cell with LiCoO$_2$ (LCO)

For full-cell fabrication, LiCoO$_2$ (LCO) cathode was used. The half-cell performance of LCO is given in supporting information in Figure 9. LCO gives a specific capacity of 165 mAh g^{-1} at 50 mA g^{-1}. The full-cells were tested at C/4 rates and the curves are presented in Figure 10. The LCO/LTO full-cell gives a specific capacity of 85 mAh g^{-1} with negligible irreversible capacity loss. The full-cell operating voltage is from 1.8 V to 2.5 V and has a plateau at 2.35 V. It was found that if the full-cell is charged beyond 2.5 V, there is a rapid decay in the specific capacity and the cell is not stable in that voltage window. The LCO/HC full-cell gives the first charging capacity of 130 mAh g^{-1}, but has a substantial capacity loss of about 60 mAh g^{-1} giving an overall cell capacity close to 70 mAh g^{-1}. The LCO/LTO-HC 50-50 full-cell also undergoes an irreversible capacity loss of 20 mAh g^{-1} but still gives an impressive specific capacity of 100 mAh g^{-1} higher than that of the LTO and HC only full-cells with LCO.

The LCO/LTO-HC 20-80 full-cell (with dramatic reduction of Li content in the anode) also performs better than the individual anode half-cells but has an irreversible capacity loss of 40 mAh g^{-1}, giving a full-cell reversible capacity close to 95 mAh g^{-1}. The important achievement in these two cases is the enhancement of operating voltage window of the full-cells and the specific capacity leading to enhanced power and energy

density of the full-cell device without any pre-treatment of the anode such as pre-lithiation.
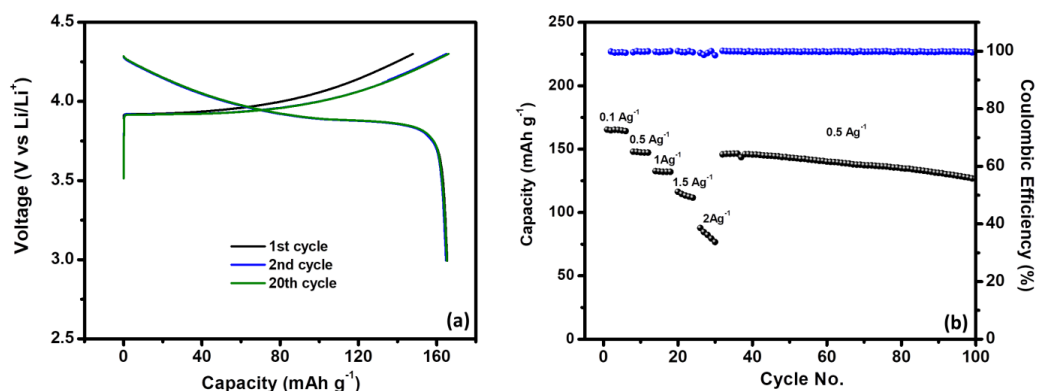
Figure 9. LCO data (a) Charge discharge curves at 50 mA g^{-1} and (b) rate performance and Coulombic efficiency.
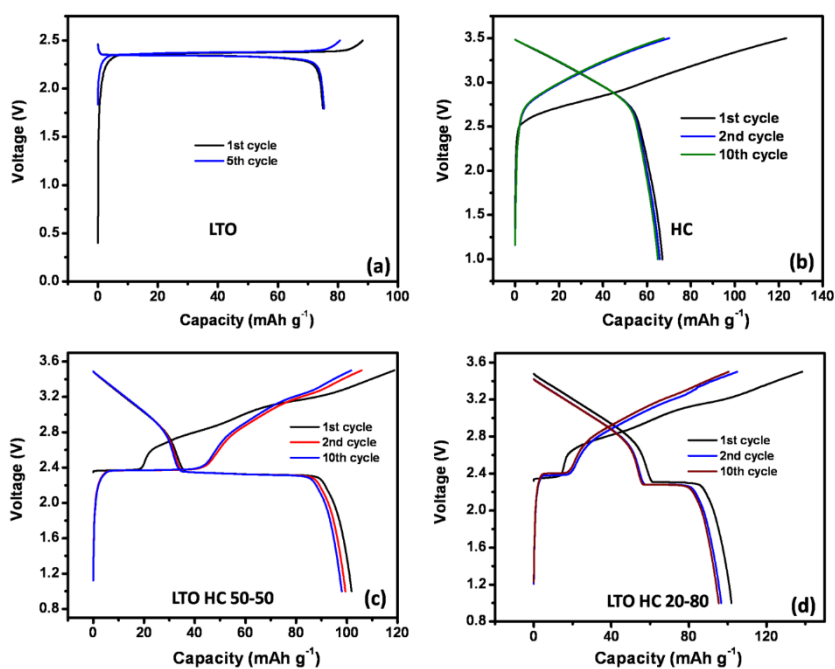
Figure 10. Full cell charge discharge curves at C/4 rate of (a) LCO/LTO; (b) LCO/HC; (c) LCO/LTO-HC 50-50 and (d) LCO/LTO-HC 20-80.

Also, the nature of the full-cell charge discharge depends on the anode characteristic. The LCO/LTO full-cell has a plateau at 2.35 V, whereas the LCO/HC full-cell has a sloping curve with no constant operating potential, a limit in the device application. When the mixed LTO-HC 50-50 and 20-80 materials are used against LCO, a plateau

region at 2.35 V is seen with enhanced potential window up to 3.5 V giving higher specific capacity.

The full-cells were also tested at a high current density of 100 mA g^{-1} for cycling stability and the charge discharge curves are specified in Figure 11. The LCO/LTO full-cell has a specific capacity of 50 mAh g^{-1} and is stable up to 250 cycles but subsequently starts degrading. The LCO/HC full-cell gives reversible capacity of only 30 mAh g^{-1} and suffers from constant capacity fade.
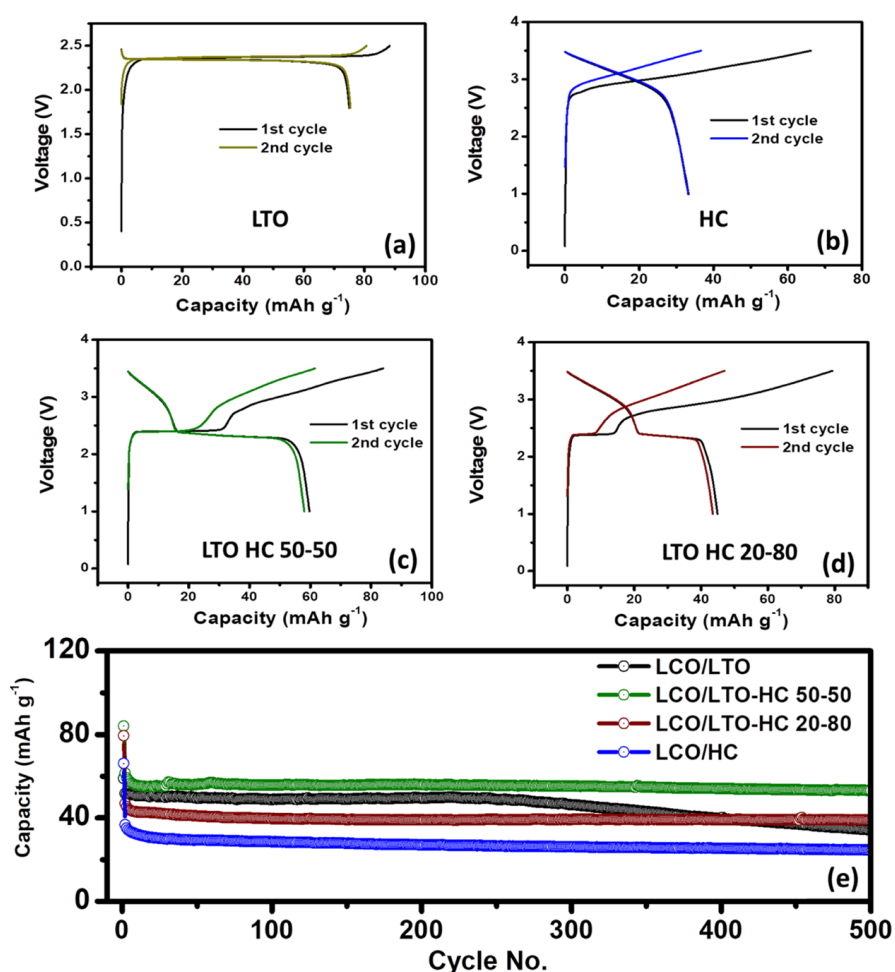
Figure 11. Full-cell performance with LCO of (a) LTO; (b) HC; (c) LTO−HC 50−50, and (d) LTO−HC 20−80 anodes. (e) Cycling stability at 100 mA g^{-1} of all full cells.

The LTO-HC 50-50 and LCO based full-cell has the highest specific capacity of 55 mAh g^{-1} and is highly stable up to 500 cycles without any capacity fading. The LCO/LTO-HC 20-80 full-cell has somewhat lower value as compared to LCO/LTO and LCO/LTO-HC 50-50 full-cells (40 mAh g^{-1}) but is still much higher than the

LCO/HC full-cell with excellent stability up to 500 cycles. The corresponding energy densities of the full cells are 34 Wh/kg for LCO/LTO and 24 Wh/kg for LCO/HC and 55 Wh/Kg for LCO/LTO-HC 50-50 and 40 Wh/kg for LCO/LTO-HC 20-80. We gain in terms of high energy density owing to enhanced operating potential window. The LCO/HC full-cell suffers from substantial irreversible capacity loss thus lacks stability as well as reversible capacity retention.

Also, when subjected to high current density of 100 mA g^{-1}, the LCO/pristine anode full-cells do not perform well whereas the LCO/LTO-HC mixed anodes are superior with the power density enhancement of the full-cells.

5.4 Conclusion

Li battery anodes are prepared by a simple physical mixing of two anode materials, namely LTO and HC, with differing strengths and weaknesses in terms of capacity and rate capability properties, in different proportions. Interestingly, the performance of such mixed anode is found to be superior to that of the individual material (LTO or HC) anodes, which can be attributed to a synergistic effect of rapid internalization and internal re-distribution of Li-ions. This condition also represents a rather unique case of laterally inhomogeneous SEI which is highly stable, possibly due to its ability for stress accommodation. In the full cells with LCO cathode, the LTO-HC mixed anodes flaunt much higher stability than only LTO or HC anode based full cells. Importantly, the Li content in the anode can be reduced by as much as 80 % and no pre-treatment is performed on the anodes to achieve a desirable level of performance. At high current density of 100 mA g^{-1} the LTO-HC mixed anodes full cell performance is excellent and the operating voltage window is also enhanced for full cell operation.

References

[1]   J.M. Tarascon, M. Armand, Issues and challenges facing rechargeable lithium batteries., Nature. 414 (2001) 359–67. doi:10.1038/35104644.

[2]   J.B. Goodenough, K. Park, The Li-ion Rechargeable Battery : A Perspective The Li-ion Rechargeable Battery : A Perspective, (2013).

[3]   G.E. Blomgren, The Development and Future of Lithium Ion Batteries, J. Electrochem. Soc. 164 (2017) A5019–A5025. doi:10.1149/2.0251701jes.

[4]   R. Marom, S.F. Amalraj, N. Leifer, D. Jacob, D. Aurbach, A review of advanced and practical lithium battery materials, J. Mater. Chem. 21 (2011) 9938. doi:10.1039/c0jm04225k.

[5]   Y. Liu, Y. Yang, Recent Progress of TiO_2 -Based Anodes for Li Ion Batteries, J. Nanomater. 2016 (2016) 1–15. doi:10.1155/2016/8123652.

[6]   T. Ohzuku, Zero-Strain Insertion Material of Li[Li[sub 1⁄3]Ti[sub 5⁄3]]O[sub 4] for Rechargeable Lithium Cells, J. Electrochem. Soc. 142 (1995) 1431. doi:10.1149/1.2048592.

[7]   K. Zaghib, M. Simoneau, M. Armand, M. Gauthier, Electrochemical study of Li4Ti5O12 as negative electrode for Li-ion polymer rechargeable batteries, J. Power Sources. 81–82 (1999) 300–305. doi:10.1016/S0378-7753(99)00209-8.

[8]   X. Sun, P. V. Radovanovic, B. Cui, Advances in spinel $Li_4 Ti_5 O_{12}$ anode materials for lithium-ion batteries, New J. Chem. 39 (2015) 38–63. doi:10.1039/C4NJ01390E.

[9]   C. Chen, H. Xu, T. Zhou, Z. Guo, L. Chen, M. Yan, L. Mai, P. Hu, S. Cheng, Y. Huang, J. Xie, Integrated Intercalation-Based and Interfacial Sodium Storage in Graphene-Wrapped Porous Li4Ti5O12 Nanofibers Composite Aerogel, Adv. Energy Mater. 6 (2016) 2–9. doi:10.1002/aenm.201600322.

[10] J. Liu, K. Song, P.A. Van Aken, J. Maier, Y. Yu, Self-supported Li4Ti5O12-C nanotube arrays as high-rate and long-life anode materials for flexible Li-ion batteries, Nano Lett. 14 (2014) 2597–2603. doi:10.1021/nl5004174.

[11] Q. Wei, F. Xiong, S. Tan, L. Huang, E.H. Lan, B. Dunn, L. Mai, Porous One-

Dimensional Nanomaterials: Design, Fabrication and Applications in Electrochemical Energy Storage, Adv. Mater. 29 (2017). doi:10.1002/adma.201602300.

[12] X. Jia, Y. Lu, F. Wei, Confined growth of Li4Ti5O12 nanoparticles in nitrogen-doped mesoporous graphene fibers for high-performance lithium-ion battery anodes, Nano Res. 9 (2016) 230–239. doi:10.1007/s12274-016-1001-5.

[13] G. Zhu, Y. Du, Y. Wang, A. Yu, Y. Xia, Electrochemical profile of lithium titanate/hard carbon composite as anode material for Li-ion batteries, J. Electroanal. Chem. 688 (2013) 86–92. doi:http://dx.doi.org/10.1016/j.jelechem.2012.07.035.

[14] J.G. Kim, M.S. Park, S.M. Hwang, Y.U. Heo, T. Liao, Z. Sun, J.H. Park, K.J. Kim, G. Jeong, Y.J. Kim, J.H. Kim, S.X. Dou, Zr4+ doping in Li4Ti5O12 anode for lithium-ion batteries: Open Li+ diffusion paths through structural imperfection, ChemSusChem. 7 (2014) 1451–1457. doi:10.1002/cssc.201301393.

[15] E. Irisarri, A. Ponrouch, M.R. Palacin, Review—Hard Carbon Negative Electrode Materials for Sodium-Ion Batteries, J. Electrochem. Soc. 162 (2015) A2476–A2482. doi:10.1149/2.0091514jes.

[16] K. Sato, M. Noguchi, A. Demachi, N. Oki, M. Endo, A Mechanism of Lithium Storage in Disordered Carbons, Science (80-.). 264 (1994) 556–558. doi:10.1126/science.264.5158.556.

[17] B. Nicholas, D. Bresser, S. Passerini, Secondary Lithium-Ion Battery Anodes : From First Commercial Batteries to Recent Research Activities Addressing the challenges in rechargeable lithium-ion battery technologies, Johnson Matthey Technol. Rev. 59 (2015) 34–44. doi:http://dx.doi.org/10.1595/205651314X685824.

[18] D.A. Stevens, J.R. Dahn, The Mechanisms of Lithium and Sodium Insertion in Carbon Materials, J. Electrochem. Soc. 148 (2001) A803. doi:10.1149/1.1379565.

[19] E. Buiel, Lithium Insertion In Hard Carbon Anode Materials For Li-Ion Batteries, J. Electrochem. Soc. 145 (1998) 1179–1183.

[20] M. Nagao, C. Pitteloud, T. Kamiyama, T. Otomo, K. Itoh, T. Fukunaga, K. Tatsumi, R. Kanno, Structure Characterization and Lithiation Mechanism of Nongraphitized Carbon for Lithium Secondary Batteries, J. Electrochem. Soc. 153 (2006) A914–

A919. doi:10.1149/1.2184908.

[21]   B. Wu, T. Liu, Q. Xia, X. Wu, Hard Carbon with Nano-Graphite Domain as High
        Performance Anode Material for Lithium-Ion Batteries, J. Electrochem. Soc. 160
        (2013) A1720–A1724. doi:10.1149/2.042310jes.

[22]   M. Noel, V. Suryanarayanan, Role of carbon host lattices in Li-ion intercalation/de-
        intercalation processes, J. Power Sources. 111 (2002) 193–209. doi:10.1016/S0378-
        7753(02)00308-7.

[23]   X.Y. Chen, C. Chen, Z.J. Zhang, D.H. Xie, X. Deng, Nitrogen-doped porous carbon
        prepared from urea formaldehyde resins by template carbonization method for
        supercapacitors, Ind. Eng. Chem. Res. 52 (2013) 10181–10188.
        doi:10.1021/ie400862h.

[24]   J. Wang, L. Shen, H. Li, X. Wang, P. Nie, B. Ding, G. Xu, H. Dou, X. Zhang, A
        facile one-pot synthesis of TiO2/nitrogen-doped reduced graphene oxide
        nanocomposite as anode materials for high-rate lithium-ion batteries, Electrochim.
        Acta. 133 (2014) 209–216. doi:10.1016/j.electacta.2014.03.095.

[25]   R. Väli, A. Jänes, T. Thomberg, E. Lust, D-Glucose Derived Nanospheric Hard
        Carbon Electrodes for Room-Temperature Sodium-Ion Batteries, J. Electrochem. Soc.
        163 (2016) A1619–A1626. doi:10.1149/2.0771608jes.

[26]   C. Wang, A.J. Appleby, F.E. Little, Electrochemical impedance study of initial
        lithium ion intercalation into graphite powders, Electrochim. Acta. 46 (2001) 1793–
        1813. doi:10.1016/S0013-4686(00)00782-9.

[27]   S.D. Xu, Q.C. Zhuang, L.L. Tian, Y.P. Qin, L. Fang, S.G. Sun, Impedance spectra of
        nonhomogeneous, multilayered porous composite graphite electrodes for Li-ion
        batteries: Experimental and theoretical studies, J. Phys. Chem. C. 115 (2011) 9210–
        9219. doi:10.1021/jp107406s.

[28]   J.P. Diard, B. Le Gorrec, C. Montella, Influence of particle size distribution on
        insertion processes in composite electrodes. Potential step and EIS theory - Part I.
        Linear diffusion, J. Electroanal. Chem. 499 (2001) 67–77. doi:10.1016/S0022-
        0728(00)00479-4.

[29] P. Szweda, P. Szweda, World ' s largest Science , Technology & Medicine Open Access book publisher Antimicrobial Activity of Honey Antimicrobial Activity of Honey, (n.d.). doi:10.1111/j.1740-8784.2012.00295.x.

[30] J. Liu, K. Tang, K. Song, P.A. van Aken, Y. Yu, J. Maier, Tiny $Li_4Ti_5O_{12}$ nanoparticles embedded in carbon nanofibers as high-capacity and long-life anode materials for both Li-ion and Na-ion batteries, Phys. Chem. Chem. Phys. 15 (2013) 20813. doi:10.1039/c3cp53882f.

[31] K. Hong, L. Qie, R. Zeng, Z. Yi, W. Zhang, D. Wang, W. Yin, C. Wu, Q. Fan, W. Zhang, Y. Huang, Biomass derived hard carbon used as a high performance anode material for sodium ion batteries, J. Mater. Chem. A. 2 (2014) 12733. doi:10.1039/C4TA02068E.

Chapter 6.

Single phase Cu_3SnS_4 nanoparticles as high capacity Li-ion battery anode

Abstract

The alloying cum conversion category materials are explored to achieve high energy density and power density Li ion batteries. Such materials have very high specific capacities and they undergo displacement reaction followed by alloying with Li. Binary sulfides fall under this category and they have specific capacity much higher than graphite. But unfortunately the sulfide dissolution and polysulfide shuttle is a big hindrance in their operation. Herein, single phase ternary metal sulfide Cu_3SnS_4 (CTS) nanoparticles with high Cu: Sn ratio are synthesized and examined for the Li ion battery anode application. A high specific capacity of 1082 mAh g^{-1} at 0.2 A g^{-1} and 440 mAh g^{-1} at a high rate of 3 A g^{-1} is realized with a superior stability tested up to 950 cycles. The CTS NPs are able to minimize the polysulfide dissolution and high Cu: Sn ratio provides excess Cu atoms as the buffer matrix for volume expansion of Sn leading to high stability and specific capacity. The comparison with reported Cu based ternary sulfides proves the same where CTS NPs stand better than other mixed phase or composite CTS materials. The full cell device with LCO cathode also performs very well giving energy density of 405 Wh/Kg at 0.1 A g^{-1}.

6.1 Introduction

The Li ion battery anodes have a wide range of specific capacity values and operating potentials.[1] While the standard Li-ion battery follows the use of $LiCoO_2$ cathode and graphite anode owing to the optimized time-tested performance of the aforementioned system, intense research is constantly being pursued on the development of novel materials for both the cathode and the anode for higher energy and power density and stability.[2] In this regard, a 40 Ah Li ion battery is reported by Attidekou et al.[3] Other alternatives like Li-air batteries[4] are also an option to achieve the desired parameters but they are not yet completely flourished. Towards cathodes, many approaches using organic materials to obtain high specific capacity have been made as they take more than one ions as compared to layered oxides.[5] But anodes are also simultaneously under continuous development.

So far we have analyzed the intercalation and alloying type anode materials. Certain compounds belong to a separate category which support dual mechanisms such as, for example, the conversion-cum-alloying type compounds (SnS_2,[6] Sb_2Se_3,[7] Sb_2S_3[8]). Along with these phosphosulphides have also been explored as Li ion battery anode.[9] These are preferred over many high capacity anode materials such as Si, Ge etc. because the latter suffer from large volume expansion and related rapid capacity decay. The conversion-cum-alloying materials also undergo volume expansion similar to the individual elements in purely alloying type materials but the corresponding consequences for the anode integrity are far less severe because the non-converted components (e. g. Cu in this case) provide a supporting structural framework. The compounds containing Sulphur (S) face additional issues, namely a) limited active material utilization, b) insulating nature of the discharge products Li_2S and Li_2S_2, and c) the dissolution of polysulfides (Li_2S_n, n higher than 4) into electrolyte that leads to the rapid capacity decay and short cycle life of the battery as shown in Figure 1.[10],[11] This causes prevents the use of Sulphur batteries in-spite of their high energy density. To solve the polysulfide dissolution problem, a specific electrolyte system- di-oxolane and dimethylether with Lithium bis-(trifluorosulfonyl) imide (LiTFSI) salt has been proposed by Linda Nazar and Manthiram groups.[14],[15]
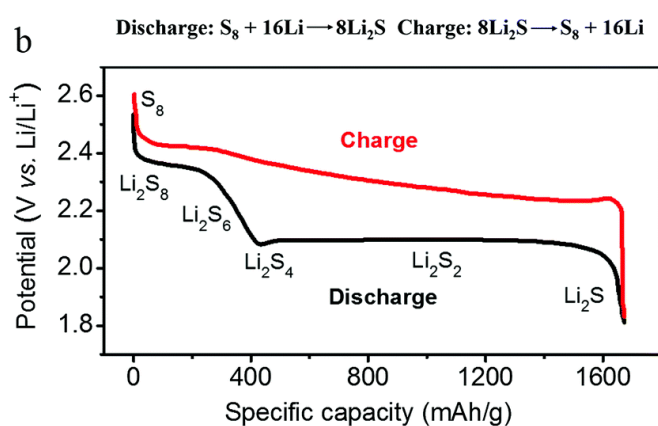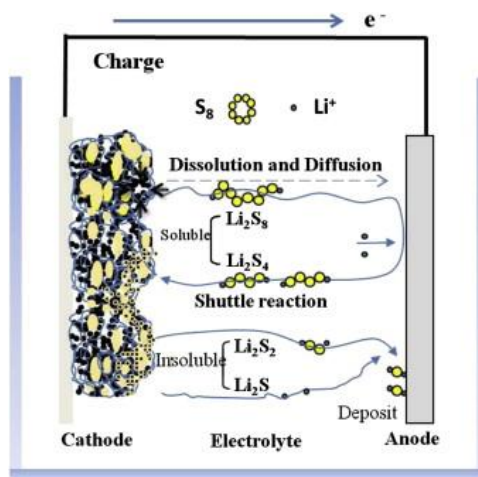
Figure 1. Polysulfide shuttle effect. Copyright Elsevier. Reproduced with permission of Ref [12]. b) Copyroght Royal Society of Chemistry. Reproduced with permission of Ref [13].

Separately, Manthiram and co-workers have developed various strategies like modifying separators by coating them with multiwall carbon nanotubes (MWCNTs) and acetylene black to avoid the polysulfide shuttle.[16],[17],[18] Apart from binary metal sulfides, ternary metal sulfides including transition metal dichalcogenides (TMDs) are a special class of materials well suited for charge storage applications owing to their unique properties. The presence of Cu, Zn into the host material or parent sulfide improves the electrical conductivity and plays a role of buffer matrix for the volume expansion. For these reasons, many ternary metal sulfides such as $NiCo_2S_4$, $CuFeS_2$, $ZnIn_2S_4$, Cu_2SnS_3 have been explored in batteries as well as supercapacitors in the as synthesized form and as composites with carbonaceous materials.[19]

Figure 2. Minimizing shuttle effect by separator modification. Copyroght Royal Society of Chemistry. Reproduced with permission of Ref [16].

Among Cu based TMDs, Cu_2SnS_3 has been used for Li- and Na-ion batteries in the form of various nanostructures as well as in composite forms.[20],[21], [22], [23], [24], [25] The higher Cu to Sn ratio compounds have either not been explored or employed in the multi-phase form in the presence of other ternary sulfides. In this report, nanoparticles of single phase ternary metal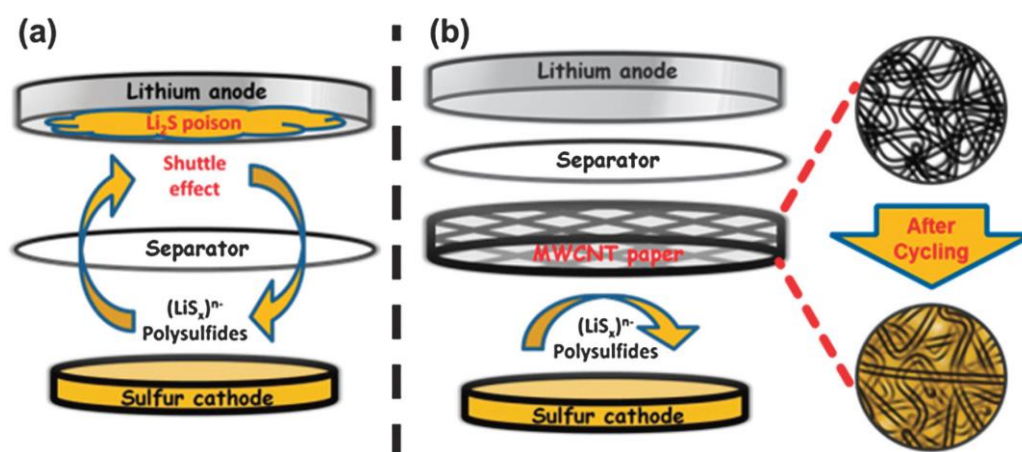 sulfide Cu_3SnS_4 (CTS) were synthesized by one step solution processing route and employed as a Li ion battery anode. The CTS NPs exhibit a high specific capacity of 1082 mAh g^{-1} at a current density of 0.2 A g^{-1} and an impressive stability of 950 cycles. The Cu-rich ternary metal sulfide renders an excellent rate performance with specific capacity of 440 mAh g^{-1} at 3 A g^{-1}.

6.2 Experimental Section

6.2.1 Materials and Methods: Synthesis of Cu_3SnS_4 Nanoparticles: The Cu_3SnS_4 nanoparticles were synthesized following the reported protocol with some modifications.[26] Briefly, the metal precursors copper acetylacetonate and tin chloride were taken in certain molar ratio with excess of thioacetamide as sulfur precursor. The reagents were taken in a three-neck vessel with formamide as the solvent and were degassed under nitrogen for half an hour with constant stirring. Then, the mixture was heated to 170 °C at a rate of 10 °C min^{-1} and kept at that temperature for 1 h. After the completion, the reaction was quenched to room temperature. The nanoparticles were obtained by centrifuging and washing with ethanol several times. The NPs were dried at 80 °C overnight.

6.2.2 Characterizations: The synthesized Cu_3SnS_4 nanoparticles were characterized using powder X-ray diffraction to investigate their crystal structure and the phase on a Bruker D8-Advance X-ray diffractometer (Germany) with CuKα radiation ($\lambda = 1.54060$ Å) at 40 kV and 30 mA. Raman spectroscopy measurements were done on a Renishaw InVia micro Raman spectrometer with an excitation wavelength of 532 nm from He-Ne laser. Transmission electron microscopy was done using JEOL, 2010F instrument at 200 kV. X-ray Photoelectron Spectroscopy (XPS) study was performed using a PHI 5000 Versa Probe II equipped with a mono-chromatic Al Ka (1486.6 eV), a X-ray source and a hemispherical analyzer.
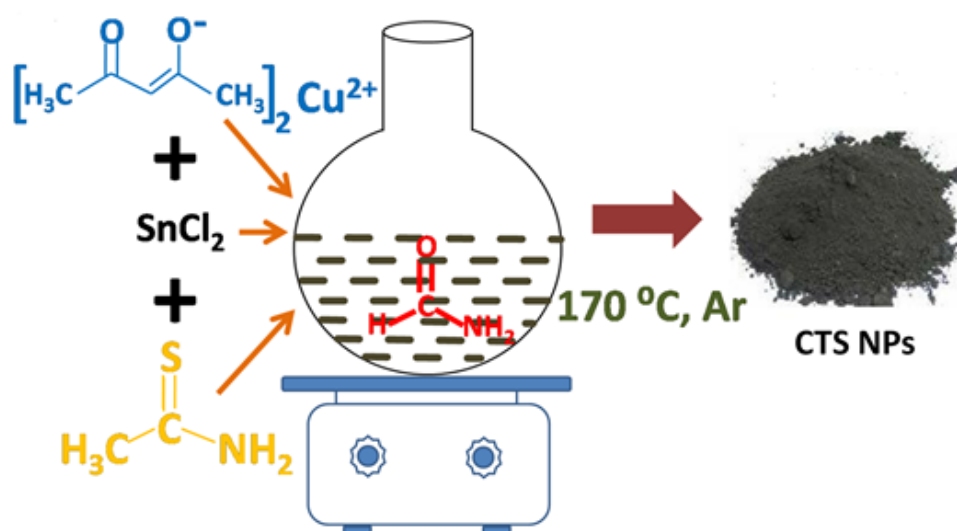
Figure 3. Synthesis protocol of CTS NPs.

Diffused reflectance spectroscopy measurement was done on Shimadzu UV-3600plus UV–VIS–NIR spectrometer to find out the band gap of the synthesized material. ICP-OES analysis was done using SPECTRO ARCOS (Germany) with smart analyzer software.

6.2.3 Electrochemical Measurements

The electrodes were prepared by making a slurry of CTS NPs, conducting carbon, and CMC binder in the weight ratio 70:20:10 in DI water. The slurry was coated onto a Cu foil and kept for drying overnight at 80 °C. The foil was then punched into 1 cm² circular discs. The CR-2032 coin cells were assembled using CTS NPs anode as

working electrodes and Li metal as reference electrode. Conducting Carbon coated Celgard 2500 was used as the separator and a commercial electrolyte with 1M LiTFSI in DOL:DME (1:1 volume) with 0.1M LiNO$_3$ as an additive. As mentioned previously, this electrilyte system is specifically choosen for sulfide based materials to minimize the dissolution of Sulphur into electrolyte and to prevent polysulfide shuttle effect. Galvanostatic charge discharge measurements were performed with BTS-Neware (China) 5V-10mA battery tester. The impedance and cyclic voltammetry were performed with VMP3 biologic system equipped with potentiostat and galvanostat channels.

6.3 Results and Discussion

6.3.1 Physical Characterisation: As emphasized in several reports for sulfide synthesis[27], it is important to note that synthesis conditions like temperature and reaction time play a crucial role in obtaining the single phase. Longer duration and temperature variation can cause the formation of binary sulfides and ternary sulfides with mix stoichiometry. Based on these studies, the CTS NPs are synthesized by a one pot solution processing route as depicted in Figure 3. The crystal structure of the Cu$_3$SnS$_4$ NPs was examined by the powder X-ray diffraction (PXRD) method. Figure 4 (a) shows the X-ray diffraction pattern with 2θ values of major diffraction peaks at 28.64, 47.82, and 56.48° representing the (0 0 1), (0 0 2), and (2 0 2) planes belonging to the orthorhombic phase of Cu$_3$SnS$_4$, which are in good agreement with the literature.[38] The appearance of diffraction peak below 2θ = 28° is strong indication of the orthorhombic phase. In this system, NPs are faceted with preferred orientation along ⟨001⟩ direction. The broadness (large full width at half maximum) of the peaks in the diffraction pattern could be attributed to the smaller size of NPs. The particles size calculated according to the Scherrer's formula is ≈5–6 nm.

Further, to confirm the phase of the NPs, Raman spectroscopy measurements were carried out. The Raman spectrum of NPs shown in Figure 4 (b) exhibits two major peaks at 291 and 329 cm^{-1} that conclusively point to the orthorhombic structure as reported in previous experiments.[39]
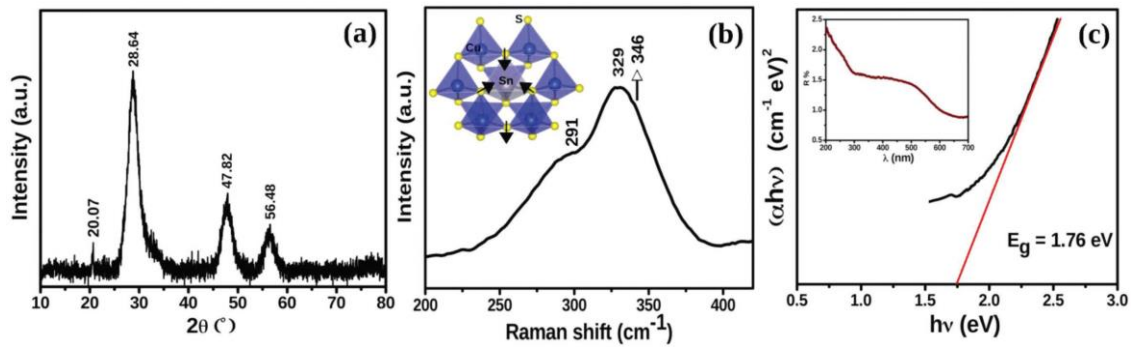
Figure 4. (a) Powder X-ray diffraction pattern of the Cu_3SnS_4 nanoparticles (b) Raman spectrum of the nanoparticles excited with 532 nm from He-Ne laser; and (c) diffuse reflectance spectrum of the nanoparticles.

Indeed, the major phonon mode around 329 cm^{-1} is associated with the breathing-like vibration of the S atoms around the Sn atom (cf. Figure 1b, inset schematic), followed by a small hump at 346 cm^{-1}, which is again a clear validation of the orthorhombic phase.[39] DRS was employed for the calculation of band gap. Figure 4 (c) presents the Tauc plot indicating the band gap of Cu_3SnS_4. The band gap was calculated using the Kubelka–Munk function F(R) given in the equation[42]

$$F(R) = \frac{(1 - R^2)}{2R}$$

where R is the diffuse reflectance of the material. The band gap obtained from the Tauc plot is 1.76 eV that corroborates with the previous reports on DRS study of this material and depicts the semi-conducting nature of this orthorhombic phase of Cu_3SnS_4.[38] The corresponding UV reflectance spectrum of the material is given in the inset of Figure 4 (c).

The composition of the material was also verified by ICP-OES with Sn to Cu ratio calculated about 1:3. The morphological investigation of the material was done using electron microscopy techniques. Figure 5 (a) shows the SEM image of the NPs. High-resolution TEM (HRTEM) images of the NPs are shown in Figure 5 (b), (c). The HRTEM micrographs present the irregular shape of the particles. The inset in Figure 5 (b) is the selected area electron diffraction (SAED) pattern of the material and the diffused rings show the polycrystalline nature of the synthesized NPs. The preferred

orientation of the Cu_3SnS_4 NPs as calculated from the lattice fringe spacing (0.36 nm) is ⟨001⟩, which is in accordance with the PXRD result.
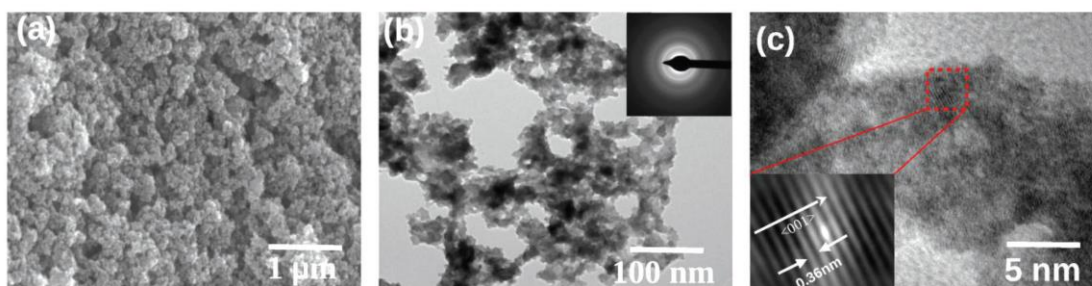
Figure 5. (a) SEM and (b), (c) TEM images of Cu_3SnS_4 nanoparticles; the inset in (b) is the SAED and the inset in (c) is the HRTEM image of the nanoparticles.
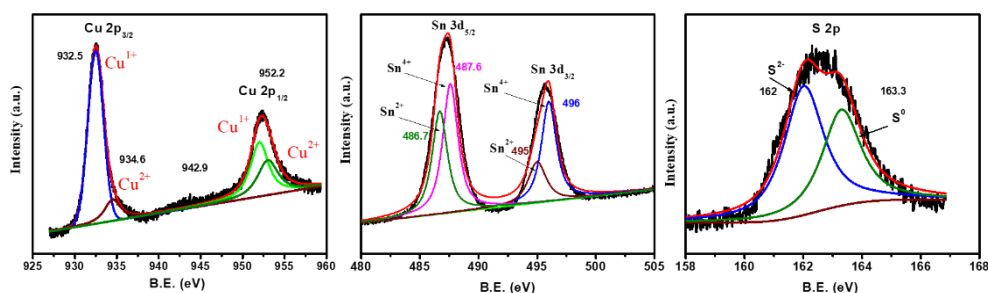
Figure 6. X-ray photoelectron spectra of CTS NPs

The XPS shown in Figure 6 reveals that the Cu $2p_{3/2}$ at 932.5 eV and Cu $2p_{1/2}$ at 952.2 eV correspond to Cu^{1+} whereas the peaks at 934.6 eV and 953 eV of the respective core levels indicate presence of Cu^{2+} in Cu_3SnS_4.[28][29] The satellite peak at 942.9 eV is also the signature of Cu^{2+} valence. Sn also exhibits two oxidation states with Sn $3d_{5/2}$ at 487.6 eV and Sn $3d_{3/2}$ at 496 eV elucidating Sn^{4+} and the peaks at 486.7 eV and 495 eV assigned to Sn^{2+}.[30][31] The S 2p core peaks at 162 eV and 163.3 eV imply the sulfide state of S.[32] This observation matches well with the literature elucidating the presence of mixed oxidation states of the elements in the material.

6.3.2 Electrochemical performance: The CTS NPs were employed as Li-ion battery anodes and their electrochemical characteristics are shown in Figure 3 and Figure 7. The Nyquist plot and the corresponding equivalent circuit is provided in Figure 7 (a).
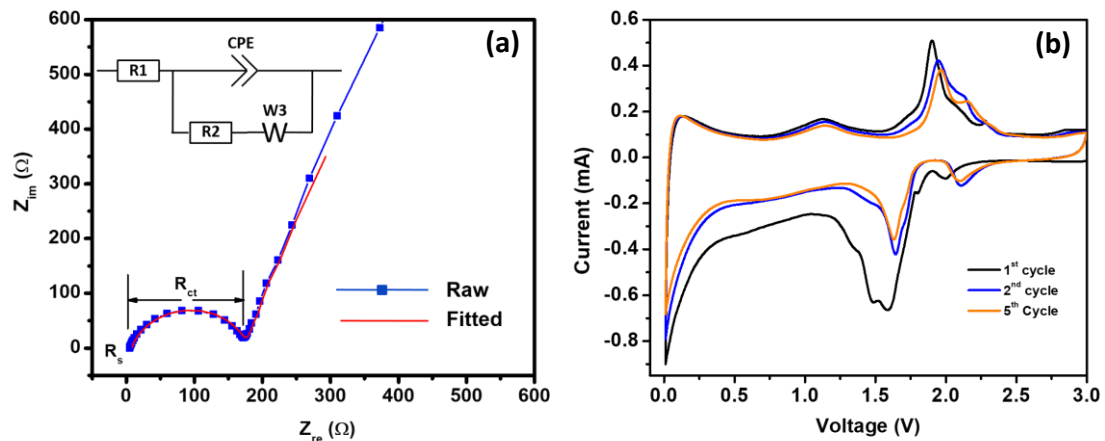
Figure 7. (a) Nyquist plot and (b) Cyclic Voltammograms of CTS NPs.

R_1 is the internal resistance; R_2 and CPE correspond to the charge transfer resistance and constant phase element. The Warburg impedance representing the lithium ion diffusion is denoted as W3. The CTS NPs exhibit a very low internal resistance implying that the electrolyte accessibility to the electrode surface is good as the particle size is small whereby the ion diffusion pathway is shortened. The cyclic voltammetry curves from 3 V to 0.01 V at a scan rate of 0.1 mV s^{-1} are given in Figure 7 (b). During the first cathodic scan, the peak at 2 V corresponds to the conversion of Cu_3SnS_4 to Cu and Sn. The broad peak around 1.5 V is due to the Li_2S evolution leading to the high first discharge specific capacity hence irreversible capacity loss.[25] The hump below 0.5 V is the signature of the Li_xSn species. In the anodic scan, the broad hump is due to metallic Sn presence.[33].[34] The de-lithiation peaks from 1.0 V to 2.25 V evince the recombination of Cu and Sn species.[35] The peaks vary in intensity in subsequent cycles owing to the slow dissolution of sulfides in electrolyte during charge discharge process.[22]

The results of the galvanostatic charge discharge measurements performed in the voltage range 0.01 V to 3.0 V are presented in Figure 8. Figure 8 (a) exhibits voltage plateaus at 0.6 V, 1.1-1.3 V, 2-2.4 V as reflected in the CV curves as well. The possible mechanism of lithiation in CTS NPs is provided in the equation below.

$$Cu_3SnS_4 + xLi \longrightarrow 4Li_2S + 3Cu^0 + Li_xSn \quad (2 \leq x \leq 4) \tag{1}$$
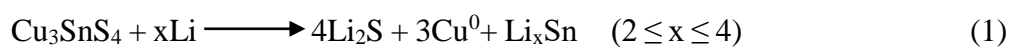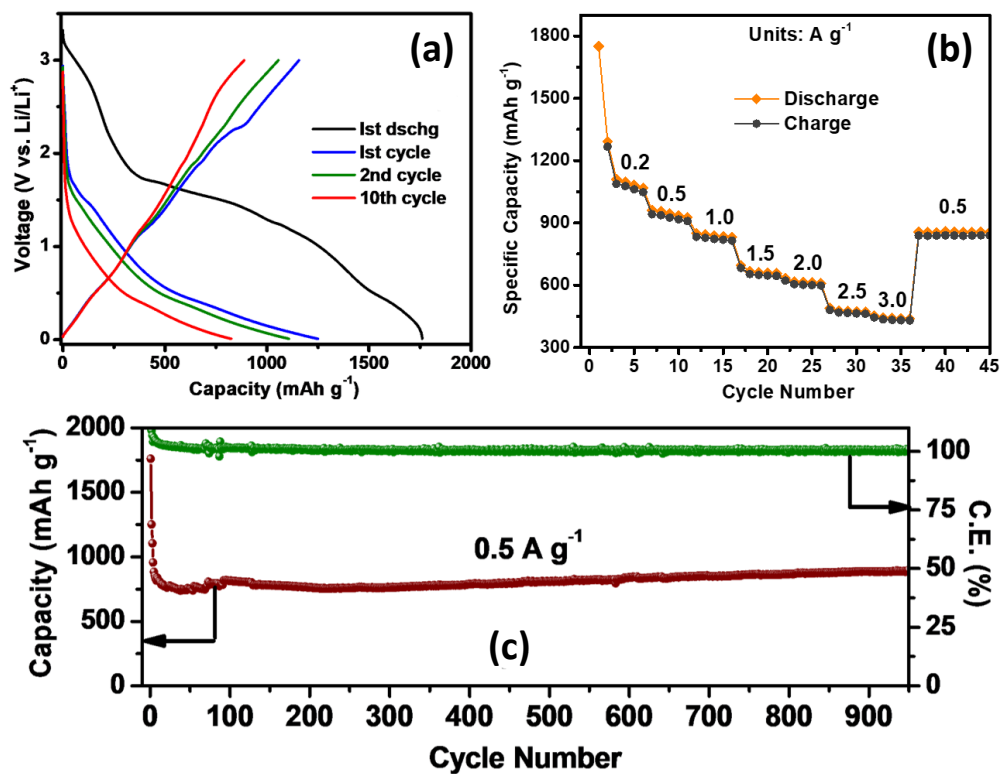
Figure 8. (a) Galvanostatic charge discharge profiles; (b) Rate performance for different current densities; and (c) cycling stability at 0.5 A g^{-1} and the corresponding Coloumbic Efficiency of CTS NPs.

The CTS NPs are seen to have an excellent rate performance (Figure 8b) with the specific capacities of 1082 mAh g^{-1}, 940 mAh g^{-1}, 835 mAh g^{-1}, 659 mAh g^{-1}, 614 mAh g^{-1}, 475 mAh g^{-1} and 440 mAh g^{-1} at current densities of 0.2 A g^{-1}, 0.5 A g^{-1}, 1 A g^{-1}, 1.5 A g^{-1}, 2 A g^{-1}, 2.5 A g^{-1} and 3 A g^{-1}, respectively. When brought back to 0.5 A g^{-1}, the CTS NPs electrode recovers to the initial capacity. The high cycling stability of CTS NPs is shown in Figure 8 (c) at a fairly high current density of 0.5 A g^{-1}. After 950 cycles of charge discharge, the CTS NPs exhibit specific capacity of 890 mAh g^{-1}.

This reflects a remarkable stability for a sulfide material. The reason for this splendid performance of CTS NPs could be the high Cu: Sn ratio in the CTS phase along with its nano phase character. Cu atoms in the structure act as a support framework for accommodating the volume expansion strain corresponding to Sn. A comparison of battery performance of various Cu-Sn-S ternary metal sulfides with different compositions is given in Table 1.
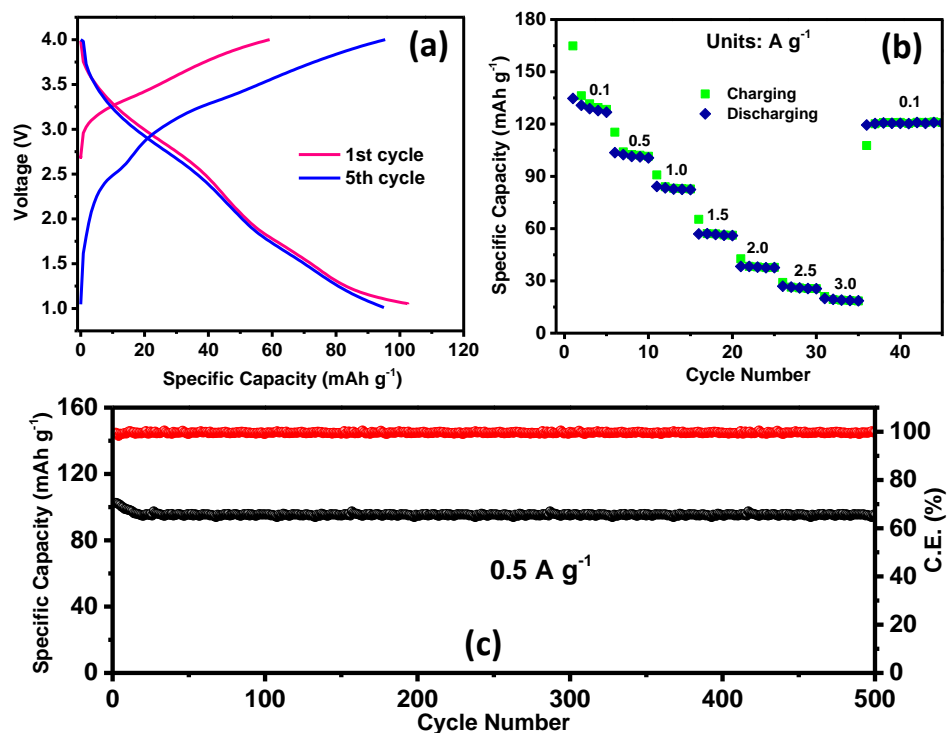
Figure 9. (a) Galvanostatic charge discharge profiles; (b) Rate performance; and (c) cycling stability and Coloumbic Efficiency at 0.5 A g-1 of LCO//CTS NPs Full Cell.

It is evident that the Cu rich ternary sulfide reported here clearly stands out among all in terms of its rate capability, long term cycling stability, and high specific capacity.

Further, full cell of CTS NPs anode is demonstrated as well using $LiCoO_2$ (LCO) cathode. The half-cell performance of LCO is provided in our previous work.[37] The cells were tested in the range 4-1 V. The CTS NPs anode was pre-lithiated prior to the full cell fabrication to compensate for the first cycle loss. The charge discharge profiles are given in Figure 9 (a). The LCO//CTS NPs full cell rate performance in Figure 9 (b) expresses the high rate capability of full cell device. The LCO//CTS NPs full cell is highly stable upto 500 cycles as clear from Figure 9 (c) with specific capacity of 95 mAh g^{-1} at 0.5 A g^{-1}. The corresponding energy density of the device is 405 Wh/kg when charged at low current density of 0.1 mA g^{-1} and 285 Wh/Kg at 0.5 A g^{-1}.

Composition	Morphology	Surface Area (m² g⁻¹)	First Discharge Capacity (mAh g⁻¹)	First Reversible Capacity	Reversible Capacity (mAh g⁻¹) And capacity retention (%)	Current Density (mA g⁻¹)	No. of Cycles
Cu_2SnS_3[25]	Cabbage like structure	22.4	1021	842	621, 69%	100	50
Cu_2SnS_3[21]	Nanosheets	-	586	403	178, 44%	30	50
Cu_2SnS_3 /rGO composite[23]	Hollow Microspheres	-	1514.6	1170	425.6, 36%	100	100
Cu_2SnS_3 /rGO composite[24]	Nanoparticles	-	1200	750	561, 74%	100	100
Cu_2SnS_3[20]	Hollow Microspheres	-	1316	500	190, 38%	100	50
Cu_2SnS_3[22]	Mesoporous Spheres	17.9	913	891	436, 49%	100	50
Cu_2SnS_3[34]	Nanoparticles	-	910	780	500, 64%	156.8 (0.2C)	200
Cu-Sn-S[34]	Mixed phase of Cu_2SnS_3 NPs and Cu_3SnS_4+ Cu_4SnS_4 NTs	102.11	1000	900	774, 83%	176 (0.2C)	200
Cu-Sn-S/SnS2/rGO composite[36]	Multiphase of $Cu_2Sn_3S_7$+ Cu_2SnS_3 + SnS_2submicron spheres	-	1043.1	900	965, 92%	500	300
Cu_3SnS_4 **This Work**	**Nanoparticles**	**80**	**1760**	**1150**	**890, 82%**	**500**	**950**

Table 1. Comparison of various Cu-Sn-S compounds for Li ion battery.

6.4 Conclusion

In conclusion, we have synthesized 5-10 nm nanoparticles of pure phase Cu-rich ternary metal sulfide Cu_3SnS_4 by a single step solution processing route. It is demonstrated that the material is capable of performing very well as a Li ion battery anode without the need of any composite forming material such as rGO or CNTs, unlike several published reports on metal sulfides. The severe capacity fading due to polysulfide dissolution in electrolyte common in Sulphur based anodes is significantly resolved which is evident from the impressive battery performance of the anode based on CTS NPs with a high specific capacity of 1082 mAh g⁻¹ at 0.2 A g⁻¹ and long term stability of 950 cycles at

0.5 A g^{-1} with specific capacity of 890 mAh g^{-1}. The rate performance shows the ability of CTS anode to withstand high currents without much capacity degradation. The full cell device of CTS NPs with LCO cathode delivers a high energy density (405 Wh/kg when charged at low current density of 0.1 mA g^{-1} and 285 Wh/Kg at 0.5 A g^{-1}) with long term stability of 500 cycles at a high current density proving the suitability of CTS NPs anode for commercial applications.

References

[1]   M. Armand, J.-M. Tarascon, Building better batteries, Nature. 451 (2008) 652–657. doi:10.1038/451652a.

[2]   J.M. Tarascon, M. Armand, Issues and challenges facing rechargeable lithium batteries., Nature. 414 (2001) 359–67. doi:10.1038/35104644.

[3]   P.S. Attidekou, S. Lambert, M. Armstrong, J. Widmer, K. Scott, P.A. Christensen, A study of 40 Ah lithium ion batteries at zero percent state of charge as a function of temperature, J. Power Sources. 269 (2014) 694–703. doi:10.1016/j.jpowsour.2014.06.064.

[4]   Y. Chen, S.A. Freunberger, Z. Peng, O. Fontaine, P.G. Bruce, Charging a Li–O2 battery using a redox mediator, Nat. Chem. 5 (2013) 489–494. doi:10.1038/nchem.1646.

[5]   M. Miroshnikov, K.P. Divya, G. Babu, A. Meiyazhagan, L.M. Reddy Arava, P.M. Ajayan, G. John, Power from nature: Designing green battery materials from electroactive quinone derivatives and organic polymers, J. Mater. Chem. A. 4 (2016) 12370–12386. doi:10.1039/c6ta03166h.

[6]   W. Sun, X. Rui, D. Yang, Z. Sun, B. Li, W. Zhang, Y. Zong, S. Madhavi, S. Dou, Q. Yan, Two-Dimensional Tin Disulfide Nanosheets for Enhanced Sodium Storage, ACS Nano. 9 (2015) 11371–11381. doi:10.1021/acsnano.5b05229.

[7]   W. Luo, A. Calas, C. Tang, F. Li, L. Zhou, L. Mai, Ultralong Sb2Se3Nanowire-Based Free-Standing Membrane Anode for Lithium/Sodium Ion Batteries, ACS Appl. Mater. Interfaces. 8 (2016) 35219–35226. doi:10.1021/acsami.6b11544.

[8]   Z. Yi, Q. Han, Y. Cheng, Y. Wu, L. Wang, Facile synthesis of symmetric bundle-like Sb2S3 micron-structures and their application in lithium-ion battery anodes, Chem.

Commun. 52 (2016) 7691–7694. doi:10.1039/C6CC03176E.

[9]   S. Sarkar, D. Mukherjee, S. Sampath, Layer-type palladium phosphosulphide and its
        reduced graphene oxide composite as electrode materials for metal-ion batteries, J.
        Power Sources. 362 (2017) 80–85. doi:10.1016/j.jpowsour.2017.06.074.

[10]   P.P.R.M.L. Harks, C.B. Robledo, T.W. Verhallen, P.H.L. Notten, F.M. Mulder, The
        Significance of Elemental Sulfur Dissolution in Liquid Electrolyte Lithium Sulfur
        Batteries, Adv. Energy Mater. 7 (2017) 1601635. doi:10.1002/aenm.201601635.

[11]   Y. Yang, G. Zheng, Y. Cui, A membrane-free lithium/polysulfide semi-liquid battery
        for large-scale energy storage, Energy Environ. Sci. 6 (2013) 1552.
        doi:10.1039/c3ee00072a.

[12]   S. Jeong, D. Bresser, D. Buchholz, M. Winter, S. Passerini, Carbon coated lithium
        sulfide particles for lithium battery cathodes, J. Power Sources. 235 (2013) 220–225.
        doi:10.1016/j.jpowsour.2013.01.084.

[13]   Z.W. Seh, Y. Sun, Q. Zhang, Y. Cui, Designing high-energy lithium-sulfur batteries,
        Chem. Soc. Rev. 45 (2016) 5605–5634. doi:10.1039/c5cs00410a.

[14]   Q. Pang, X. Liang, C.Y. Kwok, L.F. Nazar, Advances in lithium-sulfur batteries based
        on multifunctional cathodes and electrolytes, Nat. Energy. 1 (2016) 1–11.
        doi:10.1038/nenergy.2016.132.

[15]   X. Yu, J. Joseph, A. Manthiram, Suppression of the polysulfide-shuttle behavior in
        Li–S batteries through the development of a facile functional group on the
        polypropylene separator, Mater. Horizons. 3 (2016) 314–319.
        doi:10.1039/C6MH00043F.

[16]   Y.-S. Su, A. Manthiram, A new approach to improve cycle performance of
        rechargeable lithium–sulfur batteries by inserting a free-standing MWCNT interlayer,

Chem. Commun. 48 (2012) 8817. doi:10.1039/c2cc33945e.

[17] F. Zeng, Z. Jin, K. Yuan, S. Liu, X. Cheng, A. Wang, W. Wang, Y. Yang, High performance lithium–sulfur batteries with a permselective sulfonated acetylene black modified separator, J. Mater. Chem. A. 4 (2016) 12319–12327. doi:10.1039/C6TA02680J.

[18] L. Luo, S.-H. Chung, A. Manthiram, A trifunctional multi-walled carbon nanotubes/polyethylene glycol (MWCNT/PEG)-coated separator through a layer-by-layer coating strategy for high-energy Li–S batteries, J. Mater. Chem. A. 4 (2016) 16805–16811. doi:10.1039/C6TA07709A.

[19] P. Kulkarni, N. Sanna Kotrappanavar, G.R. Balakrishna, D.H. Nagaraju, M.V.V. Reddy, Nanostructured binary and ternary metal sulfides: Synthesis methods and its application in energy conversion and storage devices, J. Mater. Chem. A. 5 (2017) 22040–22094. doi:10.1039/C7TA07329A.

[20] Z. Zhang, Y. Fu, C. Zhou, J. Li, Y. Lai, EDTA-Na2-assisted hydrothermal synthesis of Cu2SnS3 hollow microspheres and their lithium ion storage performances, Solid State Ionics. 269 (2015) 62–66. doi:10.1016/j.ssi.2014.11.022.

[21] L. Shi, W. Wang, C. Wu, J. Ding, Q. Li, Synthesis of Cu2SnS3 nanosheets as an anode material for sodium ion batteries, J. Alloys Compd. 699 (2017) 517–520. doi:10.1016/j.jallcom.2017.01.023.

[22] B. Qu, M. Zhang, D. Lei, Y. Zeng, Y. Chen, L. Chen, Q. Li, Y. Wang, T. Wang, Facile solvothermal synthesis of mesoporous Cu2SnS3 spheres and their application in lithium-ion batteries, Nanoscale. 3 (2011) 3646. doi:10.1039/c1nr10401b.

[23] Z. Zhang, C. Zhou, M. Jia, Y. Fu, J. Li, Y. Lai, Synthesis of copper tin sulfide/reduced graphene oxide composites and their electrochemical properties for lithium ion batteries, Electrochim. Acta. 143 (2014) 305–311.

doi:10.1016/j.electacta.2014.07.159.

[24] H.C. Tao, S.C. Zhu, X.L. Yang, L.L. Zhang, S.B. Ni, Reduced graphene oxide
      decorated ternary Cu2SnS3as anode materials for lithium ion batteries, J. Electroanal.
      Chem. 760 (2016) 127–134. doi:10.1016/j.jelechem.2015.11.025.

[25] B. Qu, H. Li, M. Zhang, L. Mei, L. Chen, Y. Wang, Q. Li, T. Wang, Ternary
      Cu2SnS3 cabbage-like nanostructures: large-scale synthesis and their application in
      Li-ion batteries with superior reversible capacity, Nanoscale. 3 (2011) 4389.
      doi:10.1039/c1nr10784d.

[26] Y. Park, H. Jin, J. Park, S. Kim, Simultaneous phase and size control in the synthesis
      of Cu2SnS3 and Cu2ZnSnS4 nanocrystals, CrystEngComm. 16 (2014) 8642–8645.
      doi:10.1039/C4CE01079E.

[27] T.J. Huang, R.L. Guang-Ren, X. Yin, C. Tang, G. Qi, H. Gong, Effect of sulfide
      precursor selection on the nucleation, growth, and elemental composition of
      Cu2ZnSnS4nanocrystals, Cryst. Growth Des. 17 (2017) 73–79.
      doi:10.1021/acs.cgd.6b01217.

[28] H. Liu, Z. Chen, Z. Jin, Y. Su, Y. Wang, A reduced graphene oxide supported
      Cu3SnS4 composite as an efficient visible-light photocatalyst, Dalt. Trans. 43 (2014)
      7491. doi:10.1039/c4dt00070f.

[29] Y. Xiong, Y. Xie, G. Du, H. Su, From 2D framework to quasi-1D nanomaterial:
      Preparation, characterization, and formation mechanism of Cu3SnS4 nanorods, Inorg.
      Chem. 41 (2002) 2953–2959. doi:10.1021/ic0200242.

[30] N. Tipcompor, S. Thongtem, T. Thongtem, Effect of microwave radiation on the
      morphology of tetragonal Cu_3SnS_4 synthesized by refluxing
      method, Superlattices Microstruct. 85 (2015) 488–496.
      doi:10.1016/j.spmi.2015.06.015.

[31]   H. Hu, Z. Liu, B. Yang, X. Chen, Y. Qian, Template-mediated growth of
        Cu3SnS4nanoshell tubes, J. Cryst. Growth. 284 (2005) 226–234.
        doi:10.1016/j.jcrysgro.2005.07.004.

[32]   X. Lin, A. Steigert, M.C. Lux-Steiner, A. Ennaoui, One-step solution-based synthesis
        and characterization of kuramite Cu3SnS4 nanocrystals, RSC Adv. 2 (2012) 9798.
        doi:10.1039/c2ra21777e.

[33]   T.J. Kim, C. Kim, D. Son, M. Choi, B. Park, Novel SnS2-nanosheet anodes for
        lithium-ion batteries, J. Power Sources. 167 (2007) 529–535.
        doi:10.1016/j.jpowsour.2007.02.040.

[34]   J. Lin, J.M. Lim, D.H. Youn, K. Kawashima, J.H. Kim, Y. Liu, H. Guo, G.
        Henkelman, A. Heller, C.B. Mullins, Self-Assembled Cu-Sn-S Nanotubes with High
        (De)Lithiation Performance, ACS Nano. 11 (2017) 10347–10356.
        doi:10.1021/acsnano.7b05294.

[35]   L. Fu, X. Wang, J. Ma, C. Zhang, J. He, H. Xu, J. Chai, S. Li, F. Chai, G. Cui,
        Graphene-Encapsulated Copper tin Sulfide Submicron Spheres as High-Capacity
        Binder-Free Anode for Lithium-Ion Batteries, ChemElectroChem. 4 (2017) 1124–
        1129. doi:10.1002/celc.201700100.

[36]   F. Lin, W. Xiaogang, M. Jun, Z. Chuanjian, H. Jianjiang, X. Hongxia, C. Jingchao, L.
        Shizhen, C. Fenglian, C. Guanglei, Graphene-Encapsulated Copper tin Sulfide
        Submicron Spheres as High-Capacity Binder-Free Anode for Lithium-Ion Batteries,
        ChemElectroChem. 4 (2017) 1124–1129. doi:10.1002/celc.201700100.

[37]   N. Sharma, D. Puthusseri, M.O. Thotiyl, S. Ogale, Hard Carbon and $Li_4Ti_5O_{12}$-
        Based Physically Mixed Anodes for Superior Li-Battery Performance with
        Significantly Reduced Li Content: A Case of Synergistic Materials Cooperation, ACS
        Omega. 2 (2017) 8818–8824. doi:10.1021/acsomega.7b01659.

Appendix A

A flexible Li ion battery for drug delivery application

The rechargeable batteries span a long range of application and are being used in medical areas as well. The implantable medical devices (IMDs) need to be equipped with a skin compatible, light weight and portable power source for their easy operation. Flexible batteries can be used to serve this purpose. Metal organic frameworks (MOFs) are interesting materials owing to their properties and structural tunability. In this work, a Fe metal based MOF with terephthalic acid and naphthalene dicarboxylic acid as linkers is employed as an anode in Li ion battery. The Fe-MOF gives 700 mAh g^{-1} specific capacity at 50 mA $g^{-1}$and 600 mAh g^{-1} at 250 mA g^{-1} which increases to 825 mAh g^{-1} after 100 cycles with stability of more than 1000 cycles. The full cell with $LiCoO_2$ cathode shows very robust rate performance and gives 38 mAh g^{-1} specific capacity in two minutes charging time. The energy density of the full cell at 500 mA g^{-1} is 360 Wh/kg. The full cell is highly stable up to 1000 cycles. The flexible device made by free standing MOF and LCO electrodes using lamination sheet cover is used to heat a transdermal patch so that it can be used for drug delivery application.

The following paper has been published based on the work presented in this chapter.

A.1 Introduction

Rechargeable batteries have been the topic of interest past few decades. The urge for using alternative energy resources to minimize use of fossil fuels has led to enormous interest in energy harvesting and conversion devices. They have been used in hybrid vehicles to reduce pollution. They have found their utilization in the medical field as well. Now-a-days, implantable medical devices (IMDs) are quite handy for the medical community. The common IMDs include pacemakers, neuro-stimulator, drug pump etc. All these are either to monitor the parameters such as pulse rate constantly or for the controlled drug delivery.[1] All these devices require external charging for their function or they have limited use due to their non-rechargeable nature and how to power them during continuous operation is still a question. The skin patchable batteries come to play here for the solution of aforementioned problems. The batteries come on flexible platforms and are stretchable to provide ease of carrying. Much of the focus is on optimizing the current requirement to operate the miniaturized IMDs as they will need μA current and to develop micro batteries for the IMDs. There have been reports of capsule batteries which can be swallowed and operate inside the body but they are on early stage of development. Moreover, they last for a limited time of less than 24 hours. The batteries for IMDs like MEMS, NEMS etc., are micro batteries which can be either thick film or thin film coupled externally to the IMDs as the power source.[2] In this context many research groups have reported flexible batteries which are mostly Li-ion. One of such example is paper battery developed by Yi Cui's group. In this work they reported a flexible, thin battery using commercial LTO (anode) and LCO (cathode) on carbon nanotube (CNT) film to make it free standing. They introduced the printing paper as the separator.[2] Another Li-ion bendable battery was reported by Koo et al. employing polydimethylsiloxane (PDMS) as flexible substrate with thin film LCO as cathode and Li as anode.[3]

Metal organic frameworks (MOFs) are a very interesting class of materials and have unique properties which can be tuned easily. MOFs have been used frequently in many applications such as gas storage, separation, catalysis etc.[4][5][6] The organic aromatic components i.e. the linkers can act as Li insertion sites; thus use of MOFs in batteries are quite tempting. The ease of tailoring the flexibility and increase the pore size

provides the room of their exploration as anodes in batteries. There have been many reports on the application of MOFs in alkali ion batteries.[7][8][9]

In this work, a MOF with Fe as metal and terephthalic acid and naphthalene dicarboxylic acid as ligands is employed as an anode in Li ion battery. The Fe-MOF gives 700 mAh g^{-1} specific capacity at 50 mA g^{-1} and 600 mAh g^{-1} at 250 mA g^{-1} which increases to 825 mAh g^{-1} after 100 cycles with stability of more than 1000 cycles. The full cell with $LiCoO_2$ cathode shows very robust rate performance and gives 38 mAh g^{-1} specific capacity at 30C rate which is just two minutes charging time. The energy density of the full cell at 500 mA g^{-1} is 360 Wh/kg. The full cell is highly stable up to 1000 cycles. The flexible device made by free standing MOF and LCO electrodes using lamination sheet cover is used to heat a transdermal patch and it generates 52 °C in fully charged state. So it is proven that the flexible battery can be used for drug delivery application.

A.2 Experimental Section

A.2.1 Synthesis of Fe-MOF: The Fe-MOF was synthesized by following already reported protocol with modifications using hydrothermal route. Specifically, iron sulfate heptahydrate ($FeSO_4.7H_2O$), copper chloride (CuCl) and three ligands teraphthalic acid (H_2BDC), naphthalene dicarboxylic acid (H_2NDC) and 9,10-anthraquinone were taken in certain molar ratio and added all together in DMF. The solution was sonicated for 30 minutes and transferred into a Teflon liner and sealed. The hydrothermal bomb was kept at 160 °C for 3 days and then allowed to cool down to room temperature. The sample was filtered and washed with DMF many times. It was then soaked in DMF and DCM sequentially to remove any residual impurities. Finally, it was dried to obtain a reddish-brown crystals.

A.2.2 Material Characterization

Powder X-Ray diffraction was done using Bruker D8-Advance X-ray Diffractometer (Germany) with Cu kα (wavelength = 1.5418 Å). Scanning electron microscopy (SEM) was done using FEI Nova Nano 450 SEM. The Fourier transform infrared spectroscopy (FTIR) was done using a NICOLET 6700 FTIR spectrophotometer.

A.2.3 Electrochemical measurements: The anode coating was done using a slurry of Fe-MOF, Super-P and PVDF binder in weight ratio 80:10:10 in NMP solvent. The slurry was coated onto a Cu foil and dried overnight at 80 °C. After that it was punched into circular discs of diameter 1 cm. The half cells were fabricated using $LiCoO_2$ (LCO) cathode and the coating was done on Al foil using same weight ratio of LCO with Super-P and PVDF. The half cells were fabricated using Fe-MOF anode as working and Li foil as counter as well as reference electrode. The electrolyte used was commercial $LiPF_6$ EC: DMC (1:1 volume ratio) with 5% FEC as additive and whatmann separator.

A.2.4 Fabrication of flexible device: The MWCNTs were sonicated with conducting carbon and Triton X-100 and then mixed with Fe-MOF. The slurry was dispersed in PDMS and spread on a glass plate and kept for drying at 130 °C for 24 hours to get a free standing film. The cathode free standing electrodes were also synthesized by the same method. The polypropylene membrane was used as separator and the assembly was sealed in lamination sheet to get a flexible device. Galvanostatic charge discharge measurements were done with BTS-Neware (China) 5V, 10mA battery tester. The impedance and cyclic voltammetry were done with VMP3 biologic system equipped with potentiostat and galvanostat channels.

A.3 Results and Discussion

The powder XRD was performed to check the phase purity of the MOF and the PXRD pattern matches very well with the simulated one. The SEM images show the morphology of the MOF crystals which are octahedron shape. The other characterizations are being carried out for further analysis of the MOF properties.
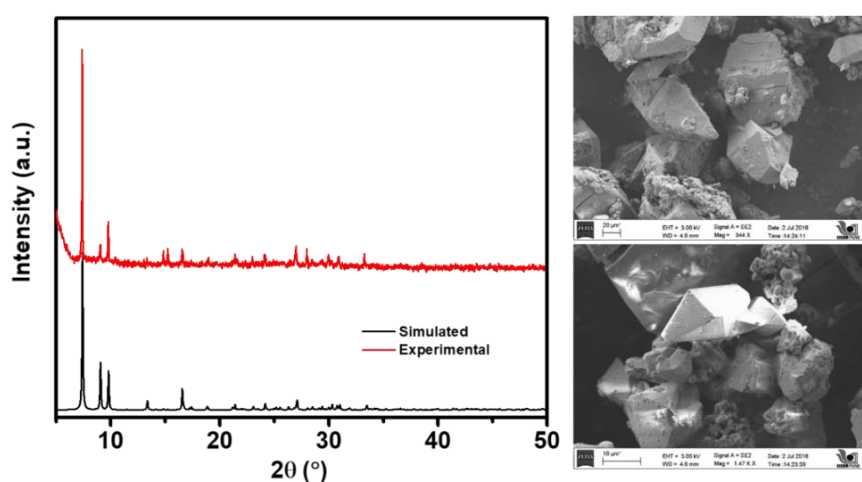
Figure 1. PXRD and SEM images of MOF.

A.3.1 Electrochemical Data

The Nyquist plot from impedance spectroscopy shows that the MOF has very low series resistance and charge transfer resistance as well. This is a very good signature for the anode application as it facilitates easy charge transfer from electrolyte to the surface and then to bulk of the electrode. The cyclic voltammetry measurements in Figure 2 show the intercalation peaks of the anode after the formation of solid electrolyte interphase (SEI) in the first cycle.
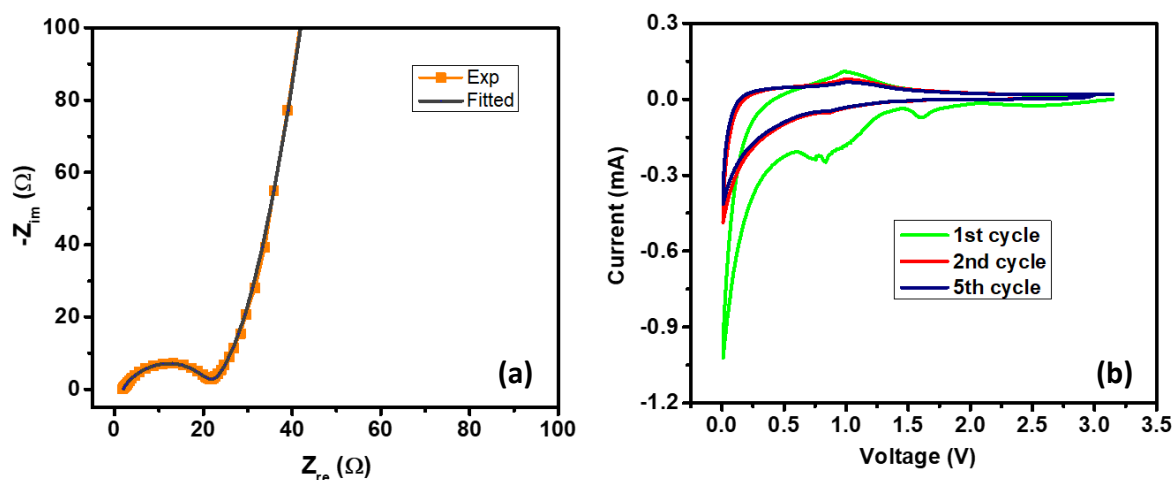
Figure 2. Nyquist plot and cyclic voltammograms of MOF electrode.

A.3.2 Determination of the charge discharge behavior: To find the mechanism of the charge discharge behavior and to determine the quantitative analysis of diffusive and capacitive contributions, cyclic voltammetry at different scan rates was carried out (Figure 3 (a)). The capacitive process comprises of electric double layer formation as well as surface redox reactions. The scan rate dependence of CV current can be expressed as below according to the power law:

$$i(V) = av^b$$

where i(V) is the current, a and b are the constant parameters and v is the scan rate. The value of b can be determined from the slope of log (i) vs. log (v) plot in Figure 3 (b) and it determines the nature of the charge storage.[10] For diffusion controlled process, b is 0.5 and for capacitive behavior b is 1. Now in this case, the slope of log (i) vs. log (v) plot is 1.02 which infers the dominance of capacitive contribution in charge transfer.

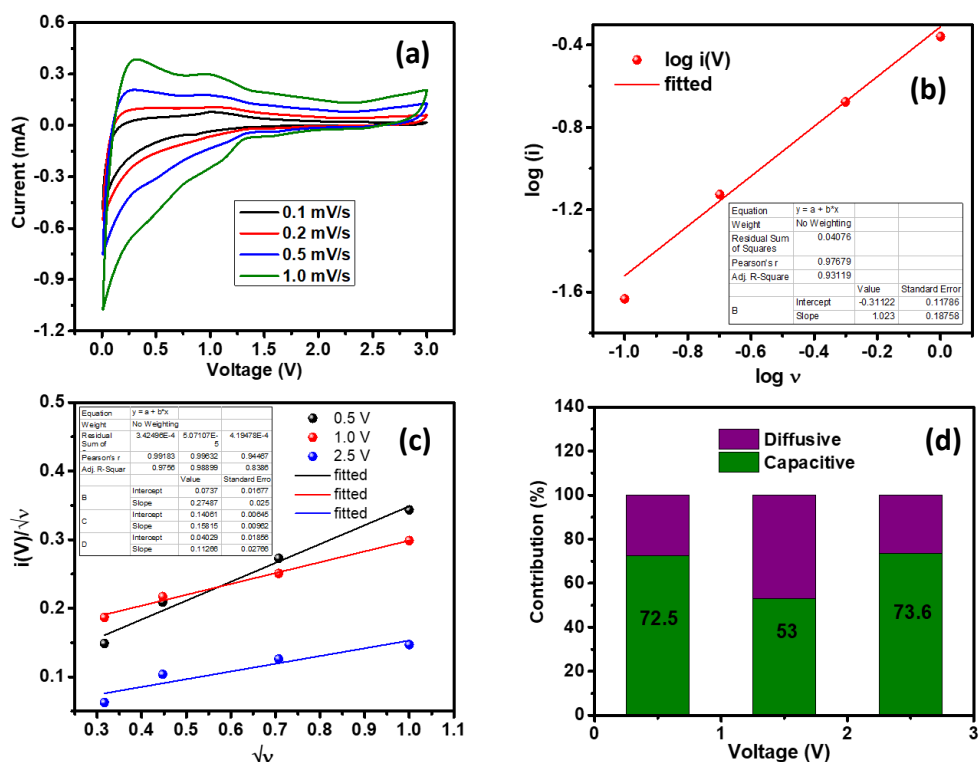Figure 3. (a) Multiscan rate CV, (b) log (i) vs. log ν plot, (c) i(V)/$\sqrt{\nu}$ vs. $\sqrt{\nu}$ plot and (d) Estimation of diffusive and capacitive current percentages at various potentials.

The total amount of current at any fixed potential can be expressed using the following equation:

$$i(V) = s_1\nu + s_2\sqrt{\nu}$$

Here, s_1 and s_2 are the constant corresponding to the capacitive and diffusive currents respectively. These constants can be estimated from the i(V)/$\sqrt{\nu}$ vs $\sqrt{\nu}$ plot knowing the $\sqrt{\nu}$ dependence of diffusion controlled process, where the slope of the graph is the measure of s_1 and the intercept represents s_2.[11] From this the ratio of capacitive and diffusive current at a given potential is calculated and given in Figure 3 (d). It is evident from the bar plots that the charge transfer is capacitive in nature which is quite usual for the porous materials such as MOFs. It elucidates that the current contribution from capacitive behavior is greater than intercalation.

From the charge discharge curves given in Figure 4 (a), no redox behavior is found and only intercalation and capacitive nature are seen. The cycling at 250 mA g^{-1} shows specific capacity of 600 mAh g^{-1} which increases to 825 mAh g^{-1} after 100 cycles.
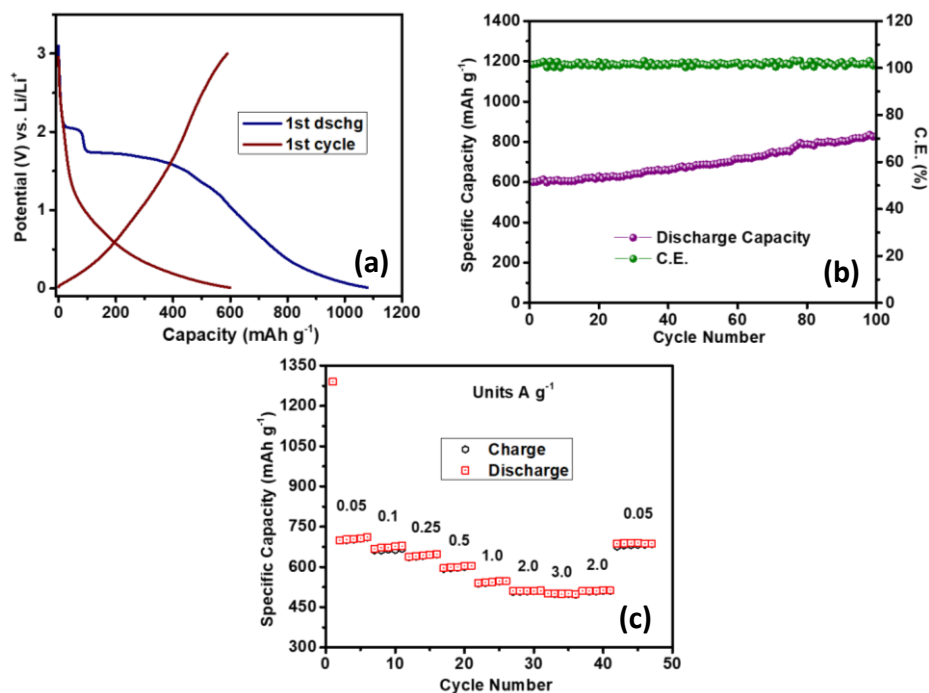
Figure 4 (a) The charge discharge curves at 250 mA g^{-1}, (b) cycling at same current density and (c) rate performance.

This is because of the capacitive behavior of the anode leading to adsorption of more number of ions as the electrolyte percolates in to the bulk. The porous materials such as MOFs tend to show this behavior. The MOF anode shows excellent rate performance with capacity of almost 500 mAh g^{-1} at a high rate of 3 A g^{-1}. It shows the same trend at 1 A g^{-1} but gets stable at 2 A g^{-1} with a stable value with no further increase in capacity. The MOF based anode is highly stable up to 1100 cycles as seen from Figure 5.
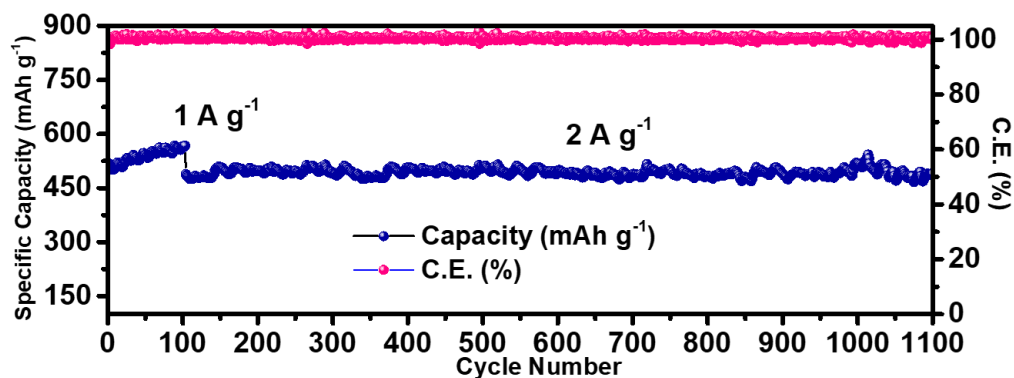
Figure 5. Long term cycling stability of MOF based anode.
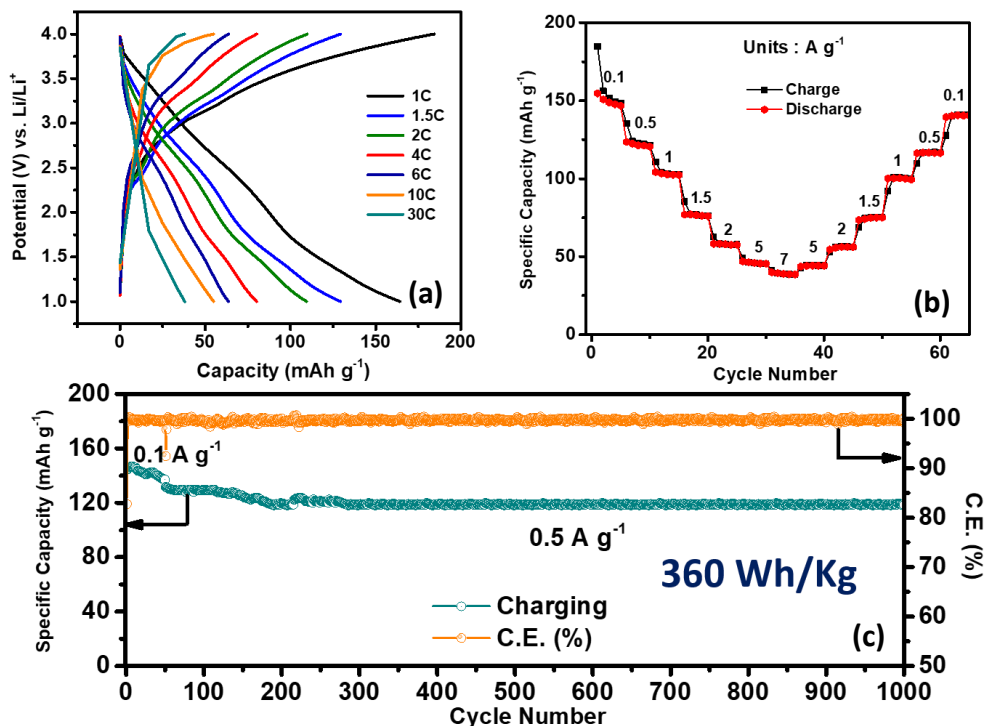
Figure 6. (a) C-rate charge discharge curves (b) rate performance and (c) cycling stability of LCO//MOF anode full cell.

A.3.3 Full cell performance: The full cells were made using MOF as anode and LCO as cathodes. The full cell exhibits high capacity at high C-rates as seen in Figure 6 (a).
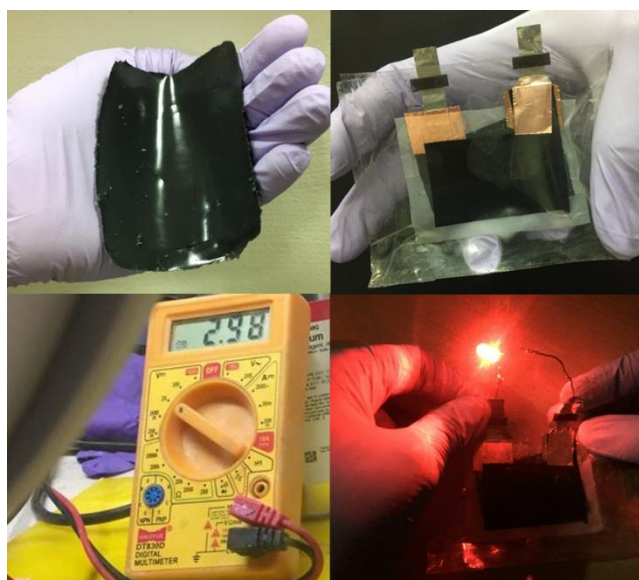
Figure 7. Flexible device fabrication process.

The rate performance is given in Figure 6 (b) where the device shows 150 mAh g^{-1} at 50 mA g^{-1} and even at a very high rate of 7 A g^{-1} it still gives almost 40 mAh g^{-1}. The

stability of full cell at 500 mA g^{-1} is also investigated and it is highly stable up to 1000 cycles giving 120 mAh g^{-1} which is equivalent to 360 Wh/kg of energy density.

A.3.4 Flexible device for drug delivery patch: The flexible device fabrication is shown in Figure 6. The flexible device is connected to the transdermal patch and it is able to generate 52 °C in bare patch and 55 °C when the patch has water on the top. IR camera imaging in Figure 8 showing that the flexible device is compatible with the transdermal patch and is capable to generate appropriate heating for drug delivery.

A.4 Conclusions

A Fe MOF is employed as an anode material for Li ion battery. The MOF is synthesized by hydrothermal route. The phase purity is checked by PXRD. The half-cell gives a very good rate performance and shows a high specific capacity and cycling stability. The full cell with LCO cathode has good C-rate performance and is very stable up to 1000 cycles. The flexible device is used to heat the transdermal patch and is able to generate desired temperature.

Bare Patch   **Patch with Water**

Figure 8. IR images of transdermal patch connected to MOF based flexible battery.

References

[1]   W. Khan, E. Muntimadugu, M. Jaffe, A.J. Domb, Focal Controlled Drug Delivery, (2014). doi:10.1007/978-1-4614-9434-8.

[2]   American Heart Association, Implantable Medical Devices, (2012) 395. doi:10.1145/634067.634234.
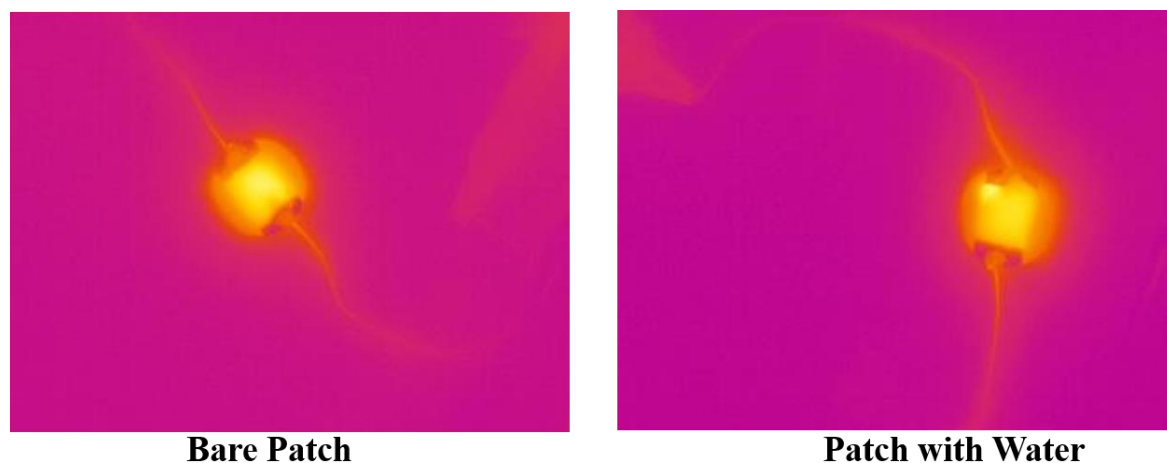
[3]   M. Koo, K. Il Park, S.H. Lee, M. Suh, D.Y. Jeon, J.W. Choi, K. Kang, K.J. Lee, Bendable inorganic thin-film battery for fully flexible electronic systems, Nano Lett. 12 (2012) 4810–4816. doi:10.1021/nl302254v.

[4]   X. Li, F. Cheng, S. Zhang, J. Chen, Shape-controlled synthesis and lithium-storage study of metal-organic frameworks Zn4O(1,3,5-benzenetribenzoate)2, J. Power Sources. 160 (2006) 542–547. doi:10.1016/j.jpowsour.2006.01.015.

[5]   T. Gong, X. Lou, E.Q. Gao, B. Hu, Pillared-Layer Metal-Organic Frameworks for Improved Lithium-Ion Storage Performance, ACS Appl. Mater. Interfaces. 9 (2017) 21839–21847. doi:10.1021/acsami.7b05889.

[6]   G. Férey, F. Millange, M. Morcrette, C. Serre, M.L. Doublet, J.M. Grenèche, J.M. Tarascon, Mixed-valence Li/Fe-based metal-organic frameworks with both reversible redox and sorption properties, Angew. Chemie - Int. Ed. 46 (2007) 3259–3263. doi:10.1002/anie.200605163.

[7]   Q. Liu, L. Yu, Y. Wang, Y. Ji, J. Horvat, M.L. Cheng, X. Jia, G. Wang, Manganese-based layered coordination polymer: Synthesis, structural characterization, magnetic property, and electrochemical performance in lithium-ion batteries, Inorg. Chem. 52 (2013) 2817–2822. doi:10.1021/ic301579g.

[8]   T. An, Y. Wang, J. Tang, Y. Wang, L. Zhang, G. Zheng, A flexible ligand-based wavy layered metal-organic framework for lithium-ion storage, J. Colloid Interface Sci. 445 (2015) 320–325. doi:10.1016/j.jcis.2015.01.012.

[9]   B.W. Byles, N.K.R. Palapati, A. Subramanian, E. Pomerantseva, The role of electronic and ionic conductivities in the rate performance of tunnel structured manganese oxides in Li-ion batteries, APL Mater. 4 (2016). doi:10.1063/1.4948272.

[10]   K.V. Sankar, R.K. Selvan, The ternary MnFe2O4/graphene/polyaniline hybrid composite as negative electrode for supercapacitors, J. Power Sources. 275 (2015) 399–407. doi:10.1016/j.jpowsour.2014.10.183.

[11]   V. Augustyn, P. Simon, B. Dunn, Pseudocapacitive oxide materials for high-rate electrochemical energy storage, Energy Environ. Sci. 7 (2014) 1597–1614. doi:10.1039/c3ee44164d.

Appendix B

Table B1. Comparison table of Si-C composite performance with literature.

Composite	Process	Morphology	Specific capacity (mAh g^{-1})	Current density (mA g^{-1})	Cycles	Reference
Macroporous Silicon/ pyrolysed PAN	Etching and pyrolysis	Free standing holy porous film	1200	200 µA cm^{-2}	20	Chem. Mater., 2012, 24, 2998−3003.
Silicon Nanowires	VLS on SS substrate	Nanowires	3000	200	200	Nat Nanotech., 2008, 3, 31-35.
Silicon/pitch Carbon	Electrospinning and pyrolysis	Nanofibers	1000	840	50	Electrochimica Acta, 2016, 220, 511–516.
Silicon/ resin Carbon	Pyrolysis	Nanorods	627	100	220	Electrochimica Acta, 2012, 71, 194– 200.
Silicon/ alginate carbon	Electrospinning and pyrolysis	Nanoporous Microspheres	1000	50	50	J. Phys. Chem. C, 2011, 115, 14148–14154.
Silicon/ CNT	CVD	Si NPs embedded nanotubes	1000	420	100	ACS Nano, 2010, 4, 2233-2241.
Silicon/CNT sponge	CVD	Nanotube sponge	1200	800	50	Adv. Energy Mater. 2011, 1, 523–527.
Silicon/ Graphene paper	Pyrolysis	Silicon embedded sheets	1500	100	100	Electrochimica Acta, 2016, 188, 777–784.

Silicon/ N-doped graphene	Hydrothermal	Nanosheets	750	500	80	Sci. Reports, 2015, 5, 15665-15675.
Silicon NPS/Carbon Nanofibers	Pyrolysis	Nanofibers	600	50	50	J. Mater. Chem., 2011, 21, 811–818
Si/Carbon	**Freeze drying and Pyrolysis**	**Si NPs embedded sheets**	**1450**	**500**	**250**	**This work**

Summary and Outlook

Research content: In this work, alkali ion batteries are discussed and certain new materials and architectures useful as anode in Li and Na ion batteries have been synthesized and tested for their performance. The various types of batteries and the importance as well as the issues of alkali ion batteries have been elaborated in the beginning to set the motivation for developing novel materials for the batteries. The various types of anode materials are particularly the topic of interest in this work and their storage mechanism and the shortcomings associated with those materials with respect to their charge storage mechanism have been explained. Based on that, different approaches have been adapted to address those shortcomings and enhance the performance of the system under consideration.

Methodology development

Search for better anodes for Li ion batteries and superior Na ion batteries have been the prime motivation in the domain of battery research. Along those lines, this work presents certain new methodologies which can be helpful to design and synthesis the new materials for Li and Na ion batteries. The novel synthesis of Na ion battery anode from a natural seed gel derived hard carbon is discussed in chapter 3. Although the pyrolysis route is very common for the synthesis of carbon, the precursor selection is important to ensure the desired properties in the final product. The natural seed gel consists of carboxylic acid and hydroxyl groups which provide -OH functionalities to the hard carbon. The freeze drying route to dry the gel also helps in retaining the structure rather than destroying the properties by conventional heating method. The volume expansion of Si is very huge problem and a big hindrance in commercialization of Si based anodes. The core-shell and composites methods are usually relied upon to provide the buffer for volume expansion. In chapter 4, a uniform carbon caging is achieved by the gel synthesis route. As the precursor seeds are subjected to swelling in the Si NPs aqueous dispersion, the Si NPs are uniformly loaded into the gel and in the final composite to give an impressive performance. Chapter 5 develops a strategy of simple physical mixing of two different anode materials and achieving superior results in mixed anodes than the individual counterparts. This way one avoids the cumbersome techniques to make the composite of the two compounds and could achieve the desired outcome. In chapter 5, the material design is chosen in such a manner that the excess ratio of one element can resolve the volume expansion and sulfide dissolution

simultaneously. The one pot synthesis under certain conditions affirms the pure phase rather than multiphase compound which is very crucial for better results. This is proven with the comparison of the material synthesized with already known compounds in the literature which are either multiphasic or with less ratio of the buffer element. In appendix a metal organic framework (MOF) has been used as a Li ion battery anode. The full cell flexible device is made using free standing electrodes where MOF is anode and $LiCoO_2$ (LCO) is cathode. The flexible device is used to heat a transdermal patch for drug delivery.

Relevance of results

In this thesis, each working chapter is based on one type of charge storage mechanism in the anode materials, where the target of solving the issue related to each type of material is established and attempts are made to achieve the same. The results obtained are seen to have accomplished the goal of enhancing the performance metrics of the device. The hard carbon synthesized for the application as anode for Na ion battery is shown to be comparable in performance with few reports and better than many of them. The comparison with commercially used hard carbon also renders the same impression giving the possibility of commercialization to the natural seed gel derived hard carbon. Achieving high stability for Si anode is indeed a challenge for the researchers working in Li ion battery. The present work establishes a gel route for uniform loading of Si NPs to get Si-carbon composite where Si is encapsulated in the carbon cage. The carbon caging provides the long term stability with high specific capacity to the Si NPs which is indeed a major achievement. The LCO//LTO system is the most used one at the commercial scale and is known for its good stability and robustness. The low specific capacity of LTO makes the overall energy density of the device very low and restricts the employment of this system in the applications with high energy density requirement. The physically mixed LTO and hard carbon anode with mere 20wt % of LTO is seen to have higher specific capacity and an excellent rate capability which otherwise is not achievable in case of carbon based materials as the nanopores are not able to adsorb ions at high rates. The mixed anodes are cycled up to 3000 cycles and show no degradation. The full cells with mixed anodes also are better in terms of energy density as well as stability making the problem relevant for the community. The high specific capacity sulfides are always considered as a good choice to design high energy density

devices. But, the polysulfide formation during cycling leading to capacity fading prevents their implication in real application. The last chapter of this thesis offers a possible solution to this problem by proposing a ternary metal sulfide with a high ratio of buffer element to minimize the sulfur dissolution.

When compared with the same class of materials, the ternary metal sulfides stands out among those which do not have the high ratio of passive element which acts only as matrix rather than participating in charging or those which are impure with multiphase characteristics.

Future direction

The basic goal of alkali ion battery research is to uplift the energy and power density of the alkali ion batteries so that their performance can satisfy the ever increasing demands of the battery driven gadgets and systems. Moreover, the batteries should be low cost, robust and safe. In certain cases they need to be flexible, with the growing interest in wearable devices. The following problems are proposed for further research in the immediate future based on this understanding.

I. The full cells in this thesis in chapter 5 and 6 are made with proposed anodes with $LiCoO_2$ (LCO) as cathode. They have a good energy density and stability but these can be further enhanced by choosing a different cathode material other than LCO. Specifically, the polyanionic cathode $Li_3V_2(PO_4)_3$ (LVP) which is better than LCO in terms of stability and capacity can be employed for the better performance of the full cells. As the LCO//LTO system is the most used one at the commercial scale[1] and is known for its good stability and robustness; with the improved performance of LTO and hard carbon mixed anode, thus the variation of cathode can lead to enhancement in the power density as well as the energy density of the system. This can be one of the future directions of the present work. The ionic liquid electrolytes could be utilized for the stability of the devices as well.

II. The cathodes play a crucial role in determining the power density of the battery. The cathodes used in alkali ion batteries are layered oxides. They have high potential window of up to 4-5 V. However, their specific capacities are limited by the one electron reaction they undergo during charging discharging. In certain cases like polyanionic compounds like $Na_3V_2(PO4)_3$ (NVP), the electron uptake is even less than

one. The conversion reaction compounds have very high capacities as they are capable of undergoing multiple electron transfer. Iron trifluoride (FeF_3) is such an interesting cathode with operating potential of 2.74 V due to the presence of highly ionic Fe-F bonds and it has theoretical capacity of 700 mAh g^{-1}.[2][3] But this cathode has low ionic conductivity and it undergoes almost 50 % volume expansion during lithiation.[4] Already there have been reports of making its composites with carbonaceous materials and downsizing the particle size but the results are not impressive enough to achieve commercialization. A core shell approach is proposed here as a future direction which can serve two purposes simultaneously; where a robust cathode material such as LVP or NVP can act as a shell to protect the FeF_3 from degradation during lithiation and can increase the potential window of the core shell cathode to 4 V which otherwise would be only 2.74 V.

III. Metal batteries are a very good candidate to bring the above considerations pertaining to high performance in to reality. The metal ion batteries can achieve very high energy density and power density because of the following reasons: the specific capacity of Li is 3800 mAh g^{-1} and has the lowest electrochemical potential of -3.04 V.[5] When coupled with any cathode material, the potential difference would be highest as compared to any other cathode anode combination giving rise to high power density. Unfortunately, the dendrite formation during plating/ stripping and the cell shortening due to the growth of dendrites are the biggest challenges in their implementation. The unstable SEI formation causing performance degradation effecting the cycle life is yet another issue to be resolved. The electrolyte additives to stabilize the SEI formation, using solid electrolytes to prevent short circuiting and coating of metal with protective layers have been till date the preventive measures to develop durable metal batteries. The use of foils as host for plating and stripping seems to be promising but the plating of the foil with Li metal and then extracting it to further use as Li containing anode is not feasible on the commercial scale. This is because the processing complications and safety issues associated with bulk Li metal handling in real systems. Recently, the metal infiltration into the distinct carbon forms has been employed to make Li metal anodes with the host matrix. The free standing carbonaceous materials such as reduced graphene oxide (rGO) and wood carbon has been used for the aforementioned task. rGO and wood carbon has been used as metal infiltration matrix for Li as well as Na metal batteries.[5][6][7] Apart from this, Ni foam owing to its porous and conducting nature

has also been proposed as matrix for the same.[8] The free standing matrix provides the ease of metal infiltration and device fabrication eliminating the plating/ stripping and cell opening and refabricating processes.[9] Thus, the free standing conducting aerogels could also be fruitfully examined as the host matrix for metal infusion, as they are flexible and robust, and can be molded into desired shapes. The easy synthesis of aerogels, cheap precursors and eco-friendly synthesis strategies make them a good candidate for metal containing anodes.

References

[1]   C. Vaalma, D. Buchholz, M. Weil, S. Passerini, A cost and resource analysis of sodium-ion batteries - Supplementary Information, (2018).

[2]   L. Zhang, S. Ji, L. Yu, X. Xu, J. Liu, Amorphous FeF3/C nanocomposite cathode derived from metal-organic frameworks for sodium ion batteries, RSC Adv. 7 (2017) 24004–24010. doi:10.1039/c7ra03592f.

[3]   D. Andre, S.J. Kim, P. Lamp, S.F. Lux, F. Maglia, O. Paschos, B. Stiaszny, Future generations of cathode materials: An automotive industry perspective, J. Mater. Chem. A. 3 (2015) 6709–6732. doi:10.1039/c5ta00361j.

[4]   G. Ali, J.H. Lee, W. Chang, B.W. Cho, H.G. Jung, K.W. Nam, K.Y. Chung, Lithium intercalation mechanism into FeF3·0.5H2O as a highly stable composite cathode material, Sci. Rep. 7 (2017) 1–8. doi:10.1038/srep42237.

[5]   Y. Zhang, W. Luo, C. Wang, Y. Li, C. Chen, J. Song, J. Dai, E.M. Hitz, S. Xu, C. Yang, Y. Wang, L. Hu, High-capacity, low-tortuosity, and channel-guided lithium metal anode, Proc. Natl. Acad. Sci. 114 (2017) 3584–3589. doi:10.1073/pnas.1618871114.

[6]   W. Luo, Y. Zhang, S. Xu, J. Dai, E. Hitz, Y. Li, C. Yang, C. Chen, B. Liu, L. Hu, Encapsulation of Metallic Na in an Electrically Conductive Host with Porous Channels as a Highly Stable Na Metal Anode, Nano Lett. 17 (2017) 3792–3797. doi:10.1021/acs.nanolett.7b01138.

[7]   X. Hu, Z. Li, Y. Zhao, J. Sun, Q. Zhao, J. Wang, Z. Tao, J. Chen, Quasi–solid state rechargeable Na-CO2batteries with reduced graphene oxide Na anodes, Sci. Adv. 3 (2017) 1–8. doi:10.1126/sciadv.1602396.

[8]   S. Sen Chi, Y. Liu, W.L. Song, L.Z. Fan, Q. Zhang, Prestoring Lithium into Stable 3D Nickel Foam Host as Dendrite-Free Lithium Metal Anode, Adv. Funct. Mater. 27 (2017) 1–10. doi:10.1002/adfm.201700348.

[9]   Z. Liang, D. Lin, J. Zhao, Z. Lu, Y. Liu, C. Liu, Y. Lu, H. Wang, K. Yan, X. Tao, Y. Cui, Composite lithium metal anode by melt infusion of lithium into a 3D conducting scaffold with lithiophilic coating, Proc. Natl. Acad. Sci. 113 (2016) 2862–2867.

List of publications

1. *Neha Sharma*, Yogesh Gawli, Absar Ahmad, Musthafa Muhammad, Satishchandra Ogale; Nanotubular hard carbon derived from natural seed gel for high performance Na ion battery anode, **Chemistry Select, 2017**, 2, 6909-6915.

2. *Neha Sharma*, Dhanya Puthusseri, Musthafa Muhammed, Satishchandra Ogale*; A hard carbon and $Li_4Ti_5O_{12}$ based physically mixed anode for superior Li-battery performance with reduced Li content: A case of synergistic materials cooperation, **ACS Omega 2017**, *2* (12), pp 8818–8824.

3. Malik Wahid, Dhanya Puthusseri, Yogesh Gawli, *Neha Sharma*, Satishchandra Ogale*; Hard Carbons for Sodium-Ion Battery Anodes: Synthetic Strategies, Material Properties, and Storage Mechanisms; **ChemSusChem 2018**, 11, 506 –526.

4. Aniruddha Basu, Kingshuk Roy, *Neha Sharma*, Shyamapada Nandi, Ramanathan Vaidhyanathan, Sunit Rane, Chandrashekhar Rode, Satishchandra Ogale*; CO_2 Laser Direct Written MOF-Based Metal-Decorated and Heteroatom-Doped Porous Graphene for Flexible All-Solid-State Microsupercapacitor with Extremely High Cycling Stability; **ACS Appl. Mater. Interfaces**, **2016**, 8 (46), 31841-48.

5. Santosh K. Singh, Kamal K. Mishra**, Neha Sharma**, Aloke Das; Direct Spectroscopic Evidence for an n-π* Interaction, **Angew.Chem. Int.Ed.**; 2016, 55, 7801 –7805.

6. Prabhsharan Kaur, Mun-Sik Shin, *Neha Sharma*, Namarta Kaur, Anjali Joshi, So-Ryong Chae, Jin-Soo Park, Moon-Sung Kang, Satpal Singh Sekhon; Non-covalent functionalization of graphene with poly(diallyl dimethylammonium) chloride: Effect of a non-ionic surfactant; **International Journal of Hydrogen Energy**, **2015**, 40(3), 1541-1547.

7. Prabhsharan Kaur, Mun-Sik Shin, Anjali Joshi, Namarta Kaur, *Neha Sharma*, Jin-Soo Park and S. S. Sekhon; Interactions between Multiwall Carbon Nanotubes and Poly(diallyl dimethylammonium) Chloride: Effect of the Presence of a Surfactant; **J. Phys. Chem. B 2013**, 117, 3161−3166.

8. *Neha Sharma*, Deodatta Phase, Musthafa Ottakam Thotiyl*, Satishchandra Ogale*; Single phase Cu_3SnS_4 nanoparticles for robust high capacity Li-ion battery anode; **ChemElectroChem, (just accepted).**

9. Thripuranthaka M, *Neha Sharma*, Tilak Das, Swapnil Varhade, Satish S. Badadhe, Musthafa Ottakam Thotiyl, Mukul Kabir* and Satishchandra Ogale*; A Combined Experimental and Computational Study of Gas Sensing by Cu_3SnS_4 Nanoparticulate Film: High Selectivity, Stability, and Reversibility for Room Temperature H_2S Sensing, **Advanced Materials Interfaces 2018**, 5, 1701492-1701500.

10. *Neha Sharma*, Sabine Szunerits, Rabah Boukherroub, Musthafa Ottakam Thotiyl and Satishchandra Ogale; A Fe-MOF based robust high capacity Li ion battery anode and demonstration of its use in flexible battery for skin patchable drug delivery system, (*submitted*).